

NUMERICAL INVESTIGATION OF FREE SURFACE AND PIPE FLOW
PROBLEMS BY SMOOTHED PARTICLE HYDRODYNAMICS

A THESIS SUBMITTED TO
THE GRADUATE SCHOOL OF NATURAL AND APPLIED SCIENCES
OF
MIDDLE EAST TECHNICAL UNIVERSITY

BY

ALİ ERSİN DİNÇER

IN PARTIAL FULFILLMENT OF THE REQUIREMENTS
FOR
THE DEGREE OF DOCTOR OF PHILOSOPHY
IN
CIVIL ENGINEERING

AUGUST 2017

Approval of the thesis:

**NUMERICAL INVESTIGATION OF FREE SURFACE AND PIPE FLOW
PROBLEMS BY SMOOTHED PARTICLE HYDRODYNAMICS**

submitted by **ALİ ERSİN DİNÇER** in partially fulfillment of the requirements for
the degree of **Doctor of Philosophy in Civil Engineering Department, Middle East
Technical University** by,

Prof. Dr. Gülbin Dural Ünver
Dean, Graduate School of **Natural and Applied Sciences** _____

Prof. Dr. İsmail Özgür Yaman
Head of Department, **Civil Engineering** _____

Prof. Dr. Zafer Bozkuş
Supervisor, **Civil Engineering Dept., METU** _____

Examining Committee Members:

Prof. Dr. A. Burcu Altan Sakarya
Civil Engineering Dept., METU _____

Prof. Dr. Zafer Bozkuş
Civil Engineering Dept., METU _____

Assoc. Prof. Dr. Yakup Darama
Civil Engineering Dept., Atılım Üniversitesi _____

Assist. Prof. Dr. Ekin Talia Tokyay Sinha
Civil Engineering Dept., METU _____

Assist. Prof. Dr. Aslı Numanoğlu Genç
Civil Engineering Dept., Atılım Üniversitesi _____

Date: _____

I hereby declare that all information in this document has been obtained and presented in accordance with academic rules and ethical conduct. I also declare that, as required by these rules and conduct, I have fully cited and referenced all material and results that are not original to this work.

Name, Last name : Ali Ersin Dinçer

Signature :

ABSTRACT

NUMERICAL INVESTIGATION OF FREE SURFACE AND PIPE FLOW PROBLEMS BY SMOOTHED PARTICLE HYDRODYNAMICS

Dinçer, Ali Ersin

Ph.D. in Department of Civil Engineering

Supervisor : Prof. Dr. Zafer Bozkuş

August 2017 ; 98 pages

In the present study, a two-dimensional (2D) computer code for free surface and pipe flows is developed by using Smoothed Particle Hydrodynamics (SPH) approach. For free surface flow problem, idealized dam break problems are investigated numerically. The results of three recently published experimental studies are used to validate the numerical solutions. In addition to mesh-free particle method, SPH with a novel boundary treatment model proposed in the present study, mesh-based methods with turbulence and laminar modelling are used to simulate the dam break problem. It is confirmed that SPH can be used to predict the behavior of dam-break induced flows. In addition, the computational time of SPH decreases with the proposed boundary model which is seminal for fluid-structure interaction problems with SPH.

Liquid slug flow driven by pressurized air in inclined and horizontal pipes with a downstream elbow is investigated numerically for the application of SPH in pipe flows. As the liquid slug hits the elbow, the impact pressure and the associated force generated at the elbow may damage pipe supports as well as the pipe itself. The slug arrival velocity and slug length (i.e. mass) at the elbow directly affect that pressure. In order to calculate these slug parameters just before the impact an improved one-

dimensional (1D) model proposed in the literature is used. At the elbow, pressure variation with respect to time is calculated with SPH. The obtained numerical data are validated with previously published experimental results. For both short and long slugs, calculated peak pressures and pressure variations show great agreement with those of measured peak pressures and pressure variations.

Keywords: smoothed particle hydrodynamics, SPH, dam-break, open channel flow, pipe flow, slug flow, boundary model.

ÖZ

SERBEST YÜZEYLİ AKIMLARIN VE BORU AKIMLARININ YUMUŞATILMIŞ PARÇACIK DİNAMİĞİ YÖNTEMİYLE SAYISAL OLARAK İNCELENMESİ

Dinçer, Ali Ersin

Doktora, İnşaat Mühendisliği Bölümü

Tez Yöneticisi : Prof. Dr. Zafer Bozkuş

Ağustos 2017 ; 98 Sayfa

Bu çalışmada, serbest yüzeyle akımların ve boru akımlarının modellenmesi için Yumuşatılmış Tanecik Hidrodinamiği (SPH) yöntemini kullanan bir bilgisayar kodu geliştirildi. Serbest yüzeyle akım için, idealize edilmiş baraj yıkılma problemleri sayısal olarak incelendi. Sayısal modellemenin doğrulanması için, son zamanlarda yayınlanmış üç deneysel çalışmanın sonucu kullanıldı. Baraj yıkılmasını modellemek için, meshden bağımsız parçacık yöntemi olan ve bu çalışmada yeni bir sınır modeli ile güçlendirilen SPH'e ek olarak, türbülans ve laminar akım yaklaşımlarını kullanan mesh'e bağımlı yöntemler de kullanıldı. Baraj yıkılmasından dolayı oluşan akımın davranışının modellenmesi için SPH yönteminin kullanılabilmesi teyit edildi. Buna ek olarak, SPH için yeni önerilen sınır yönteminin işlem süresini kısalttığı görüldü. Ayrıca, bu sınır yöntemi yapı-sıvı etkileşimi için ufuk açıcudur.

Mansabında dirsek bulunan eğimli veya yatay borulardaki basınçlı hava ile itilen sıvı parçacığı akımı, boru sistemlerindeki akımın SPH ile modellenmesi için sayısal olarak incelendi. Sıvı parçacığı dirseğe vurunca, dirsekte oluşan pik (darbe) veya çarpma basıncı ve bu basınçtan kaynaklı kuvvet, boru mesnetlerine ve boruya zarar verebilir.

Sıvı parçacığının dirseğe varış hızı ve dirsekteki uzunluğu (ya da kütlesi) doğrudan bu basıncı etkiler. Çarpmadan hemen önceki sıvı parçacığı hızını ve kütlesini hesaplamak için literatürde bulunan iyileştirilmiş bir boyutlu bir yöntem kullanıldı. Dirsekteki zamana bağlı basınç değişimi SPH ile hesaplandı. Bulunan sayısal sonuçlar yayınlanmış deney değerleriyle doğrulandı. Hem kısa hem de uzun sıvı parçacıkları için hesaplanan pik basınçlar ve basınç değişimlerinin, deneylerde ölçülen pik basınç ve basınç değişimleri ile büyük bir uyum içinde olduğu gözlemlendi.

Anahtar Kelimeler: yumuşatılmış tanecik hidrodinamiği, SPH, baraj yıkılması, açık kanal akım, boru akımı, sıvı parçacığı akımı, sınır yöntemi

To My Wife

ACKNOWLEDGEMENTS

I would never have been able to finish my dissertation without the guidance of my committee members, help from friends, and support from my family and wife.

I would like to express my sincere gratitude to my advisor Prof. Dr. Zafer Bozkuş for the continuous support of my Ph.D study and related research, for his patience, motivation, and immense knowledge. His guidance helped me in all the time of research and writing of this thesis. I always knew that his door is open to me regardless of his busy schedule. I could not have imagined having a better advisor and mentor for my Ph.D study.

I would also like to thank Prof. Dr. A. Burcu Altan Sakarya for her constant support, encouragement and guidance throughout my time in METU. I am also grateful to her for accepting to be one of the members of my thesis committee. Besides, I would like to thank Assoc. Prof. Dr. Yakup Darama for his insightful comments and encouragement. I am also grateful to Asst. Prof. Dr. Talia Ekin Tokyay Sinha for her guidance. She was a reliable source of practical Computational Fluid Dynamics knowledge and willing to share all the knowledge she has. I would also like to thank Asst. Prof. Dr. Aslı Numanoğlu Genç for her interest in my work. Moreover, I would like to acknowledge Assoc. Prof. Dr. Arris S. Tijsseling of Eindhoven University of Technology for his ideas that definitely improved the quality of my Ph.D study. I have also greatly benefited from his modifications and corrections about the concepts discussed in this study.

I will always be indebted to the members of Hydromechanics Division of Civil Engineering Department at METU, Prof. Dr. Mustafa Göğüş, Prof. Dr. Nuray Tokyay, Prof. Dr. İsmail Aydın and Assoc. Prof. Dr. Mete Köken for their help. I gained a lot from their vast hydromechanics knowledge and I was fortunate to work with such a talented group of professors. Additionally, special thanks go to Necla Çankaya Lostar. She is the big sister of our laboratory and always helped me whenever I need.

My time at METU was made enjoyable in large part due to the many friends that became a part of my life. I will never forget our trips at holidays, chit-chats at tea times, night outs and many more memories we shared with Ezgi Köker and Ezgi Budak. I am also grateful to Ahmet Nazım Şahin for his constructive ideas about our studies. Special thanks go to Emre Haspolat who always laughed at my jokes even they are about him for being such a giving person. I am also thankful to Abdullah Demir for his friendship and contributions to this study. I always felt the support of my colleagues during my time at METU. It would have been a lonely work place without them.

Cüneyt Yavuz and Kutay Yılmaz also deserve special thanks. We have experienced many adventures with them and I will always remember our enjoyable times. I am also grateful to Serkan Gökmener, Emre Kavak and Abidin Berhan Melek. I enjoyed our talks about sports, computers, cars and many more things. Many thanks to Hüseyin Gündoğdu and Eyup Uğur, our laboratory workers.

I want to thank my life-long friends Burak Ali Uzun, Samet Dursun and Salih Erakman. I always felt their supports throughout my life. I am also grateful to my late friends Onur Aslan and Ayça Aslan. I will always remember our trips to Russia and other places, games we played and times we shared.

I would also like to say a heartfelt thank to my aunt Prof. Dr. Nazire Nergiz Dinçer for always believing in me and encouraging me to follow my dreams. She is like a sister to me and I cannot express her contributions to my life, sufficiently.

Lastly but not leastly, my deep and sincere gratitude to my family for their continuous and unparalleled love, help and support. I am grateful to my sister, Zehra Esin, for always being there for me as a friend. I am forever indebted to my parents, Ahmet Emin and Hasibe, for giving me the opportunities and experiences that have made me who I am. They selflessly encouraged me to explore new directions in life and seek my own destiny. I cannot express my gratitude to my wife, Ezgi, in words for her continued support, encouragement, love and most importantly for being my eternal sunshine. This journey would not have been possible without them, and I dedicate this milestone to them.

TABLE OF CONTENTS

ABSTRACT	v
ÖZ.....	vii
ACKNOWLEDGEMENTS	x
TABLE OF CONTENTS	xii
LIST OF TABLES	xv
LIST OF FIGURES.....	xvi
LIST OF SYMBOLS	xix
CHAPTERS	1
1. INTRODUCTION	1
1.1 General.....	1
1.2 Mesh-based Methods.....	2
1.3 Mesh-free Methods.....	3
1.4 The SPH Method	3
1.5 Literature Review on SPH.....	3
1.6 Scope of the Study	7
2. NUMERICAL MODEL.....	9
2.1 SPH Model	9
2.1.1 Smoothing Function (Kernel).....	11

2.1.2	Governing Equations.....	13
2.1.3	Artificial Viscosity.....	18
2.1.4	Incompressible Flow Treatment.....	20
2.1.5	Boundary Treatment.....	22
2.1.6	Lagrange Multipliers for SPH boundaries	27
2.1.7	Neighboring Particle Search Algorithm.....	30
2.1.8	Time Integration and Time Stepping	32
2.2	RANS and LES equations	35
2.3	VOF Equations	37
2.4	The Implementation of SPH Formulations into Computer Code.....	38
3.	APPLICATION OF SPH ON FREE SURFACE FLOWS.....	41
3.1	Introduction to Dam Break Problem	41
3.2	Description of Models used in Experimental Studies	44
3.3	Results	47
3.3.1	Free Surface Profiles	47
3.3.2	Velocity Calculations	53
3.3.3	Pressure Calculations	57
3.4	Discussion of Results	58
4.	APPLICATION OF SPH ON PIPE FLOWS	61
4.1	Introduction to Slug Flow in a Pipe.....	61
4.2	Improved One-Dimensional Model.....	65

4.3	Experimental Setups	66
4.4	Numerical Models	68
4.5	Results of the simulations for the Experiments of Bozkuş et al. (2004)	70
4.6	Results of the simulations for the Experiments of Bozkuş (1991)	76
4.7	Discussion of Results.....	80
5.	CONCLUSIONS.....	81
5.1	Summary and Conclusions	81
5.2	Future Works	82
	REFERENCES.....	85
	CURRICULUM VITAE	97

LIST OF TABLES

TABLES

Table 3.1 The parameters used in SPH	45
Table 3.2 Parameters used in mesh-based methods	47
Table 3.3 Relative approximate difference between numerical and experimental results for (in %)	56

LIST OF FIGURES

FIGURES

Figure 2.1 Representation of kernel	11
Figure 2.2 Forces to derive momentum equation in the x-direction on an infinitesimal flow element.....	15
Figure 2.3 Sketch of boundary particles (Monaghan and Kos, 1999).....	24
Figure 2.4 Ghost particle technique (single boundary tangent treatment)	25
Figure 2.5 Geometry of Contact.....	28
Figure 2.6 Contact Force	28
Figure 2.7 Particle Motion	29
Figure 2.8 Linked-list algorithm for searching the nearest neighboring particles in 2D	32
Figure 2.9 Flow chart of SPH code	40
Figure 3.1 Experimental setup of Ozmen-Cagatay and Kocaman (all units are in m)	44
Figure 3.2 Experimental setup of LaRocque et al. (2013a) (all units are in m).....	45
Figure 3.3 Experimental setup of Lobovský et al. (2014) (all units are in m)	46
Figure 3.4 Particle Representation of experimental setup of Lobovský et al. (2014)	46
Figure 3.5 Comparison of free surface profiles between the experiments of Ozmen-Cagatay and Kocaman (2010) and the numerical simulations without turbulence effects	49

Figure 3.6 Comparison of free surface profiles between the experiments of Ozmen-Cagatay and Kocaman (2010) and the numerical simulations with turbulence effects	50
Figure 3.7 Comparison of free surface profiles between the experiments of LaRocque et al. (2013a) and the numerical simulations without turbulence effects.....	52
Figure 3.8 Comparison of free surface profiles between the experiments of LaRocque et al. (2013a) and the numerical simulations with turbulence effects.....	52
Figure 3.9 Free surface profiles at $t = 0.1599$ (a), 0.2766 (b) and 0.3733 (c) seconds. (Top frames from experiments, bottom frames from simulations, Lobovský et al., 2014).	53
Figure 3.10 Downstream velocity profiles for $T = 11.44$ and $h_0=0.30$ m of LaRocque et al. (2013a).....	55
Figure 3.11 Numerical simulation of velocity profiles for different bed slopes.....	57
Figure 3.12 Impact pressures measured and calculated at pressure sensor for experimental data of Lobovský et al. (2014)	58
Figure 4.1 Slug motion with holdup (taken from Tijsseling et al., 2016).....	66
Figure 4.2 Experimental setup used in Bozkuş et al. (2004)	67
Figure 4.3 Initial liquid slug in an inclined pipe Bozkuş et al. (2004).....	67
Figure 4.4 Experimental setup of Bozkuş (1991) in original work	68
Figure 4.5 Boundary and initial ($t=0$) conditions used in SPH setup (not to scale)...	70
Figure 4.6 Pressure history at the elbow for a 24 kg slug and driving pressures of: (a) 3 bar, (b) 4 bar and (c) 5 bar.....	73
Figure 4.7 Pressure history at the elbow for a 40 kg slug and driving pressures of: (a) 3 bar, (b) 4 bar and (c) 5 bar.....	75

Figure 4.8 Particle distribution and flow separation at the elbow at $t = 0.015$ s (not to scale).....	76
Figure 4.9 Pressure history at the elbow for an initial slug length of 2.74 m and an initial air pressure of 138 kPa.....	77
Figure 4.10 Pressure history at the elbow for an initial slug length of 2.74 m and an initial air pressure of 138 kPa.....	78
Figure 4.11 Pressure history at the elbow for an initial slug length of 3.35 m and an initial air pressure of (a) 138 kPa, (b) 207 kPa.....	79

LIST OF SYMBOLS

f	function of space
δ	Dirac delta function
\mathbf{x}	position vector (m)
m	mass of a particle (kg)
ρ	density (kg/m ³)
V	volume (m ³)
\mathbf{n}	unit normal vector
R	relative distance between two particles
h	smoothing length (m)
W	kernel function
τ	shear stress
\mathbf{u}	velocity vector (m/s)
μ	dynamic viscosity of fluid
π_{ij}	Monaghan-type artificial viscosity
c	speed of sound (m/s)
λ_g	free-path length of gas particles
P	pressure (Pa)

L	characteristics length scale
V_b	fluid bulk velocity
r_0	initial spacing between the fluid particles (m)
\mathbf{a}	acceleration vector (m/s^2)
\mathbf{I}	identity matrix
ν_t	eddy viscosity
μ_t	turbulent viscosity
φ	coefficient of thermal expansion
Pr_t	turbulent Prandl number
β	the holdup coefficient in slug flow
A	full pipe area (m^2)

CHAPTER 1

INTRODUCTION

1.1 General

The simulation of complex problems in science and engineering has been an important topic. One of the best ways to understand the behavior of the real life engineering systems is to perform experiments. However, performing experiments is expensive and requires large areas in laboratories or on site. In order to avoid large, time consuming and expensive experiments, the physical problem can be translated into a numerical model. Numerical simulation is often superior to traditional experimental methods in terms of acquiring data that cannot be directly observed and measured via experiments (Liu & Liu, 2003) and studying systems under peak conditions.

In order to numerically simulate a physical problem which involves fluid flow, computational fluid dynamics (CFD) is used. Since the number of calculations is too many, computers are necessary in CFD. Usually there are three main fundamentals in CFD, namely, pre-processing, solver and post-processing. First, in pre-processing mathematical model and corresponding governing equations are specified and computational domain is defined. Defining appropriate boundary and initial conditions is necessary in the implementation of the governing equations. In CFD, the conservation of mass, momentum and energy is used to establish governing equations. To solve the numerical problem, computational domain should be divided into a number of sub-domains, i.e. grids or particles that represent the characteristics of materials in the problem should be generated. The accuracy of the solution is heavily dependent on the number of grids or particles. In general, with the increase of the cells or particles, the accuracy of the simulation increases. Secondly, in solver, the governing equations are integrated usually with respect to time. A computer code in a

programming language is necessary to implement the numerical simulation. Finally, in post-processing the solution is analyzed and validated.

In the discretization of the computational domain, mesh-based and mesh-free or meshless methods can be used.

1.2 Mesh-based Methods

Finite difference, finite element and finite volume methods are the three most popular numerical discretization mesh-based methods. The finite difference method (FDM) is the oldest and useful for structured geometries. However, it is not very common due to limitations in the problems involving irregular geometries. In finite element method (FEM), the computational domain is subdivided into smaller parts or elements and residual equations are integrated over the domain. The integration takes place over each element (Liu & Quek, 2013; Zienkiewicz, Taylor, & Zhu, 2013). In finite volume method (FVM), partial differential equations are represented in the form of algebraic equations. The implementation of FVM for unstructured meshes is easier. While, in structural mechanics FEM is more popular, FDM and FVM are commonly used in CFD. Although FEM is more stable than FVM, it requires more memory.

The Eulerian and the Lagrangian descriptions are the main fundamental frames of mesh-based methods. In the Lagrangian grid method, grid is fixed on the material and it moves with the material. On the other hand, Eulerian grid is fixed on the space and it does not change while materials flow across it.

Mesh-based methods are commonly used in CFD. Despite their great success, they suffer difficulties in many aspects. The mesh generation for complex geometries is not an easy task. Determination of the locations of free-surfaces and deformable boundaries is also very hard in Eulerian mesh-based methods. Especially for the problems involving high deformations such as explosion, the limitations of mesh-based methods are more apparent.

1.3 Mesh-free Methods

Mesh-free methods are based on the interaction of particles or nodes with all their surrounding counterparts without using any pre-defined meshes. Among the mesh-free methods, element free Galerkin (EFG) method in which mesh for integration is necessary has been applied to many solid mechanics problems (Hirohisa, Kawashima, & Miyamura, 2000). In Meshless Local Petrov-Galerkin (MLPG), a global background mesh for integration is not necessary. MLPG has also been applied to solid and fluid mechanics problems (Lin & Atluri, 2001; Liu & Gu, 2001). Reproducing kernel particle method (RKPM) (Liu & Tu, 2002), point interpolation method (PIM) (Liu & Gu, 2001), mesh-free weak-strong (MWS) form method are three other mesh-free methods. Among all the mesh-free methods, smoothed particle hydrodynamics (SPH) is the most popular mesh-free particle method. It was originally developed for astrophysical problems, then it was extended to other areas.

1.4 The SPH Method

In SPH, the material (fluid in CFD) is divided into a set of particles which have the material properties. These particles move according to governing equations which will be discussed in Chapter 2. SPH is a Lagrangian method and has an adaptive nature so the random particle distribution do not affect the formulation of SPH. This nature enables SPH to deal with problems including large deformation and free-surfaces. Due to Lagrangian formulation and particle approximation, SPH particles carry all the material properties and move according to internal and external forces unlike other mesh-free methods (Liu & Liu, 2003).

1.5 Literature Review on SPH

SPH method was firstly developed to simulate astrophysics problems such as the binary stars and stellar collisions in the late 1970s by Gingold & Monaghan (1977) and Lucy (1977). Then, Monaghan (1994) used SPH to simulate free-surface problems in hydrodynamics. He investigated whether incompressible flows or arbitrary boundaries can be simulated with SPH. In order to simulate incompressible flow, he

used an artificial fluid which was more compressible than the real fluid. To treat boundary conditions, he used boundary particles which impose forces on the fluids. Different hydrostatic problems were tested and the results were compared with the available experimental and numerical data in the literature.

Morris, Fox & Zhu (1997) simulated incompressible fluids flowing with low Reynolds numbers by using weakly compressible fluid by SPH algorithm and compared their results with the solutions of Poiseuille and Couette flows. The boundary treatment they proposed, which is explained in detail in the next chapter, is still in use in many SPH codes.

Chen, Beraun & Jih (1999) developed a corrective SPH method in order to solve tensile instability and boundary deficiency problems. In their method, large density differences between the phases were simulated with density re-initialization approach. They also developed corrective kernel estimation.

Morris (2000) proposed an SPH method to simulate surface tension between two fluids having the same density and viscosity. He did not address problems with multi-phase flows in which the fluids have high viscosity and density ratios.

Colagrossi & Landrini (2003) implemented SPH method to treat two dimensional, two-phase interfacial flows with low density ratio by simulating a classical dam break problem with two phase approach. They developed novel particle evolution equations to improve stability and eliminate untrue surface-tension effects. They also used a modified artificial viscosity. Comparison with other numerical solvers such as shallow water theory and experiments were given. Results show that air-water flows with interface breaking and air entrapment can be simulated qualitatively with the proposed method. However, the quantitative results did not always show a good agreement.

Hu & Adams (2006) modified SPH equations in order to solve the discontinuity in the problems having more than one fluid. The equations they developed were in terms of particle number density and can be easily changed to continuous form across a density discontinuity.

Crespo, Gómez-Gesteira & Dalrymple (2008) simulated dam break problems over a dry bed and wet bed with SPH. The experimental results of free surfaces and wave front velocities after a dam break were compared with the numerical simulations. 2D SPH model was proved to be a suitable tool to simulate dam break flows. The open channel part of the present study shows minor similarities with the study of Crespo et al., (2008). Although free surfaces after a dam break were simulated with SPH many times, the simulation of velocity profiles reported in the studies is rare. In the open channel part of the present study, in addition to the simulation of free surfaces, velocity profiles are also calculated. The main difference between the studies is that Crespo et al., (2008) calculated the horizontal velocities of wave front. However, in the present study, the velocities at different downstream locations after a dam break were recorded in the simulation.

Monaghan & Kajtar (2009) developed a method to simulate complicated boundaries. The first applications of Monaghan's boundary conditions did not give very satisfactory results, because a particle moving parallel to the boundary at a constant distance can feel a non-uniform normal force and a tangential force. In this new method, they used radial forces to simulate boundary forces. The method works well for both concave and convex boundaries.

Staubach (2010) studied real-time performance of SPH method and presented an implementation guideline in his bachelor thesis. The handling of collision between fluid particles was investigated in the study. Spiky kernel was used instead of 6th degree polynomial kernel, which is frequently used in the implementation of SPH, to smooth out pressure force contributions. In addition, 6th order degree polynomial kernel cannot create repulsive forces between particles.

Lee et al., (2008) presented two algorithms of SPH methods, for weakly compressible and truly incompressible fluids. The algorithms are then applied to three dimensional open channel flows. In SPH algorithm for weakly compressible fluid, an equation of state in which pressures were calculated from density variations was used and for incompressible SPH, Poisson equations were solved to find pressures. In the simulation of three dimensional (3D) water collapse in a tank, incompressible SPH

predicted pressures satisfactorily, while the results of weakly compressible SPH were not realistic.

Johnsson (2011) used SPH model in order to simulate hydraulic jump. SPH was used in the numerical model, since simulation of highly disturbed free-surface flows is relatively complex in grid-based methods. He investigated whether SPH can capture the characteristics of a hydraulic jump and the effect of the number of particles used in SPH on the representation of the system. In the simulations, LS-DYNA, a commercially available software package was used. Numerical results were compared with the experimental data they obtained. According to the results, SPH could capture the characteristics of a hydraulic jump.

Kao & Chang (2012) simulated dam break – induced flood and inundation with SPH. In their model, instead of 3D Navier – Stokes equations, 2D shallow water equations (SWE) were used. They gave attention to different boundary conditions, wetting/drying moving interfaces, free-surface discontinuities and complex topography variations. They concluded that the proposed 2D-SPH-SWE method was applicable for 2 dimensional flood and inundation simulations.

Hou (2012) simulated unsteady conduit flows with SPH for his doctoral thesis. Water hammer phenomena for rapid filling and emptying of the pipelines and slug motions in closed conduit systems were simulated. A 1D SPH model was developed and applied to these systems. In order to simulate slug motion, both 1D and 2D SPH models were used. The results were closer to the experimental data than any other numerical results in the literature such as Method of Characteristics (MOC) and rigid column theories.

Barreiro, Crespo, Domínguez & Gómez-Gesteira (2013) studied on modelling coastal engineering problems with DualSPHysics, an open source software which uses SPH to simulate free-surface flow. In order to obtain faster solution, they assumed that the fluid was slightly compressible and Tait's equation of state originally developed by Peter G. Tait in 1888 was used to correlate the pressure and the density. According to this equation, a small oscillation in density causes large pressure variations. First, they compared the experimental results of wave heights with the simulations. After the

feasibility of SPH method was confirmed, they applied SPH to coastal protection problem. According to the results, SPH is an accurate model in wave propagation in coastal areas and wave impact on structures.

Hou, Tijsseling & Bozkuş (2014) calculated the impact force with respect to time on the elbow due to liquid slug flow in a horizontal pipe with a 90⁰ elbow at the end. They found the velocities and other parameters such as slug length and driving air pressure before the slug arrives the elbow by using a 1D model developed by Bozkuş, (1991). By using this data, a developed 2D SPH model was used to predict the flow separation at the elbow. Finally, knowing the contraction coefficient, an improved 1D SPH model was developed. The results of simulations were compared with the experimental data of Bozkuş, (1991). The results were in great agreement.

Aureli, Dazzi, Maranzoni, Mignosa & Vacondio (2015) investigated the capability of three models, 2D depth-averaged model, 3D Eulerian two-phase model (by using FLUENT) and 3D SPH model (with DualSPHysics) by conducting experiments for a dam break problem. Their purpose was to estimate the force due to impact of a wave occurred after dam-break on a structure. All the models were capable of simulating the increase on peak impact force with the increasing initial headwater depth. Due to three dimensional effects, 2D depth-averaged model was not as successful as 3D models to predict force time series on the structure. Load impulse was reproduced better with SPH solver.

There are many more studies about SPH. The related past studies are given and explained wherever they are applicable in the context.

1.6 Scope of the Study

In the present study, a computer code is developed to implement SPH method on open-channel flows and closed-conduit systems. For the open-channel part, a novel boundary treatment method proposed in the present study is used. The boundary method improves the computational efficiency. As can be seen from the literature review, the application of SPH on closed conduit systems is very rare. In fact, the

algorithm to calculate the slug flow in a piping system proposed here is the first so far to the best of the knowledge of the author.

The source code provided by Liu and Liu (2003) is modified and extended considerably to numerically simulate the problems in the study. In order to simulate closed-conduit flows, modified and extended source code in FORTRAN is combined with a code developed by the author in MATLAB.

The layout of the study is as follows: In Chapter 2, basic ideas and necessary formulations of SPH and other numerical models used in the calculations are given. In addition, computer implementation of SPH code is also explained in this chapter. In Chapter 3, three experiments about free surface flows found in the literature are simulated with SPH. The same experiments are also simulated with a commercially available, open-source software which uses mesh-based methods. Then, in Chapter 4 two experiments about pipe flows conducted by Bozkuş (1991) and Bozkuş et al. (2004) are modelled with SPH and compared with previous simulations in the literature. Finally, in Chapter 5 conclusions are drawn.

CHAPTER 2

NUMERICAL MODEL

2.1 SPH Model

The integral representation of an arbitrary function $f(\mathbf{x})$ in SPH model can be expressed as:

$$f(\mathbf{x}) = \int f(\mathbf{x}') \delta(\mathbf{x} - \mathbf{x}') d\mathbf{x}' \quad (2.1)$$

where f is a function of space, \mathbf{x} is the position vector and $\delta(\mathbf{x} - \mathbf{x}')$ is the Dirac delta function, represented by:

$$\delta(\mathbf{x} - \mathbf{x}') = \begin{cases} 1 & \mathbf{x} = \mathbf{x}' \\ 0 & \mathbf{x} \neq \mathbf{x}' \end{cases} \quad (2.2)$$

By replacing Dirac delta function with smoothing function,

$$f(\mathbf{x}) = \int f(\mathbf{x}') W(\mathbf{x} - \mathbf{x}', h) d\mathbf{x}' \quad (2.3)$$

where W is the smoothing kernel function or simply kernel. By imagining that the fluid is divided into N small elements with masses m_1, m_2, \dots, m_N , the particle representation of SPH can be shown as:

$$f(\mathbf{x}_i) \approx \sum_{j=1}^N \frac{m_j}{\rho_j} f(\mathbf{x}_j) W(\mathbf{x}_i - \mathbf{x}_j, h) \quad (2.4)$$

where N is the number of particles in support domain and

$$d\mathbf{x}' = \Delta V_j = \frac{1}{\rho_j} \rho_j \Delta V_j = \frac{1}{\rho_j} m_j \quad (2.5)$$

where ρ is the density and V is the volume and m is the mass of a particle. According to Monaghan (2005), the error in Equation (2.4) is $O(h^2)$ or better. However, due to the disordered motion of particle, the error cannot be estimated exactly in the SPH equations. Although the particles move in a disordered manner, they are still governed by fluid dynamics equations. Therefore, SPH is more correct than just interpolation of quantities from randomly disordered particle arrays would propose.

The integral interpolant representation of the gradient function can be stated as:

$$\nabla f(\mathbf{x}) = \int \nabla f(\mathbf{x}') W(\mathbf{x} - \mathbf{x}', h) d\mathbf{x}' - \int f(\mathbf{x}') \nabla W(\mathbf{x} - \mathbf{x}', h) d\mathbf{x}' \quad (2.6)$$

Integrating by parts of Equation (2.6),

$$\nabla f(\mathbf{x}) = - \int f(\mathbf{x}') \nabla W(\mathbf{x} - \mathbf{x}', h) d\mathbf{x}' + \int f(\mathbf{x}') W(\mathbf{x} - \mathbf{x}') \mathbf{n}_{x'} dS \quad (2.7)$$

where \mathbf{n} is the unit normal vector to the surface, S . On the right hand side (RHS) of the above equation, the first integral is over the volume of the domain, while the second integral is over the boundary of the domain. Through the boundary domain, either the function or the kernel tends to be zero. Therefore, the second integral on the RHS can be neglected for most of the fluid problems. Then the gradient function becomes:

$$\nabla f(\mathbf{x}) = - \int f(\mathbf{x}') \nabla W(\mathbf{x} - \mathbf{x}', h) d\mathbf{x}' \quad (2.8)$$

This equation can be stated in summation form as:

$$\nabla f(\mathbf{x}) = - \sum_{j=1}^N \frac{m_j}{\rho_j} f(\mathbf{x}_j) \nabla W(\mathbf{x}_i - \mathbf{x}_j, h) \quad (2.9)$$

Thus, the derivative of any function in SPH equation is obtained by directly differentiating the kernel function. This is one of the most important advantages of SPH summation.

2.1.1 Smoothing Function (Kernel)

There are different smoothing functions proposed in literature. In Figure 2.1, schematic representation of kernel can be seen. The main idea is that the effect of a neighboring particle to a particle of interest decreases while the distance between the particles increases.

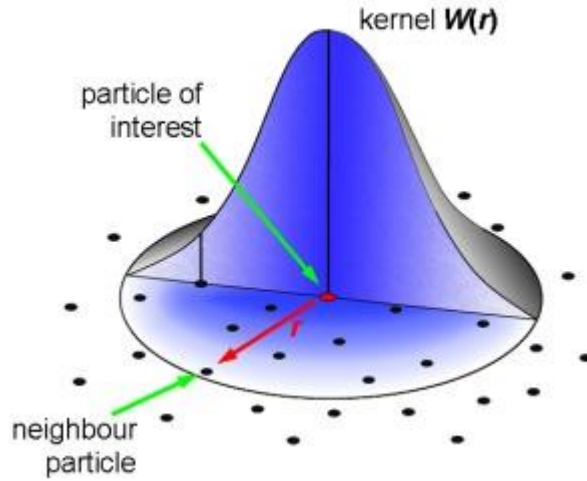


Figure 2.1 Representation of kernel

Lucy (1977) proposed bell-shaped function as kernel:

$$W(R, h) = \alpha_d \begin{cases} (1 + 3R)(1 - R)^3 & R \leq 1 \\ 0 & R > 1 \end{cases} \quad (2.10)$$

where $\alpha_d = \frac{5}{4h}$ for one-dimensional, $\alpha_d = \frac{5}{\pi h^2}$ for two-dimensional and $\alpha_d = \frac{105}{16\pi h^3}$ for three-dimensional space. R is the relative distance between two particles, i.e. $R = \frac{|x_i - x_j|}{h}$ and h is the smoothing length and can be taken close to the initial spacing between two fluid particles.

Gingold & Monaghan (1977) used Gaussian kernel:

$$W(R, h) = \alpha_d e^{-R^2} \quad (2.11)$$

where $\alpha_d = \frac{1}{h\pi^{0.5}}$, $\frac{1}{h\pi^2}$, $\frac{1}{h^3\pi^{1.5}}$ for one, two and three dimensional space, respectively.

Although Gaussian kernel is stable, accurate and smooth for higher order derivatives it is not really compact and does not reach zero theoretically resulting in large support domain and more particles, so it is computationally more expensive.

Monaghan & Lattanzio (1985) proposed cubic spline or B-spline kernel function:

$$W(R, h) = \alpha_d \begin{cases} \frac{2}{3} - R^2 + \frac{1}{2}R^3 & 0 \leq R < 1 \\ \frac{1}{6}(2 - R)^3 & 1 \leq R < 2 \\ 0 & R \geq 2 \end{cases} \quad (2.12)$$

where $\alpha_d = \frac{1}{h}$ for one-dimensional, $\alpha_d = \frac{15}{7\pi h^2}$ for two-dimensional and $\alpha_d = \frac{3}{2\pi h^3}$ for three-dimensional problems.

Johnson, Stryk & Beissel (1996) proposed quadratic smoothing function,

$$W(R, h) = \alpha_d \left(\frac{3}{16}R^2 - \frac{3}{4}R + \frac{3}{4} \right) \quad (2.13)$$

where $\alpha_d = \frac{1}{h}$, $\frac{1}{h^2\pi}$ and $\frac{5}{4h^3\pi}$ for one, two and three dimensional space, respectively. In this function, while the particles move apart from each other, the magnitude of derivative decreases, conversely, while the particles approach each other it increases. This is useful in the problems having trouble with compressive instability.

Bell-shaped, Gaussian, cubic spline and quadratic smoothing functions are all included in the developed computer code. According to the problem, one of these kernels is chosen. In this study, the results by using cubic spline function are presented. Actually, other kernels have also been applied to some simulations and the results did not significantly change. However, minor differences in computational time were observed.

2.1.2 Governing Equations

Navier-Stokes equations for density approximation of SPH can be expressed in two approaches. In the first approach, summation density approach, SPH approximations are directly applied to the density itself. For a particle i , summation density approximation can be expressed as:

$$\rho_i = \sum_{j=1}^N m_j W_{ij} \quad (2.14)$$

where,

$$W_{ij} = W(\mathbf{x}_i - \mathbf{x}_j, h) = W(|\mathbf{x}_i - \mathbf{x}_j|, h) = W(R_{ij}, h) \quad (2.15)$$

and,

$$R_{ij} = \frac{|\mathbf{x}_i - \mathbf{x}_j|}{h} \quad (2.16)$$

where, i is the given particle, j is the particle which is in the support domain of particle i , m_j is the mass of particle j , N is the number of particles in the support domain of particle i and R_{ij} is the relative distance between two particles.

Another approach for density approximation is the continuity density in which continuity equation is used to approximate density. Continuity equation in Lagrangian frame is given as:

$$\frac{D\rho}{Dt} = -\rho \nabla \cdot \mathbf{u} \quad (2.17)$$

By combining equation (2.9) with equation (2.17), the continuity density approximation is obtained. In the equation, ρ is the fluid density, \mathbf{u} is the flow velocity vector field. The transformations can be followed in the studies of Liu and Liu (2003). From this point on, α and β are used to show the coordinate directions in the equations.

$$\frac{d\rho_i}{dt} = \sum_{j=1}^N m_j (\mathbf{u}_{ij}^\beta) \frac{\partial W_{ij}}{\partial \mathbf{x}_i^\beta} \quad (2.18)$$

In the equations (2.14) and (2.18), j cannot be equal to i . In the code, this limitation is taken into consideration. From equation (2.18) it is seen that, the gradient of kernel function directly affects the contribution of the relative velocities to density approximation. Both summation density and continuity density approaches are included in the developed code. Since in the summation density approach, all the densities should be calculated before the calculation of other parameters, the computational time is higher. In addition, for the problems having free surfaces, density drops to zero discontinuously. However, in the summation density approach, this discontinuous drop cannot be observed, because particles at the surface have their densities smoothed over a length $2h$. In the simulation of the problems with free surface, continuity density approach may give more accurate results. Although, using the summation density approach is preferable for general fluid problems (Liu & Liu, 2003) continuity density is used in the simulations of this study.

By applying Newton`s second law to an infinitesimal flow element, momentum equation is derived. The infinitesimal flow element and the forces on the element are shown in Figure 2.2. In the derivation of momentum equation, on the contrary of the notation used in the present study, the coordinate directions are represented as x , y and z instead of α , β and ζ .

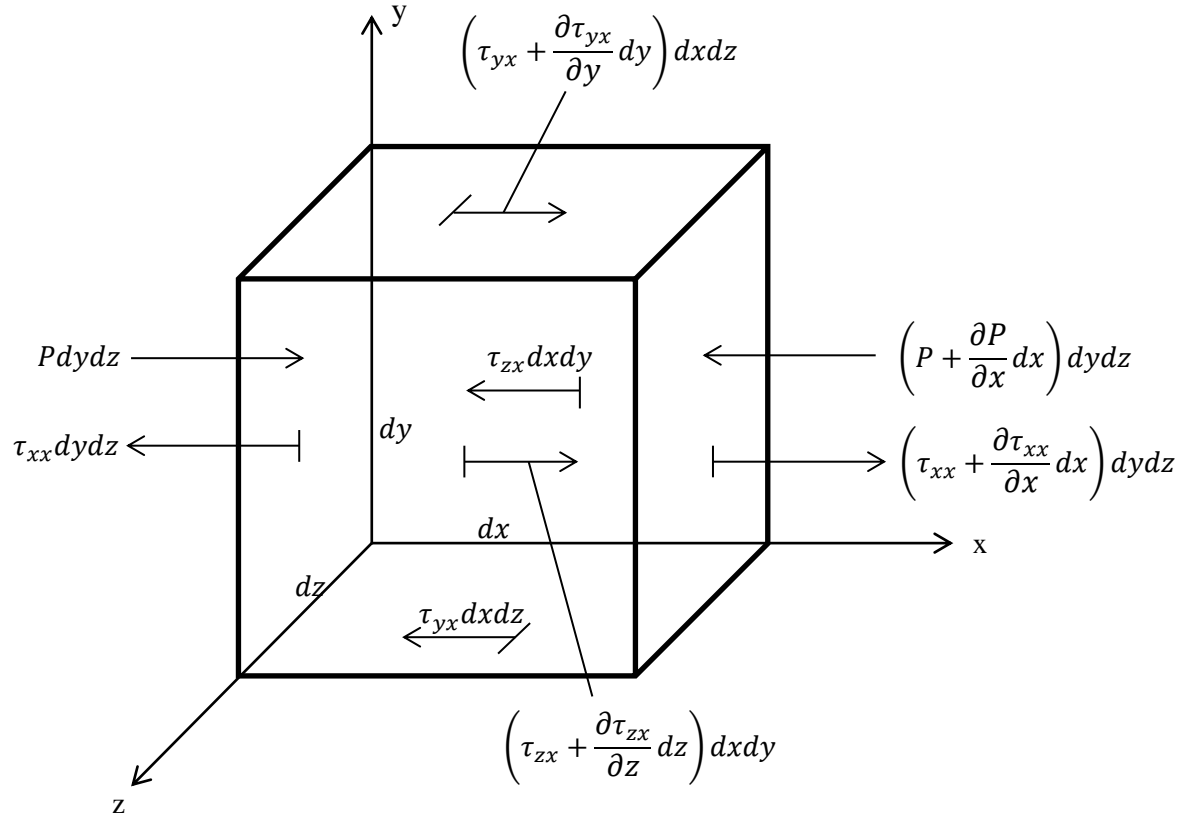


Figure 2.2 Forces to derive momentum equation in the x-direction on an infinitesimal flow element

According to Newton`s second law, the resultant force on an element can be stated as the multiplication of its mass and its acceleration. Then, the x component of the net force on an infinitesimal flow element can be expressed as:

$$\sum F_x = \delta m a_x \quad (2.19)$$

where δm is the incremental mass of the fluid element and a_x is the x component of the acceleration. The body forces and the surface forces form the total net force on a fluid element can be given as:

$$\sum F_x = \left(-\frac{\partial P}{\partial x} + \frac{\partial \tau_{xx}}{\partial x} + \frac{\partial \tau_{yx}}{\partial x} + \frac{\partial \tau_{zx}}{\partial x} \right) dx dy dz + f_x \rho dx dy dz \quad (2.20)$$

where τ_{xx} , τ_{yx} and τ_{zx} show the stress in x direction exerted on a plane perpendicular to x , y and z axis, respectively, f_x is the body force per unit mass in the x direction and P is the pressure. The mass of a fluid element can be shown as:

$$\delta m = \rho d_x d_y d_z \quad (2.21)$$

Then, Equation (2.20) becomes:

$$\delta m a_x = \left(-\frac{\partial P}{\partial x} + \frac{\partial \tau_{xx}}{\partial x} + \frac{\partial \tau_{yx}}{\partial y} + \frac{\partial \tau_{zx}}{\partial z} \right) \frac{\delta m}{\rho} + f_x \delta m \quad (2.22)$$

By replacing a_x by $\frac{Du_x}{Dt}$

$$\rho \frac{Du_x}{Dt} = \left(-\frac{\partial P}{\partial x} + \frac{\partial \tau_{xx}}{\partial x} + \frac{\partial \tau_{yx}}{\partial y} + \frac{\partial \tau_{zx}}{\partial z} \right) + f_x \rho \quad (2.23)$$

Equation (2.23) shows the x component of the momentum equation. Similarly, y and z components can be shown as:

$$\rho \frac{Du_y}{Dt} = \left(-\frac{\partial P}{\partial y} + \frac{\partial \tau_{xy}}{\partial x} + \frac{\partial \tau_{yy}}{\partial y} + \frac{\partial \tau_{zy}}{\partial z} \right) + f_y \rho \quad (2.24)$$

$$\rho \frac{Du_z}{Dt} = \left(-\frac{\partial P}{\partial z} + \frac{\partial \tau_{xz}}{\partial x} + \frac{\partial \tau_{yz}}{\partial y} + \frac{\partial \tau_{zz}}{\partial z} \right) + f_z \rho \quad (2.25)$$

For a Newtonian fluid, shear stress is proportional to time rate of strain and can be defined as:

$$\tau_{xx} = \lambda \nabla \cdot \mathbf{u} + 2\mu \frac{\partial u_x}{\partial x} \quad (2.26)$$

$$\tau_{yy} = \lambda \nabla \cdot \mathbf{u} + 2\mu \frac{\partial u_y}{\partial y} \quad (2.27)$$

$$\tau_{zz} = \lambda \nabla \cdot \mathbf{u} + 2\mu \frac{\partial u_z}{\partial z} \quad (2.28)$$

$$\tau_{xy} = \tau_{yx} = \mu \left(\frac{\partial u_y}{\partial x} + \frac{\partial u_x}{\partial y} \right) \quad (2.29)$$

$$\tau_{xz} = \tau_{zx} = \mu \left(\frac{\partial u_z}{\partial x} + \frac{\partial u_x}{\partial z} \right) \quad (2.30)$$

$$\tau_{yz} = \tau_{zy} = \mu \left(\frac{\partial u_z}{\partial y} + \frac{\partial u_y}{\partial z} \right) \quad (2.31)$$

where μ is the dynamic viscosity of fluid and Stokes theorem can be used to calculate λ :

$$\lambda = \frac{2}{3} \mu \quad (2.32)$$

By combining the shear forces into momentum equations, the final form of momentum equations in the x , y and z directions are obtained as:

$$\begin{aligned} \rho \frac{Du_x}{Dt} = & -\frac{\partial P}{\partial x} + \frac{\partial \left(\lambda \nabla \cdot \mathbf{u} + 2\mu \frac{\partial u_x}{\partial x} \right)}{\partial x} + \frac{\partial \left(\left(\frac{\partial u_y}{\partial x} + \frac{\partial u_x}{\partial y} \right) \mu \right)}{\partial y} \\ & + \frac{\partial \left(\left(\frac{\partial u_z}{\partial x} + \frac{\partial u_x}{\partial z} \right) \mu \right)}{\partial z} + f_x \rho \end{aligned} \quad (2.33)$$

$$\begin{aligned} \rho \frac{Du_y}{Dt} = & -\frac{\partial P}{\partial y} + \frac{\partial \left(\left(\frac{\partial u_y}{\partial x} + \frac{\partial u_x}{\partial y} \right) \mu \right)}{\partial x} + \frac{\partial \left(\lambda \nabla \cdot \mathbf{u} + 2\mu \frac{\partial u_y}{\partial y} \right)}{\partial y} \\ & + \frac{\partial \left(\left(\frac{\partial u_z}{\partial y} + \frac{\partial u_y}{\partial z} \right) \mu \right)}{\partial z} + f_y \rho \end{aligned} \quad (2.34)$$

$$\begin{aligned} \rho \frac{Du_z}{Dt} = & -\frac{\partial P}{\partial z} + \frac{\partial \left(\left(\frac{\partial u_z}{\partial x} + \frac{\partial u_x}{\partial z} \right) \mu \right)}{\partial x} + \frac{\partial \left(\left(\frac{\partial u_z}{\partial y} + \frac{\partial u_y}{\partial z} \right) \mu \right)}{\partial y} \\ & + \frac{\partial \left(\lambda \nabla \cdot \mathbf{u} + 2\mu \frac{\partial u_z}{\partial z} \right)}{\partial z} + f_z \rho \end{aligned} \quad (2.35)$$

By combining Equation (2.9) with Equation (2.23) and after some transformations, SPH approximation of momentum equation in α direction can be expressed as:

$$\frac{d\mathbf{u}_i^\alpha}{dt} = - \sum_{j=1}^N m_j \left(\frac{P_i}{\rho_i^2} + \frac{P_j}{\rho_j^2} \right) \frac{\partial W_{ij}}{\partial \mathbf{x}_i^\alpha} + \sum_{j=1}^N m_j \left(\frac{\tau_i^{\alpha\beta}}{\rho_i^2} + \frac{\tau_j^{\alpha\beta}}{\rho_j^2} + \pi_{ij} \right) \frac{\partial W_{ij}}{\partial \mathbf{x}_i^\alpha} \quad (2.36)$$

where the first part on the RHS is the SPH approximation of pressure and the second part shows SPH approximations of viscous force. In the equation, P_i and P_j are the pressures of the particles i and j and π_{ij} is the so-called Monaghan-type artificial viscosity which will be explained in the next sections. Gravitational acceleration, if exists, is also directly added into Equation (2.36).

In order to force the particles to move with a velocity closer to the average velocity of the neighboring particles, the XSPH technique is used (Monaghan, 1989, 1992) according to:

$$\frac{d\mathbf{x}_i}{dt} = \mathbf{u}_i - \varepsilon \sum \frac{m_j}{\bar{\rho}_{ij}} W(\mathbf{x}_i - \mathbf{x}_j, h) \mathbf{u}_{ij} \quad (2.37)$$

where ε is taken as 0.3 (Liu & Liu, 2003) and $\bar{\rho}_{ij} = 0.5(\rho_i + \rho_j)$. By using the XSPH technique, the unphysical penetration of the particles is minimized.

2.1.3 Artificial Viscosity

By remembering the Navier-Stokes equations:

$$\rho \frac{d\mathbf{u}}{dt} = -\nabla P + \mu \nabla^2 \mathbf{u} \quad (2.38)$$

where \mathbf{u} is the velocity vector and μ is the coefficient of viscosity. By rearranging this equation:

$$\frac{d\mathbf{u}}{dt} = -\frac{1}{\rho} \nabla(P - \mu \nabla \mathbf{u}) \quad (2.39)$$

According to this equation, viscosity term can be treated as an extra pressure term. The viscosity term is divided as physical and artificial viscosity. The inclusion of physical viscosity into momentum equation of SPH approximation was explained in the previous section. The artificial viscosity, π should be proportional to:

$$\pi \approx \frac{\mu}{\rho^2} \nabla \mathbf{u} \quad (2.40)$$

where the denominator ρ^2 comes from momentum equation of SPH approximation. Monaghan & Gingold (1983) derived artificial viscosity for a gas flow. The coefficient of viscosity for a gas flow can be stated as:

$$\mu \approx \rho c \lambda_g \quad (2.41)$$

where c is the speed of sound, λ_g is the free-path length of gas particles. In SPH it is logical to replace λ_g with smoothing length h . By combining equations (2.39), (2.40) and the finite difference form of the derivative of velocity with respect to time, the equation of artificial viscosity in one dimensional form is obtained:

$$\pi_{ij} = - \left(\frac{\alpha h c_i}{\rho_i} \right) \left(\frac{\mathbf{u}_i - \mathbf{u}_j}{\mathbf{x}_i - \mathbf{x}_j} \right) \quad (2.42)$$

where α is an empirical coefficient and taken in the range of 0.1-0.01 (Monaghan, 1994). The symmetric form of π_{ij} can be obtained by using the symmetrized forms of

$$\bar{c}_{ij} = 0.5(c_i + c_j) \quad (2.43)$$

$$\bar{\rho}_{ij} = 0.5(\rho_i + \rho_j) \quad (2.44)$$

and to avoid approaching $\mathbf{x}_{ij} = \mathbf{x}_i - \mathbf{x}_j$ to zero when $\mathbf{u}_{ij} = \mathbf{u}_i - \mathbf{u}_j \neq 0$, the following equation is proposed:

$$\frac{\mathbf{u}_{ij}}{\mathbf{x}_{ij}} = \frac{\mathbf{u}_{ij} \mathbf{x}_{ij}}{\mathbf{x}_{ij}^2 + 0.001 h^2} \quad (2.45)$$

Finally, the general statement of artificial viscosity becomes:

$$\pi_{ij} = - \frac{\alpha \mu_{ij} \bar{c}_{ij} + \beta \mu_{ij}^2}{\bar{\rho}_{ij}} \quad (2.46)$$

where

$$\mu_{ij} = \frac{h(\mathbf{u}_i - \mathbf{u}_j)(\mathbf{x}_i - \mathbf{x}_j)}{r_{ij}^2 + 0.001h^2} \quad (2.47)$$

When the fluid has a significant real viscosity and flow has a low Mach number, β in Equation (2.46) can be taken as zero. Monaghan (1994) used $\alpha = 0.01$ in the simulations of dam break flow and the results he obtained are in good agreement with experimental data. In the present study, α is taken as 0.01 and β is taken as zero.

Morris et al., (1997) had trouble to find accurate results in velocity profiles while simulating Couette and Poiseuille flow when Reynolds number was low. In order to overcome this problem, they proposed a hybrid expression:

$$\pi_{ij} = - \frac{\alpha(\mu_i + \mu_j)(\mathbf{x}_i - \mathbf{x}_j)}{\rho_i \rho_j (r_{ij}^2 + 0.001h^2)} \quad (2.48)$$

where linear equation is conserved exactly while angular momentum is conserved approximately. The equations of artificial viscosity proposed by Monaghan (1994) and Morris et al., (1997) are both used in the developed code. However, no significant difference was observed in the results of simulations.

2.1.4 Incompressible Flow Treatment

SPH equations were derived for astrophysical problems in which the flow is compressible. In hydrodynamic problems, water, an almost incompressible fluid, is used. In the momentum equation, the pressure terms are calculated from the equation of state in which pressure is related to particle density. If the actual equation of state is used for the simulation of incompressible flow, extremely small time steps should be used. Therefore, calculation of pressure term is a major task in SPH problems. By accepting that a theoretically incompressible fluid is practically compressible, artificial compressibility concept was born. In SPH, the real fluid is replaced by an artificial

fluid which is more compressible. Since the speed of sound is still much larger than the speed of bulk flow, this artificial fluid gives a valid approximation. Monaghan (1994) proposed to use the following equation of state to find pressures.

$$P = B \left(\left(\frac{\rho}{\rho_0} \right)^\gamma - 1 \right) \quad (2.49)$$

where γ is taken as 7 (Monaghan, 1994) and B is used to set a maximum limit to density variation. According to Morris et al., (1997) and Schlatter (1999), B can be taken as initial pressure. In artificial compressibility concept, speed of sound should be given an importance. When the real speed of sound, 1480 m/s for water under standard conditions, is used, the real fluid is approximated as artificial fluid and the density variation becomes negligible. Therefore, the sound speed should be much smaller than the actual one to make the fluid compressible, but it also should be large enough to represent the behavior of the real fluid. According to Morris et al., (1997), the following equation can be used to calculate speed of sound.

$$c^2 = \max \left(\frac{V_b^2}{\delta}, \frac{V_b \mu}{\rho \delta L}, \frac{FL}{\delta} \right) \quad (2.50)$$

where F is the magnitude of body force, L is the characteristics length scale, V_b is the fluid bulk velocity, μ is the dynamic viscosity of fluid and

$$\delta = \frac{\rho - \rho_0}{\rho_0} \quad (2.51)$$

By using the equation of state, the speed of sound at the initial density can also be calculated as (Jones & Belton, 2006)

$$c^2 = \frac{\gamma B}{\rho_0} \quad (2.52)$$

By keeping relative density fluctuations approximately 0.01, the following equation to calculate B can be used:

$$B = \frac{100 \rho_0 u_{max}^2}{\gamma} \quad (2.53)$$

where maximum velocities in each problem should be estimated. Although for a dam break problem, it may be estimated readily ($u_{max}^2 = 2gh$), it is not always possible to estimate maximum velocities.

In the present study, for the simulations of dam break flow, B was calculated from Equation (2.53). On the other hand, for the simulations of slug flow, B value was taken as initial pressure.

2.1.5 Boundary Treatment

The application of boundary conditions in SPH is challenging, because kernel function is truncated for the particles near the boundaries. This truncation prevents second order accuracy of SPH formulation. Consequently, proper boundary treatment in SPH is an ongoing subject for researchers. If boundary treatment is improper, fluid particles may leave the computational domain or errors in the solution may occur due to kernel truncation at the boundary. There are three popular types of boundary conditions: force based method, ghost particle method and combined force based and ghost particle method. In the present study, in addition to these boundary methods, a novel boundary method is proposed which will be explained in the next section.

The main idea of force based method is the creation of boundary particles which exert a repulsive force to the center of fluid particles close to them. Usually, the magnitude of the force increases while the fluid particle approaches to the boundary, so the penetration of the fluid particles to boundaries is prevented. First, Monaghan (1994) proposed to use Lennard-Jones forces as boundary conditions. For a distance between a boundary and fluid particle, r , the force exerted to fluid particles can be expressed as:

$$f(r) = \frac{D}{r} \left(\left(\frac{r_0}{r} \right)^{p_1} - \left(\frac{r_0}{r} \right)^{p_2} \right) \quad (2.54)$$

where r_0 is the initial spacing between the fluid particles. The boundary particles are positioned with half of the initial spacing to provide a solid barrier. If $r > r_0$ the force, $f(r)$ is taken as zero. In the literature, different values for the p_1 and p_2 exponents are

suggested. In this study, p_1 is taken as 12 and p_2 is taken as 6 (Monaghan, 1994). D is the problem dependent parameter and in the present study it is taken in the same scale as the square of the largest velocity (Liu & Liu, 2003).

For another force based method, Monaghan & Kos (1999) proposed to calculate forces due to boundary particle in terms of normal and tangential vectors of fluid particles. The visualization of the method is given in Figure 2.3. The force exerted from boundary particle can be stated as:

$$\mathbf{f}(\mathbf{r}) = \mathbf{n}R(x_n)P(x_t) \quad (2.55)$$

where \mathbf{n} is the normal vector to boundary particle, x_t is the tangential distance and x_n is the normal distance. $R(y)$ can be calculated as:

$$R(y) = \frac{A \left(1 - \frac{x_n}{2r_0}\right)}{\sqrt{\frac{x_n}{2r_0}}} \quad (2.56)$$

where r_0 is the initial spacing between particles. When $\frac{x_n}{2r_0} \geq 1$, $R(y)$ is zero. A can be calculated as:

$$A = \frac{1}{h} (0.01c^2 + \beta c(\mathbf{u}_b - \mathbf{u}_f) \cdot \mathbf{n}_b) \quad (2.57)$$

where β is 1 if the particle is approaching the boundary, otherwise it is zero, \mathbf{u}_b and \mathbf{u}_f are the velocity vectors of boundary particle and fluid particle, respectively and \mathbf{n}_b is the normal vector of boundary particle. The second term in the denominator helps damp-out the motion which is perpendicular to the boundary. If $r < r_0$,

$$P(x_t) = \frac{1 + \cos\left(\frac{\pi x_t}{r_0}\right)}{2} \quad (2.58)$$

else $P(x) = 0$. In this method, when the fluid particles move parallel to boundary, the boundary particles do not exert a force and the parallel motion of the particles is not disturbed.

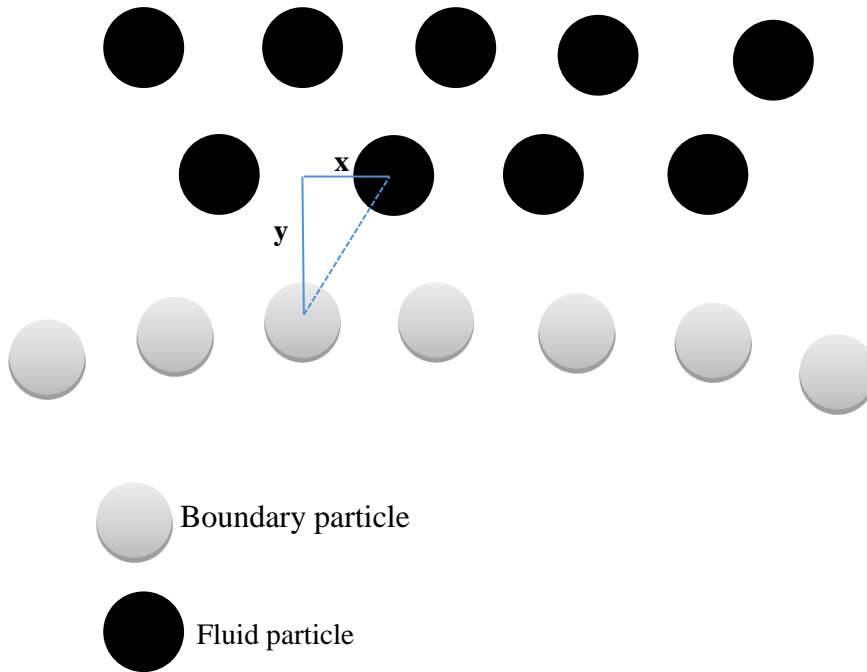


Figure 2.3 Sketch of boundary particles (Monaghan and Kos, 1999)

Monaghan (2005) modified the studies of Monaghan and Kos (1999) by changing the calculations of $R(x_n)$ and $P(x_t)$ as:

$$R(x_n) = \nabla W\left(\frac{x_n}{2r_0}\right) 0.01c^2 \quad (2.59)$$

$$P(x_t) = 1 - \frac{x_t}{r_0} \quad (2.60)$$

where $0 < x_t < r_0$, otherwise $P(x)$ is zero and c is the speed of sound.

No-slip condition may be necessary in the problems. No-slip condition is implemented by including the boundary particles in the calculation of viscous terms in the momentum equation in all the force methods. The main advantage of force methods is the easiness of the implementation of boundaries. Especially for the problems with complex boundaries, the force methods are more preferable.

In ghost particles method, when the distance between a fluid particle and the boundary is smaller than the smoothing length, a ghost particle of that fluid particle is created outside of the boundary by taking a mirror image of the fluid particle. Due to mirror image, the ghost particle moves in the opposite direction of the fluid particle. Since both particles have exact same velocities, penetration is prevented. In another and more popular approach, ghost particles are created during the particle generation. In this approach, i.e., single boundary tangent technique, the velocity of the ghost particle is calculated as:

$$\mathbf{u}_g = -\frac{x_{ng}}{x_{nf}}\mathbf{u}_f \quad (2.61)$$

where \mathbf{u}_g and \mathbf{u}_f are the velocity vectors of ghost and fluid particles, respectively, x_{ng} and x_{nf} are the normal distance from the boundary tangent of ghost and fluid particles, respectively. A schematic representation is given in Figure 2.4.

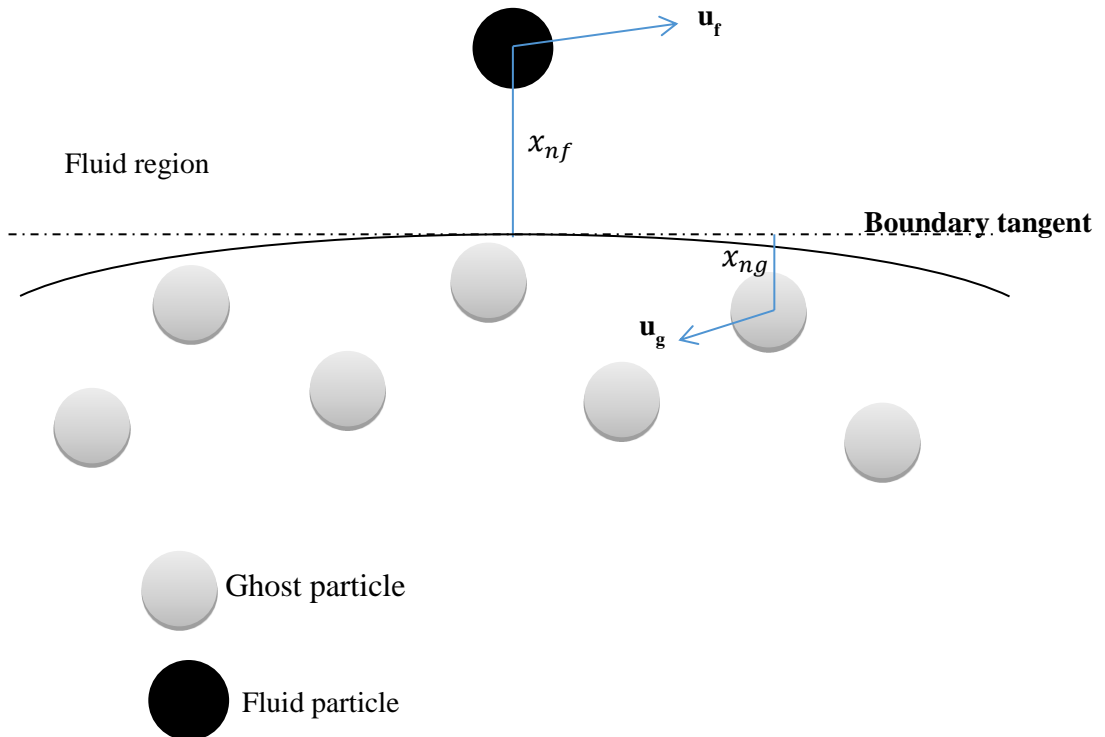


Figure 2.4 Ghost particle technique (single boundary tangent treatment)

In this method, particles are generated based on the distance and angle, so the implementation is a bit complicated. Yildiz, Rook, and Suleman (2009) proposed a modified version of this method, multiple boundary tangent method. In this method, tangent lines are computed at each time step. The handling of the curved boundary surfaces is the main advantage of this method over single boundary tangent treatment. Ghost particle method is more preferable when the pressures between the solid boundary and the fluid region are of interest (Colagrossi & Landrini, 2003).

Dalrymple and Knio (2001) proposed dynamic boundary particles technique which is a combined method of boundary force and ghost particles method. In this method, the boundary particles and ghost particles are generated at the beginning of the computation. The main difference of this technique from ghost particle method is that in this method, the positions of ghost particles are fixed. Therefore, new ghost particles are not created during the computation and the evaluation of the distance between the fluid particle and the boundary particle is not necessary, since no repulsive force is exerted to the fluid particles. Thus, the method is computationally less expensive. However, if fluid particles are approaching to the boundary with high velocities, they may penetrate the solid surface.

Ferrari, Dumbser, Toro, and Armanini (2009) used the combination of boundary force and ghost particles in their study. In the method, the boundary particles are placed to the solid interfaces but no force is exerted from boundary particles to fluid particles. The boundary particles set for each fluid particle a fictitious fluid point via local point-symmetry. These boundary interactions are added to momentum equation. Spurious pressure oscillations at the wall are not observed in this method. This method is computationally more expensive.

In the present study, Lennard-Jones forces and Lagrange multipliers boundary method, which will be explained in the next section, are used to represent the boundary conditions.

2.1.6 Lagrange Multipliers for SPH boundaries

In the present study, Lagrange multipliers boundary model is implemented to SPH for the first time in literature to the best knowledge of the author. Lagrange multipliers are mostly used to constraint the structures. The method is capable of relating nodal displacements defined on structure like $d_1 + 2d_2 = 0$, where d_1 and d_2 are nodal displacements. These type of functions are named as multi-freedom constraints (MFCs). A set of k MFCs can be written as $\mathbf{C}\mathbf{d} = \mathbf{b}$; where \mathbf{C} is a $k \times l$ matrix, l is number of degrees of freedoms. It is known that potential energy of the unconstrained finite element model is $\pi = \frac{1}{2}\mathbf{d}^T \mathbf{K}\mathbf{d} - \mathbf{d}^T \mathbf{R}$, where \mathbf{K} is the stiffness matrix and \mathbf{R} is the residual force. New potential can be calculated by imposing MFCs as $\pi_{new} = \pi + \boldsymbol{\lambda}(\mathbf{C}\mathbf{d} - \mathbf{b})$ where $\boldsymbol{\lambda}$ is a vector for corresponding forces. Writing it in incremental form Equation (2.62) is achieved.

$$\delta \mathbf{d}^T \mathbf{K}\mathbf{d} - \delta \mathbf{d}^T \mathbf{R} + \delta \boldsymbol{\lambda}(\mathbf{C}\mathbf{d} - \mathbf{b}) = 0 \quad (2.62)$$

In matrix form;

$$\begin{bmatrix} \mathbf{K} & \mathbf{C} \\ \mathbf{C}^T & \mathbf{0} \end{bmatrix} \begin{bmatrix} \mathbf{d} \\ \boldsymbol{\lambda} \end{bmatrix} = \begin{bmatrix} \mathbf{R} \\ \mathbf{b} \end{bmatrix} \quad (2.63)$$

In the present numerical model, boundary is assumed as fully constraint. Thus, \mathbf{K} term drops or becomes as an identity matrix. Instead, SPH mass matrix should be added. Finally, after transformations, set of equations in matrix form becomes;

$$\begin{bmatrix} \mathbf{M} & \mathbf{0} \\ \mathbf{0} & \mathbf{0} \end{bmatrix} \begin{bmatrix} \mathbf{a} \\ \mathbf{0} \end{bmatrix} + \begin{bmatrix} \mathbf{0} & \mathbf{C} \\ \mathbf{C}^T & \mathbf{0} \end{bmatrix} \begin{bmatrix} \mathbf{d} \\ \boldsymbol{\lambda} \end{bmatrix} = \begin{bmatrix} \mathbf{0} \\ \Delta \end{bmatrix} \quad (2.64)$$

where, Δ is overlap of water particles shown in Figure 2.5, \mathbf{a} is the acceleration vector and $\boldsymbol{\lambda}$ is force vector to push SPH particles out of the boundary which is shown in Figure 2.6.

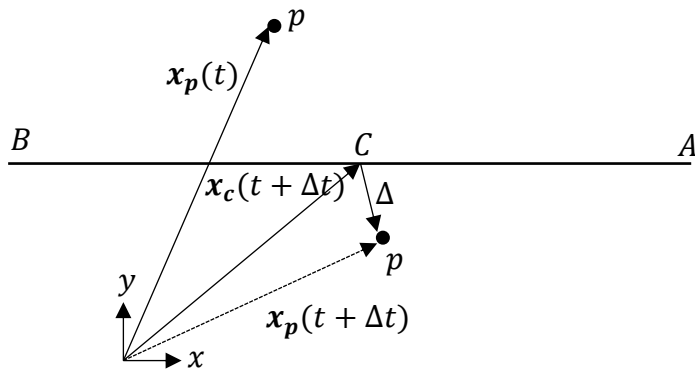


Figure 2.5 Geometry of Contact

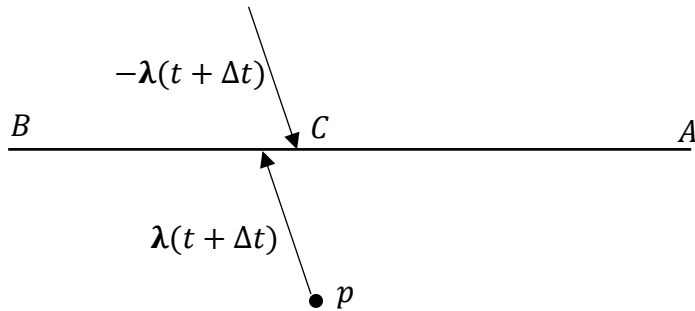


Figure 2.6 Contact Force

Considering MFC for a water particle invading the boundary, \mathbf{C} matrix becomes -1 for one water particle. In order to solve the Equation 2.64, \mathbf{a} should be written in terms of \mathbf{d} . Relation is set by following time integration scheme as seen in Figure 2.7 where \mathbf{u} is taken as the velocity vector.

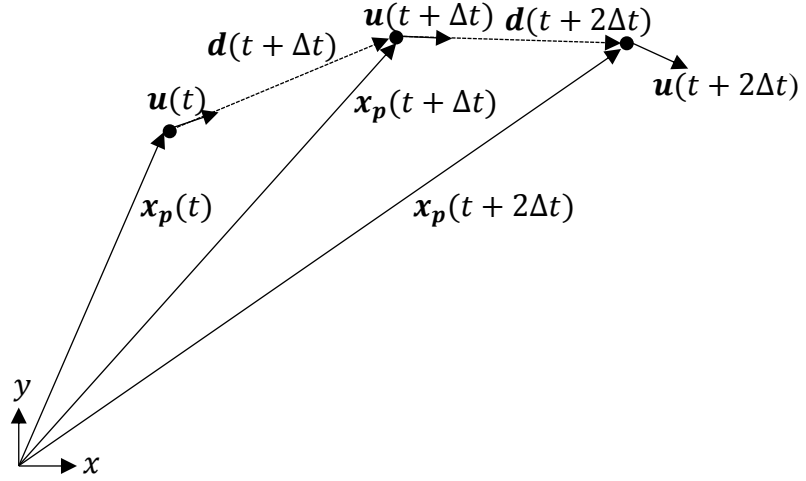


Figure 2.7 Particle Motion

Acceleration between t and $t + 2\Delta t$ is defined constant:

$$\mathbf{a} = \frac{\mathbf{u}(t + 2\Delta t) - \mathbf{u}(t)}{\Delta t} \quad (2.65)$$

Average velocity between t and $t + 2\Delta t$ is defined as,

$$\bar{\mathbf{u}} = \frac{\mathbf{u}(t + 2\Delta t) + \mathbf{u}(t)}{2} \quad (2.66)$$

$$\bar{\mathbf{u}} = \frac{\Delta \mathbf{d}}{\Delta t} = \frac{\mathbf{d}(t + 2\Delta t) + \mathbf{d}(t + \Delta t)}{\Delta t} \quad (2.67)$$

Substituting Equation (2.66) into (2.67) velocity of particle at time $t + 2\Delta t$,

$$\mathbf{u}(t + 2\Delta t) = \frac{2\Delta \mathbf{d}}{\Delta t} - \mathbf{u}(t) \quad (2.68)$$

Substituting Equation (2.68) into (2.65):

$$\mathbf{a} = \frac{\left(\frac{2\Delta \mathbf{d}}{\Delta t} - \mathbf{u}(t)\right) - \mathbf{u}(t)}{\Delta t} = \frac{2\Delta \mathbf{d} - 2\Delta t \mathbf{u}(t)}{\Delta t^2} \quad (2.69)$$

From SPH calculations, it is known that

$$\mathbf{u}(t) = \frac{\mathbf{d}(t + \Delta t)}{\Delta t} \quad (2.70)$$

Substituting Equations (2.67) and (2.70) into (2.69)

$$\mathbf{a} = \frac{2\mathbf{d}(t + 2\Delta t)}{\Delta t^2} \quad (2.71)$$

Substituting Equation (2.71) into (2.64).

$$\begin{bmatrix} \frac{2}{\Delta t^2}m\mathbf{I} & -\mathbf{I} \\ -\mathbf{I} & \mathbf{0} \end{bmatrix} \begin{bmatrix} \mathbf{d} \\ \lambda \end{bmatrix} = \begin{bmatrix} \mathbf{0} \\ \Delta \end{bmatrix} \quad (2.72)$$

Where m is mass of a water particle, \mathbf{I} is an identity $n \times n$ matrix, n is the number of particle.

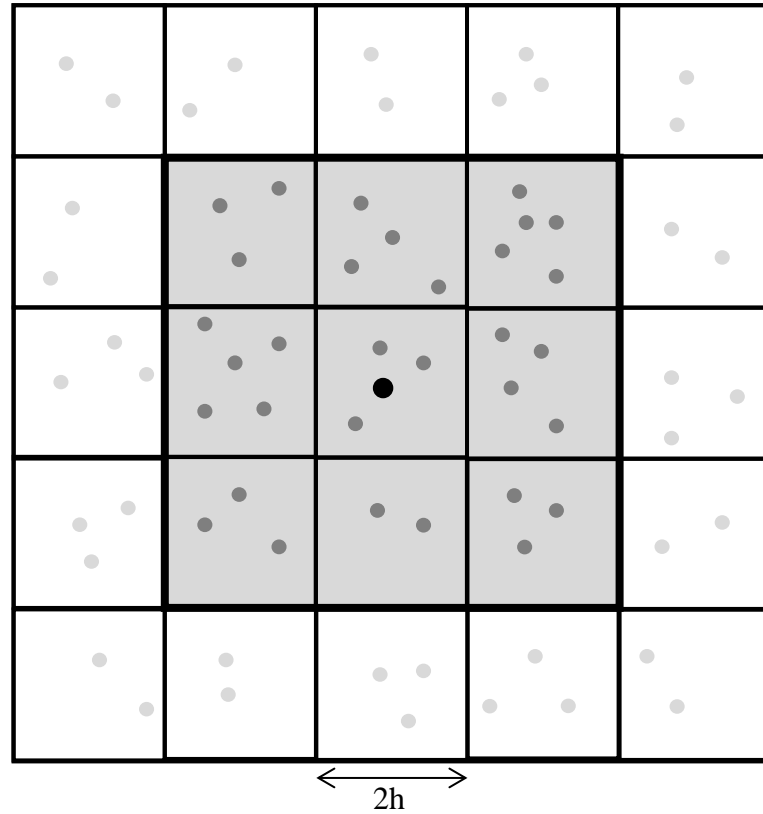
Solving Equation 2.72 for all water particles invading the solid domain will give displacements for each particle. Updated positions, velocities and accelerations are determined from Newmark Method by calculated displacement.

2.1.7 Neighboring Particle Search Algorithm

When the domain of the problem is large, SPH is very demanding in terms of computation time. Due to the characteristics of SPH, numerical integration of the governing equations is carried out for a finite number of particles which previously defined in the kernel function located in a radius called as smoothing length or radius of kernel of the interested particle. These particles are called as nearest neighboring particles (NNPs). The locations of all the particles change during simulation. NNPs should be defined in every time step. All pair search, linked-list search, tree-search (Liu & Liu, 2003), Verlet List (Viccione, Bovolín, & Carratelli, 2008), Bucket algorithm (Liu & Tu, 2002) are some popular methods to find NNPs. In the code, linked-list search algorithm is used.

All-pair search algorithm is the simplest way to define NNPs. In this algorithm, all the particles in the computation domain are checked whether they are a neighbor of the particle of interest. First, the distance of a particle to the particle of interest, r_{ij} , is defined. If this distance is less than the dimension of the support domain of the particle of interest, this particle is taken as a neighbor. For all the particles, the calculations are performed. The complexity of this algorithm is $O(N^2)$ where N is the number of particles (Liu & Liu, 2003). This means N^2 of computations should be performed. Although the application of all-pair search algorithm is simple, the computation time is clearly high. This method is preferred only for very small scale problems.

If the cells are used as bookkeeping devices, the computational time can be remarkably lowered (Monaghan & Gingold, 1983). In linked-list search algorithm, all the particles are initially assigned to cells. In order to explain the algorithm better Figure 2.8 is shown. As can be seen in the figure, the computational domain is divided into square cells with a side of $2h$ (or Kh where K can be taken as any number) (Monaghan & Lattanzio, 1985). In this method, NNPs can only be in the same grid or the immediately adjoining grids. Therefore, the search is done only for 9 grid cells for a two dimensional problem. In this way, the number of computations performed is decreased to N . When variable smoothing length is used, mesh size may not be optimal for every particle for linked-list search algorithm. In this case tree search algorithm may be used. In that case the complexity is $O(N \log N)$ (Hernquist & Katz, 1989). Since in the present study, linked-list search algorithm is used, a detailed description of other algorithms is not given here. In the studies of Monaghan (1985) and Hockney and Eastwood (1988) more detailed information about linked-list algorithm can be found.



- Particle of interest
- Nearest neighboring particle
- Particle not included in the computations for a given particle

Figure 2.8 Linked-list algorithm for searching the nearest neighboring particles in 2D

2.1.8 Time Integration and Time Stepping

Discrete SPH equations can be integrated with ordinary methods such as Runge-Kutta-Fehlberg method or Leapfrog integrator. In the code, the leapfrog integrator, a second order integrator, is used. The velocity and the position of a particle are updated half a time step by using the values of the velocity and position evaluated at the previous half time step. The equations to update position and velocity in leapfrog algorithm can be stated as:

$$\mathbf{x}(t + \Delta t) = \mathbf{x}(t) + \mathbf{u}\left(t + \frac{1}{2}\Delta t\right)\Delta t \quad (2.73)$$

$$\mathbf{u}\left(t + \frac{1}{2}\Delta t\right) = \mathbf{u}\left(t - \frac{1}{2}\Delta t\right) + \mathbf{a}(t)\Delta t \quad (2.74)$$

where $\mathbf{x}(t)$, $\mathbf{u}(t)$ and $\mathbf{a}(t)$ are the position, velocity and the acceleration vectors at time t and Δt is the time step, respectively. In the equations it is clearly seen that the integrator should be time-reversible. Another form of leap frog integrator which gives velocity at integer steps can also be seen below.

$$\mathbf{x}(t + \Delta t) = \mathbf{x}(t) + \left(\mathbf{u}(t) + \frac{\Delta t}{2}\mathbf{a}(t)\right)\Delta t \quad (2.75)$$

$$\mathbf{u}(t + \Delta t) = \mathbf{u}(t) + (\mathbf{a}(t) + \mathbf{a}(t + \Delta t))\frac{\Delta t}{2} \quad (2.76)$$

$$\mathbf{u}\left(t + \frac{1}{2}\Delta t\right) = \mathbf{u}(t) + \mathbf{a}(t)\frac{\Delta t}{2} \quad (2.77)$$

In the equation (2.76), it is clearly seen that in order to calculate $\mathbf{u}(t + \Delta t)$, the acceleration $\mathbf{a}(t + \Delta t)$ should be known and the scheme becomes implicit. However, in SPH simulations, the RHS of momentum equation i.e. the pressure force and the viscous force depend on the local velocity. Therefore, modifications should be done to adapt the integrator to SPH equations. Springel, White, and Hernquist (2001) and Nelson, Wetzstein, and Naab (2009) proposed the following modifications. First, the positions at time $\left(t + \frac{1}{2}\Delta t\right)$ is predicted as:

$$\mathbf{x}\left(t + \frac{1}{2}\Delta t\right) = \mathbf{x}(t) + \mathbf{u}(t)\frac{\Delta t}{2} \quad (2.78)$$

Then, the velocity at time $\left(t + \frac{1}{2}\Delta t\right)$ is obtained from equation (2.77) and density and other parameters are also calculated at the half time step. By knowing all the parameters, the acceleration at the half time step $\mathbf{a}\left(t + \frac{1}{2}\Delta t\right)$ can be calculated. Later, the velocity at time $(t + \Delta t)$ is calculated from,

$$\mathbf{u}(t + \Delta t) = \mathbf{u}(t) + \mathbf{a} \left(t + \frac{1}{2} \Delta t \right) \Delta t \quad (2.79)$$

and the positions can be updated by using,

$$\mathbf{x}(t + \Delta t) = \mathbf{x}(t) + (\mathbf{u}(t) + \mathbf{u}(t + \Delta t)) \frac{\Delta t}{2} \quad (2.80)$$

The modified method is also time-reversible. The main advantage of leap-frog method is the low memory storage requirement of the method. The method is also efficient for one force evaluation per step (Liu & Liu, 2003).

In order to satisfy the numerical stability, it is crucial to select correct time step value. The most popular time step criterion is Courant-Friedrichs-Lewy or CFL condition given by:

$$\Delta t_{CFL} \leq \frac{\Delta x}{c} \quad (2.81)$$

where Δx is the characteristic length scale and c is the characteristic speed (Anderson, 1995). In SPH equations, Δx can be expressed as the smoothing length, h , and speed of sound, c , is the characteristic speed. Then CFL condition in SPH equation for a particle i can be stated as:

$$\Delta t_{CFL} \leq \frac{h_i}{c} \quad (2.82)$$

If the viscous dissipation and the external force is taken into consideration, Monaghan (1989, 1992) proposed the following equations.

$$\Delta t_{CFL} \leq \frac{h_i}{c_i + (\alpha_\pi c_i + \beta_\pi \max(\phi_{ij}))} \quad (2.83)$$

$$\Delta t_{ext} \leq \left(\frac{h_i}{a_i} \right)^{\frac{1}{2}} \quad (2.84)$$

where α and β terms are used to determine the strength of artificial viscosity explained at previous sections. It should be noted that Equation (2.83) is obtained by adding the viscous term to Equation (2.82). The time step is then calculated by:

$$\Delta t = \min(0.4\Delta t_{CFL}, 0.6\Delta t_{ext}) \quad (2.85)$$

Morris et al. (1997) proposed another criterion to calculate time step by considering the viscous diffusion.

$$\Delta t = 0.125 \frac{h^2 \rho}{\mu} \quad (2.86)$$

2.2 RANS and LES equations

For a Newtonian fluid, the RANS equations in Einstein notation are:

$$\frac{\partial \rho}{\partial t} + \frac{\partial (\overline{u^\alpha \rho})}{\partial x^\alpha} = 0 \quad (2.87)$$

$$\begin{aligned} \frac{\partial (\rho_i \overline{u^\alpha})}{\partial t} + \frac{\partial (\overline{\rho u^{\alpha'} u^{\beta'}})}{\partial x^\beta} \\ = -\frac{\partial \overline{P}}{\partial x^\alpha} + \frac{\partial}{\partial x^\beta} \left[\mu \left(\frac{\partial \overline{u^\alpha}}{\partial x^\beta} + \frac{\partial \overline{u^\beta}}{\partial x^\alpha} - \frac{2}{3} \delta_{ij} \frac{\partial \overline{u^\alpha}}{\partial x^\beta} \right) \right] \\ + g_i + \frac{\partial (\overline{-\rho u^{\alpha'} u^{\beta'}})}{\partial x^\beta} \end{aligned} \quad (2.88)$$

where x^α and x^β are the Cartesian coordinate components, ρ is the density of the fluid, \mathbf{u} is Reynolds' mean velocity vector, u^α and u^β are the components of Reynolds' mean velocity vector in α and β directions, μ is the dynamic viscosity, P is the pressure, g is the gravitational acceleration and the Reynolds stress $\overline{-\rho u^{\alpha'} u^{\beta'}}$ represents the effects of turbulence. In order to determine the turbulent viscosity, a standard k- ϵ turbulence closure model can be used and the Reynolds stress is expressed as (Launder & Spalding, 1974):

$$-\overline{\rho u^{\alpha'} u^{\beta'}} = 2\rho v_t \frac{1}{2} \left(\frac{\partial \overline{u^\alpha}}{\partial x^\beta} + \frac{\partial \overline{u^\beta}}{\partial x^\alpha} \right) - \frac{2}{3} \rho k \delta^{\alpha\beta} \quad (2.89)$$

where $u^{\alpha'}$ and $u^{\beta'}$ are the fluctuating velocity components, v_t is the eddy viscosity and $v_t = C_\mu k/\epsilon$ and C_μ is taken as 0.09 for the standard k- ϵ turbulence closure model (Zhang, Nakagawa, Kawaike, & Baba, 2009) and $\delta^{\alpha\beta}$ is the Kronecker delta:

$$\delta^{\alpha\beta} = \begin{cases} 1 & \text{if } \alpha = \beta \\ 0 & \text{if } \alpha \neq \beta \end{cases} \quad (2.90)$$

For the turbulent kinetic energy and dissipation in k- ϵ turbulence model, the RANS equations are given below, respectively (Wilcox, 1998).

$$\frac{\partial(\rho k)}{\partial t} + \frac{\partial(\rho k \overline{u^\beta})}{\partial x^\beta} = P_k + P_b - \rho\epsilon - Y_M + S_k + \frac{\partial}{\partial x^\beta} \left[\left(\mu + \frac{\mu_t}{\sigma_k} \right) \frac{\partial k}{\partial x^\beta} \right] \quad (2.91)$$

$$\begin{aligned} \frac{\partial(\rho\epsilon)}{\partial t} + \frac{\partial(\rho\epsilon \overline{u^\beta})}{\partial x^\beta} \\ = C_{1\epsilon} \frac{\epsilon}{k} (P_k + C_{3\epsilon} P_b) - C_{2\epsilon} \rho \frac{\epsilon^2}{k} + S_\epsilon + \frac{\partial}{\partial x^\beta} \left[\left(\mu + \frac{\mu_t}{\sigma_\epsilon} \right) \frac{\partial \epsilon}{\partial x^\beta} \right] \end{aligned} \quad (2.92)$$

where μ_t is the turbulent viscosity, defined by:

$$\mu_t = \rho C_\mu \frac{k^2}{\epsilon} \quad (2.93)$$

and

$$P_k = -\overline{\rho u^{\alpha'} u^{\beta'}} \frac{\partial u^\beta}{\partial x^\alpha} \quad (2.94)$$

P_b is the buoyancy term, calculated by,

$$P_b = \varphi g_i \frac{\mu_t}{\rho r_t} \frac{\partial T}{\partial x^\alpha} \quad (2.95)$$

where Pr_t is the turbulent Prandtl number and taken as 0.85 and φ is the coefficient of thermal expansion. In the numerical model, $C_{1\epsilon} = 1.44$, $C_{2\epsilon} = 1.92$, $C_\mu = 0.09$,

$\sigma_k = 1.0$ and $\sigma_\epsilon = 1.3$ (Wilcox, 1998). It should be noted that RANS equations with k - ϵ turbulence closure models are simply referred as RANS equations or just RANS throughout the text.

If a filtering operation is denoted by tilde, the LES equations obtained by filtering the Navier-Stokes equations for two dimensional flows are given below.

$$\frac{\partial \tilde{\rho}}{\partial t} + \frac{\partial(\tilde{u}^\alpha \tilde{\rho})}{\partial x^\alpha} = 0 \quad (2.96)$$

$$\frac{\partial(\tilde{\rho} \tilde{u}^\alpha)}{\partial t} + \frac{\partial(\tilde{\rho} \tilde{u}^\alpha \tilde{u}^\beta)}{\partial x^\beta} = -\frac{\partial \tilde{P}}{\partial x^\alpha} + \mu \tilde{\rho} \frac{\partial^2 \tilde{u}^\alpha}{\partial x^\beta \partial x^\beta} - \frac{\partial(\overline{\tilde{\rho} \tilde{u}^\alpha \tilde{u}^\beta} - \tilde{\rho} \tilde{u}^\alpha \tilde{u}^\beta)}{\partial x^\beta} \quad (2.97)$$

where filtering operator is denoted by a tilde. In Equation (2.97), the third term in the Right Hand Side represents the effect of small scales and should be modeled. The detailed explanation about this subject can be found in the studies of (Piomelli, 1999).

2.3 VOF Equations

The volume of fluid (VOF) method is used to track the interfaces between immiscible fluids in which a transport equation is used to determine the relative volume fraction of the phases for two components fluids in each computational cell. Physical properties are calculated as weighted averages based on this fraction F which satisfies (Hirt & Nichols, 1981)

$$\frac{\partial F}{\partial t} + u^\alpha \frac{\partial F}{\partial x^\alpha} + u^\beta \frac{\partial F}{\partial x^\beta} = 0 \quad (2.98)$$

where u^α and u^β are the velocity components in α and β directions, respectively. The volume fraction can have any value between 0 and 1.

For the simulations of the mesh-based numerical methods, the OpenFOAM CFD library, has been used. The OpenFOAM library is a free, open-source library for continuum mechanics developed by OpenCFD Ltd. which has pre-configured solvers specially developed for fluid mechanics (Weller, Tabor, Jasak, & Fureby, 1998). In this study the “interFoam” solver is used for the numerical calculations. This solver

specializes for free-surface modelling and uses the VOF method for calculating interfacial flows in combination with the PISO algorithm for solving the Navier-Stokes equations.

2.4 The Implementation of SPH Formulations into Computer Code

The implementation of meshless methods are in general harder than the implementation of mesh-based methods since pre-defined grids make the establishment of discrete system equations easier (Liu & Liu, 2003). In this part, the main features of the developed SPH code are given.

The code is implemented in two-dimensional space. In the code, there are 11 subroutines and a main SPH processor. Below the features of the subroutines and SPH processor are explained:

- The initialization module is mainly used to create the particles according to the problem geometry. Initial positions and velocities of the particles are defined in this module. In addition, the boundaries are also defined by using virtual particles. Therefore, the number of virtual particles and their coordinates are defined. The type of boundary particles used for the calculations should be stated in this part. While Monaghan type of boundary particles do not evolve with time, the velocities and the positions of the ghost particles may change with time. The initial pressures (hydrostatic pressure in open channel flows and predefined pressures which were calculated from MATLAB code in closed conduit flows) should also be defined. This module includes 3 subroutines.
- The particle search module is responsible to find the interaction pairs between the particles. Linked-list search algorithm is used. For this module, 2 subroutines are used. In the first subroutine, grids in which the particles lie are created and in the second subroutine interaction pairs are determined.
- The kernel subroutine is responsible to calculate the smoothing function and its derivatives. Different kernels are defined in this subroutine, but only one kernel function should be chosen according to the problem.

- The density module is used to update density according to the formulas defined previously.
- In the force module, internal and external forces are calculated. Artificial viscosity is also included in this module because it acts as an internal force. Pressure gradients and viscous forces which are the right hand side of the Navier-Stokes equations are treated as internal forces. The pressures of the particles are calculated through an equation of state. External forces such as gravity are included in this module. The forces arising from the interaction of the fluid particles with the boundary particles and anti-penetration forces are treated as external forces.
- In the average velocity (XSPH) module, the average velocities are calculated to prevent penetration.
- The time integration module is responsible to update the momentum and the density. The positions and the velocities of the particles evolve here. The calculated forces are transformed to the accelerations and by integrating the accelerations, the velocities and the positions of the particles for the next time step is determined.
- In the output module, positions and velocities of the particles are saved at every time step. In addition, the number of time steps and the elapsed CPU time are also saved.

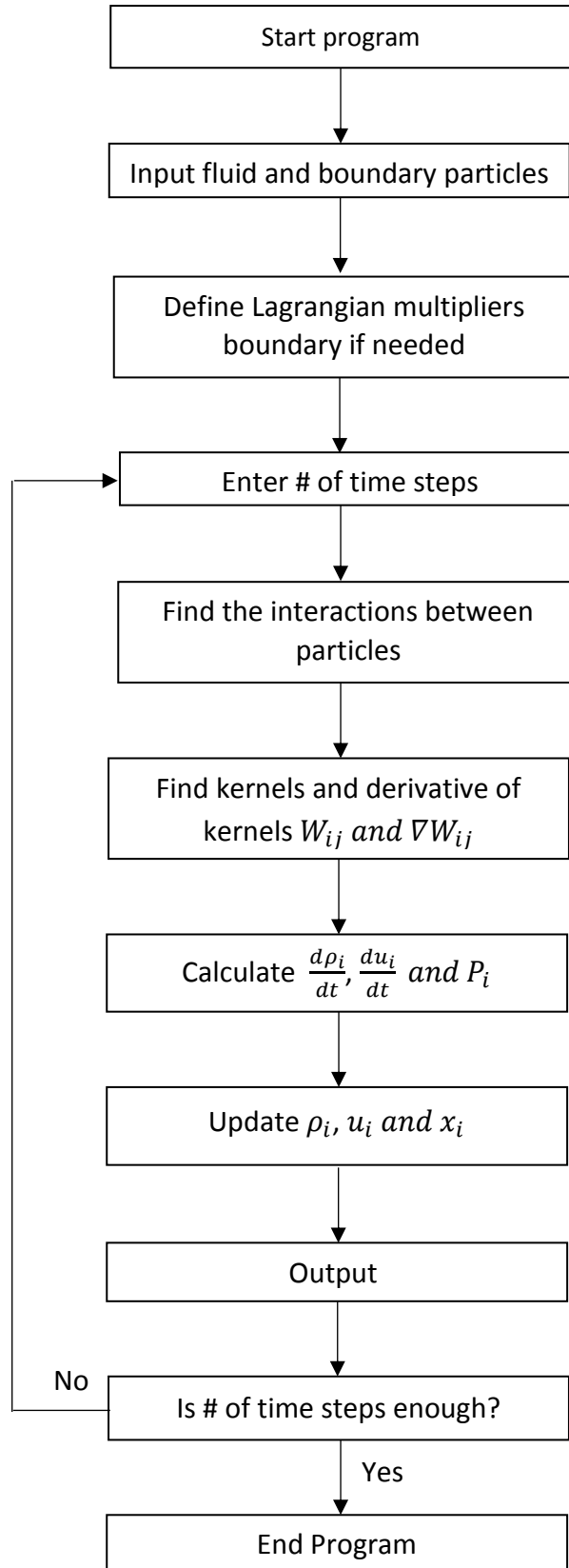


Figure 2.9 Flow chart of SPH code

CHAPTER 3

APPLICATION OF SPH ON FREE SURFACE FLOWS

In this part, idealized, two dimensional dam break problems are investigated numerically. The results of three recently published experimental studies are used to validate the numerical solutions. Among the numerical simulations, SPH method with the novel boundary model described in the previous chapter is used. On the other hand, for the mesh-based approach large eddy simulation (LES), k- ϵ turbulence models, a mesh-based laminar and Eulerian models are employed. Turbulence models are used since, downstream of the dam, turbulence may be deemed to be effective. Both free-surfaces, velocity profiles and pressures are numerically simulated. In literature, the numerical modelling of velocity profiles with SPH method in dam-break induced flows is relatively rare. The general trend of the free-surface profile and the velocity profiles of the simulation results of the SPH method are pretty close with the results of the experiments. Turbulence modelling does not improve the results significantly. It is seen that the SPH method as a mesh-free method and laminar, k- ϵ turbulence and LES models along with VOF tracking as mesh-based methods can be used for the prediction of dam break flows. However, the inclination angle of the channel may somewhat adversely affect the accuracy of k- ϵ turbulence model. In addition, the computational time of SPH decreases with the proposed boundary model. Proposed boundary model is promising for fluid-structure interaction problems with SPH.

3.1 Introduction to Dam Break Problem

The dam break problem is a very important research subject. Due to earthquakes, structural deficiencies, faulty design or maintenance problems, dams may get damaged or even entirely collapse (Bell, Elliot, & Chaudry, 1992). The correct numerical

prediction of the depth and the velocity of the wave front after a dam break are very important in order to make useful emergency plans. The studies on this subject started in the 19th century. To model a sudden dam break, Ritter (1892) developed an analytical solution which calculates the free surface profile for an instantaneous dam break problem with a frictionless, horizontal channel. The turbulence effects were not taken into consideration and the length of the reservoir and of the channel was assumed infinite. Dressler (1952) included the frictional losses between the water and the bed and expressions for the height and the velocity of the wave front were obtained. The results of Dressler and Ritter were verified by various researchers (Pohle, 1950; Whitham, 1955). Martin and Moyce (1952) made experiments for a dry bed channel and found that the wave front velocity is proportional to the square root of the initial water column height. Stoker (1957) improved the analytical studies of Ritter for a wet bed channel. For a dam-break problem, Stansby, Chegini, and Barnes (1998) made experiments in order to investigate the dry and wet bed channel situations. For a wet bed channel, immediately after a dam break, a water jet similar to a mushroom was observed. Aleixo, Soares-Frazão, and Zech (2011) studied the water surface profiles by using particle tracking velocimetry for a two dimensional dam-break problem. The experimental studies for a dam-break problem were usually made in order to investigate the water surface profile (Aziz, 2000; Miller & Chaudhry, 1989; Ozmen-Cagatay & Kocaman, 2010). Although there are lots of experimental studies for a dam break problem, there are few numerical studies which investigate the dynamics of the wave front after a sudden dam break (Lobovský, Botia-Vera, Castellana, Mas-Soler, & Souto-Iglesias, 2014). In order to model a dam break problem numerically, usually Navier-Stokes equations should be solved. Solving the full Navier-Stokes equations is computationally expensive. Therefore, by neglecting the vertical accelerations and solving 1D and 2D depth-averaged mass and momentum conservation equations, Saint-Venant or shallow water equations (SWE) are obtained. Previous researchers solved the shallow water equations by using the method of characteristics, finite element methods and derived numerical models (Elliot & Chaudhry, 1992; Fennema & Chaudhry, 1990). However, some observed hydraulic aspects may not be captured with models based on SWE (LaRocque, Imran, & Chaudhry, 2013b).

Since the dam-break problem involves highly transient gravity dominated flows the role of turbulence becomes secondary, especially in the upstream reservoir where the potential flow theory can be used to describe the flow. Unlike the conditions in the upstream, the downstream part is highly turbulent, (LaRocque, Imran, & Chaudhry, 2013a). In general, there are two mostly used turbulence models, Reynolds-Averaged Navier-Stokes (RANS) and large eddy simulation (LES). In RANS models, a variable such as velocity is decomposed into its fluctuating and Reynolds-averaged components. In the LES approach, large eddies are computed directly and only small-scale motions are modelled separately, (Zhiyin, 2015). Therefore, the range of length scales decreases. Since smaller mesh sizes must be used in LES models, the computational time is higher.

Previous researchers mainly focused on the free surface profiles while simulating dam-break flow with SPH because of the transient character of the method (Crespo et al., 2008; Lee et al., 2008). In this study, in addition to free surface profiles, velocity profiles and pressures are also determined by using SPH. Turbulence effects are not included in the developed SPH code.

In this part, three recently published experiments available in the literature are numerically simulated; Ozmen-Cagatay and Kocaman (2010), LaRocque et al. (2013a) and Lobošský et al. (2014). At first, without turbulence model, the free surface profiles and the velocity profiles of mesh-based and mesh-free methods are compared. For the mesh free-method SPH code with the proposed novel boundary condition is used. Then, the simulations are done with LES and RANS turbulence approaches. According to LaRocque et al. (2013a), RANS models using a $k-\epsilon$ model may not be suitable for dam-break problems. This statement is investigated. At the end, the improvements and limitations of proposed boundary method, the advantages of mesh-free and mesh-based methods and the effect of turbulence models for dam-break problems are presented. In the following parts, first the experimental and the numerical setups are provided in detail. Then, the comparison of the measurements and the results of the simulations are presented with concluding remarks.

3.2 Description of Models used in Experimental Studies

The experiments of Ozmen-Cagatay and Kocaman (2010) were conducted in a rectangular channel of 9 m long, 0.30 m wide and 0.34 m deep and the experimental setup is given in Figure 3.1. The plate representing the dam was located 4.65 m downstream of the reservoir entrance and the plate was removed instantaneously (0.06 s – 0.08 s) by using a mechanism. In the experiments, the initial reservoir head was taken as $h_0 = 0.25$ m and the bed level was horizontal. The free surface profiles were determined by using digital image processing.

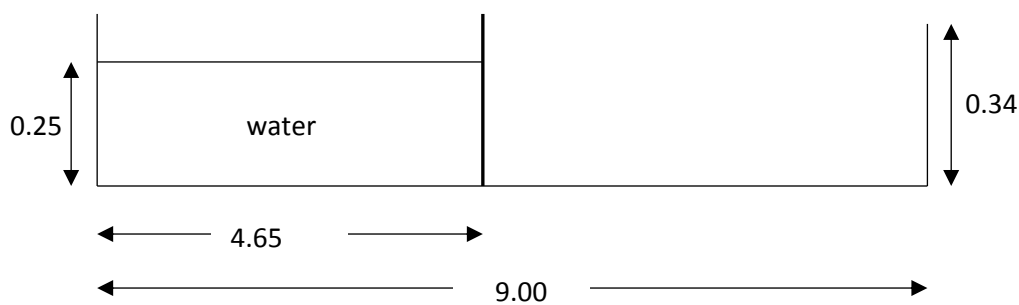


Figure 3.1 Experimental setup of Ozmen-Cagatay and Kocaman (all units are in m)

The experiments of LaRocque et al. (2013a) were conducted in a smooth wooden flume having a length of 7.31 m, a width of 0.18 m and a depth of 0.42 m with a bottom slope of 0.93% and a schematic representation can be seen in Figure 3.2. The gate was located 3.37 m downstream from the upstream end of the reservoir. The removal time of the gate was 0.21 s and 0.06 s to 0.08 s for the experiments of LaRocque et al. (2013a) and Ozmen-Cagatay and Kocaman (2010), respectively. According to Lauber and Hager (1998), the gate openings in both experiments can be considered as instantaneous.

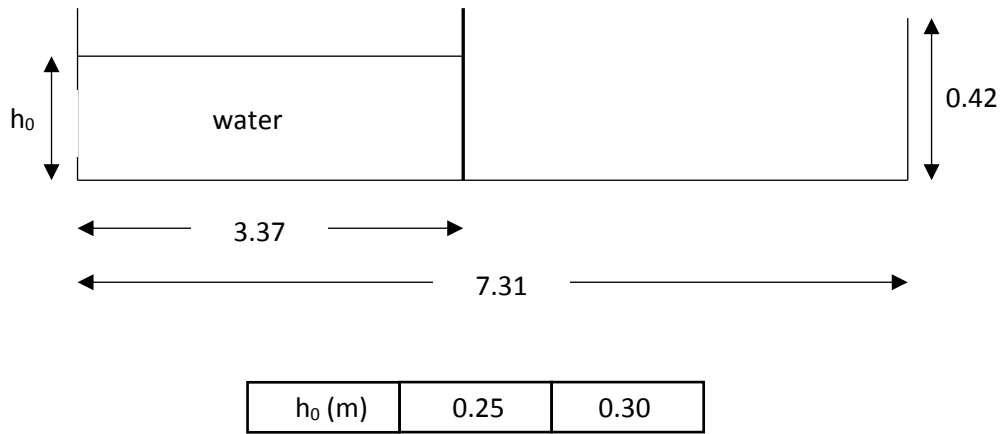


Figure 3.2 Experimental setup of LaRocque et al. (2013a) (all units are in m)

In the numerical models, the gate is removed instantaneously. In the SPH method, the initial distance between the water particles and the boundary particles was taken 0.01 m and 0.005 m, respectively. The mass of a particle is determined by multiplying the spacing between two particles (0.01 m) and the density of the particles. The number of water particles and boundary particles taken in the simulations, smoothing (kernel) lengths, minimum time steps, and simulation times are given in Table 3.1.

Table 3.1 The parameters used in SPH

The model of Ozmen-Cagatay and Kocaman (2010)				
# of Water Particles	# of Boundary Particles	Smoothing Length (m)	Time step (s)	Simulation time (s)
11625	1902	0.01	3e-5	1.50
The model of LaRocque et al. (2013a)				
# of Water Particles	# of Boundary Particles	Smoothing Length (m)	Time step (s)	Simulation time (s)
10110	1861	0.01	2.5e-5	4.00

The experiments of Lobovský et al. (2014) is used to validate the calculation of pressures. The experiments were conducted over a dry horizontal bed. A side view and the front view of the impact wall located downstream end of the experimental setup

can be seen in Figure 3.3(a) and 3.3(b), respectively. A pressure sensor was mounted to the impact wall.

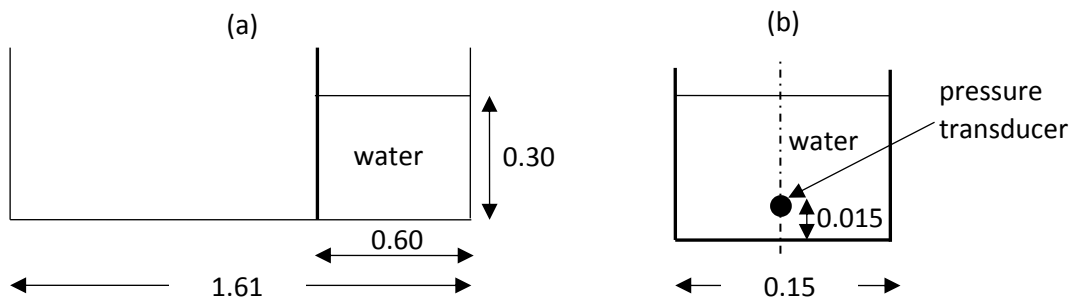


Figure 3.3 Experimental setup of Lobovský et al. (2014) (all units are in m)

In the numerical simulations of the experiment of Lobovský et al. (2014), 1860 water particles, shown with red dots in Figure 3.4 were used. The initial spacing between particles for this case is 0.01 m. Time step is calculated from CFL condition.

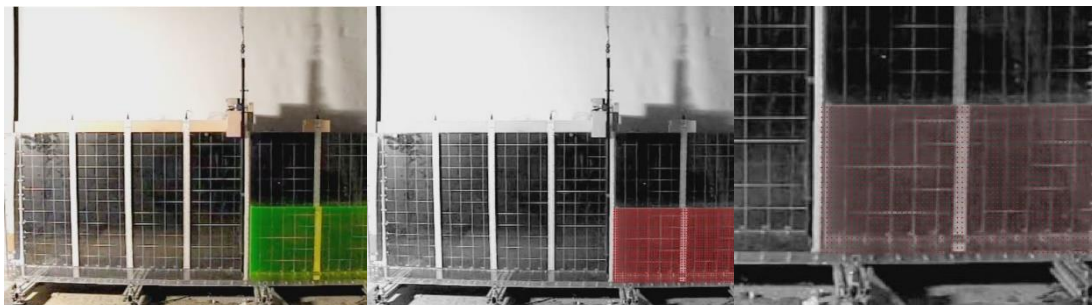


Figure 3.4 Particle Representation of experimental setup of Lobovský et al. (2014)

For the numerical simulation of laminar flow, RANS equations with $k-\epsilon$ turbulence model and LES model, the parameters are given in Table 3.2. In all the models, for the upstream end of the reservoir and for the bottom of the channel, the wall boundary with no-slip condition, for the top of the computational area, a symmetry boundary condition was used. The initial water height and length were defined according to the experimental values ($h_0 = 0.20$ m for the experiments of Ozmen-Cagatay and Kocaman and $h_0 = 0.25$ and 0.30 m for LaRocque et al., 2013a). The time step was defined according to Courant-Friedrichs-Lewy (CFL) condition.

Table 3.2 Parameters used in mesh-based methods

The model of Ozmen-Cagatay and Kocaman (2010)				
Model	Grid size in x direction (m)	Grid size in y direction (m)	Grid size in z direction (m)	Simulation time (s)
Lam.	0.005	0.005	0.01	2
RANS	0.005	0.005	0.01	2
LES	0.0015	0.0015	0.01	2
The model of LaRocque et al. (2013a)				
Model	Grid size in x direction (m)	Grid size in y direction (m)	Grid size in z direction (m)	Simulation time (s)
Lam.	0.005	0.005	0.01	2.5
RANS	0.005	0.005	0.01	2.5
LES	0.0015	0.0015	0.01	2.5

3.3 Results

3.3.1 Free Surface Profiles

The variation of the water surface for a dry bed configuration obtained from the experiments of Ozmen-Cagatay and Kocaman (2010) and from the numerical approaches are given in Figure 3.5 and Figure 3.6. In the figures, dimensionless parameters are used. The dimensionless parameters are calculated as: $T = \sqrt{\frac{g}{h_0}} t$, $Y = \frac{y}{h_0}$, $X = \frac{x}{h_0}$ where $h_0 = 0.25$ m. In the simulations, the problem is also solved with Euler equations obtained simply by ignoring the viscous term in Navier-Stokes equations. A general agreement between the measured, SPH-calculated, Eulerian and laminar flow results is seen in Figure 3.5. Although the laminar solution of the mesh-based method gives slightly overestimated results for later stages of dam-break, Euler and SPH solutions give slightly underestimated results. In Figure 3.6, turbulence effects are included. The results of turbulence models are closer to the experimental values than no turbulence models especially in the later stages of the dam break flow. There is not much difference between the results of RANS and LES turbulence models. However, RANS with k- ϵ turbulence model gives the closest results with the

experiment. LES turbulence model gives slightly underestimated results in terms of free surfaces. The small differences in the results may be due to the assumption of sudden removal of the gate. The differences between numerical and experimental results increase at the later stages of dam break. According to Hogg and Woods (2001) at the later stages of the dam break, the flow is strongly influenced by the skin friction resulting in a slow propagation of the wave front. The computational time of SPH with old boundary condition is approximately ten times higher than laminar flow and eight times higher than LES for this case. The proposed boundary method decreases the computational time by nearly 15 %. Particle distribution throughout the simulation shows minor differences for standard boundary and proposed boundary. Since the particles can move parallel to the boundary without exerting a repulsive force in proposed boundary condition, the distribution is more refined. The effect of kernel truncation at the boundary is not severe in the simulations of present study as can be seen from the simulation results.

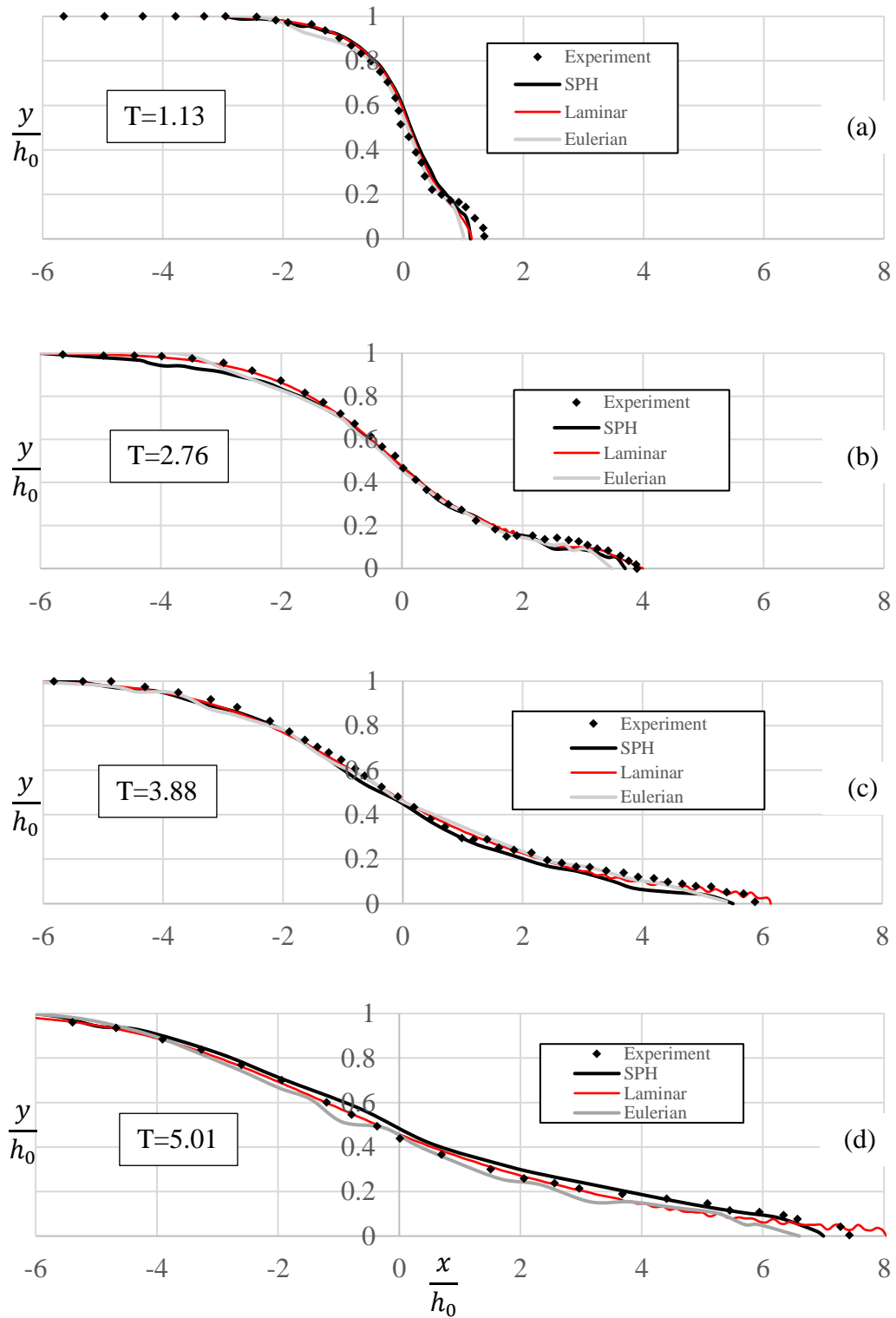


Figure 3.5 Comparison of free surface profiles between the experiments of Ozmen-Cagatay and Kocaman (2010) and the numerical simulations without turbulence effects

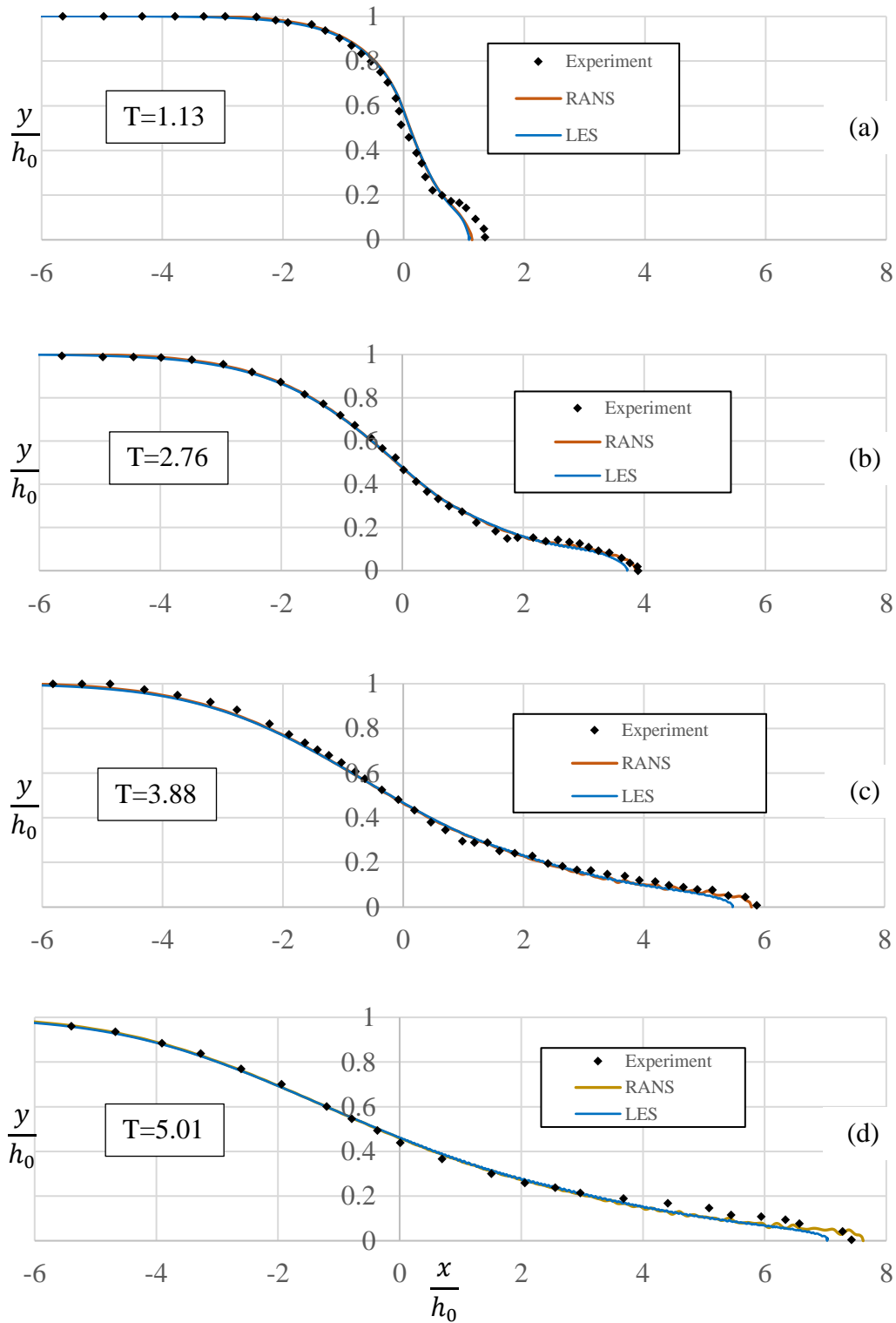


Figure 3.6 Comparison of free surface profiles between the experiments of Ozmen-Cagatay and Kocaman (2010) and the numerical simulations with turbulence effects

Free surface profiles for different times obtained from the experiments of LaRocque et al. (2013a) and numerical simulations are given in Figure 3.7 and Figure 3.8. In Figure 3.7, the comparison between the experimental, SPH, Eulerian and mesh-based laminar flow results are given. In Figure 3.8, RANS, LES and experimental results are given together. The probes were located at -0.3, -0.5, -0.7, -0.8, -0.9, -1.1 and -1.5 m upstream and at 0.2, 0.4, 0.6, 0.8, 1.0 m downstream of the gate and the measurements were done accordingly. The location and the shape of the wave front cannot be interpreted from the experimental readings. However, a general idea of the shape evolution of the free surface profile can be deduced. In the figures dimensionless data is used. As can be seen from the experimental data, there is a slight increase in water level at the upstream side of the gate due to the removal of the gate at $T = 3.13$. Since in the numerical simulations sudden gate removal was assumed, the upward movement of the water surface at the initial stages of the dam break, i.e. $T = 3.13$, is not observed. At the downstream side of the gate, all the numerical simulations give slightly underestimated results in terms of free surface level. The LES and RANS simulations give very similar results. The figures show that all the numerical solutions give good consistency with the measured data. Computational time of proposed boundary method is nearly 13% less than repulsive force boundary condition.

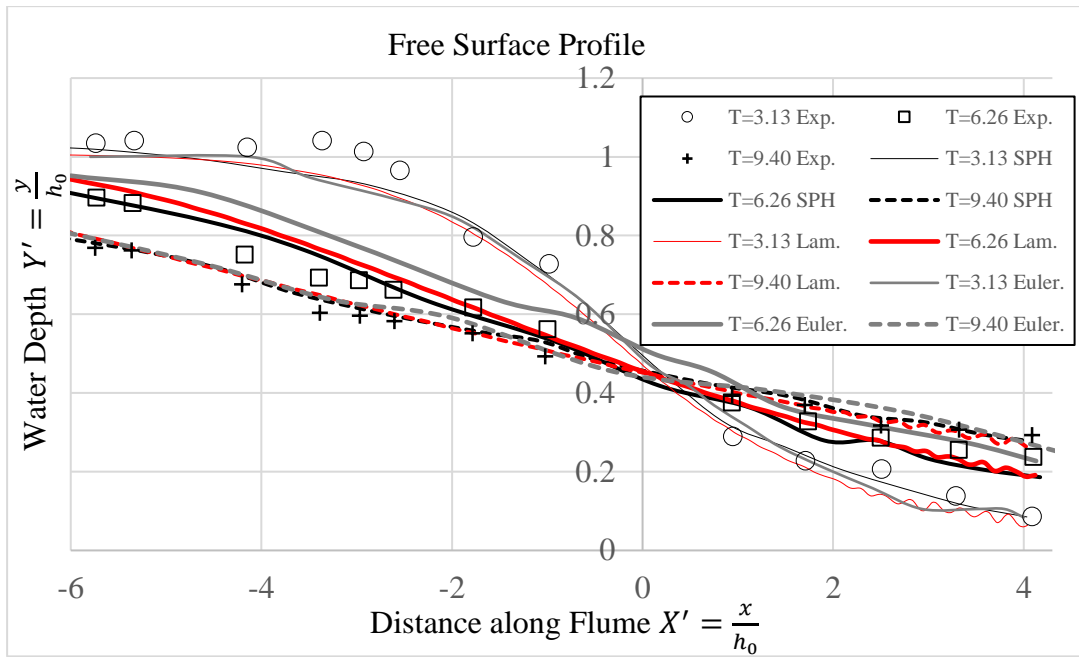


Figure 3.7 Comparison of free surface profiles between the experiments of LaRocque et al. (2013a) and the numerical simulations without turbulence effects

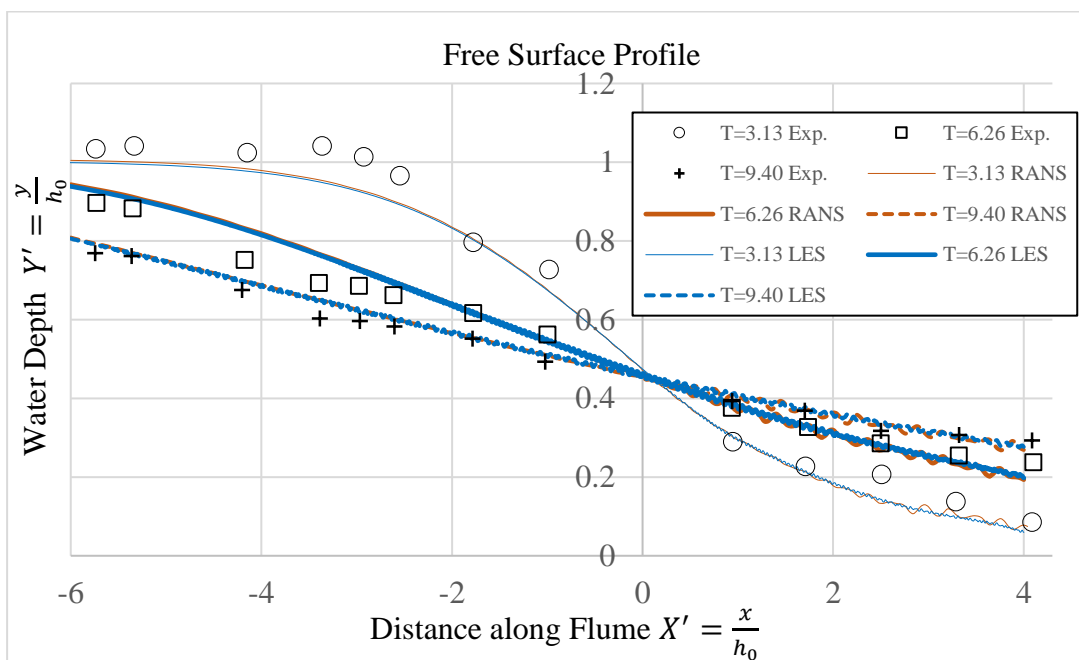


Figure 3.8 Comparison of free surface profiles between the experiments of LaRocque et al. (2013a) and the numerical simulations with turbulence effects

Figure 3.9, the measured and calculated free surface profiles from the experiments of Lobovský et al. (2014) at different times can be seen. In the figure, a1, b1 and c1 are the experimental data whereas a2, b2 and c2 are the numerical results. Due to the angle of photography in the experiments (a1, b1, c1), two free-surface profiles can be seen on the front and back wall which also can be seen in a2, b2 and c2. As shown, the measured and simulated free surfaces are in good agreement.

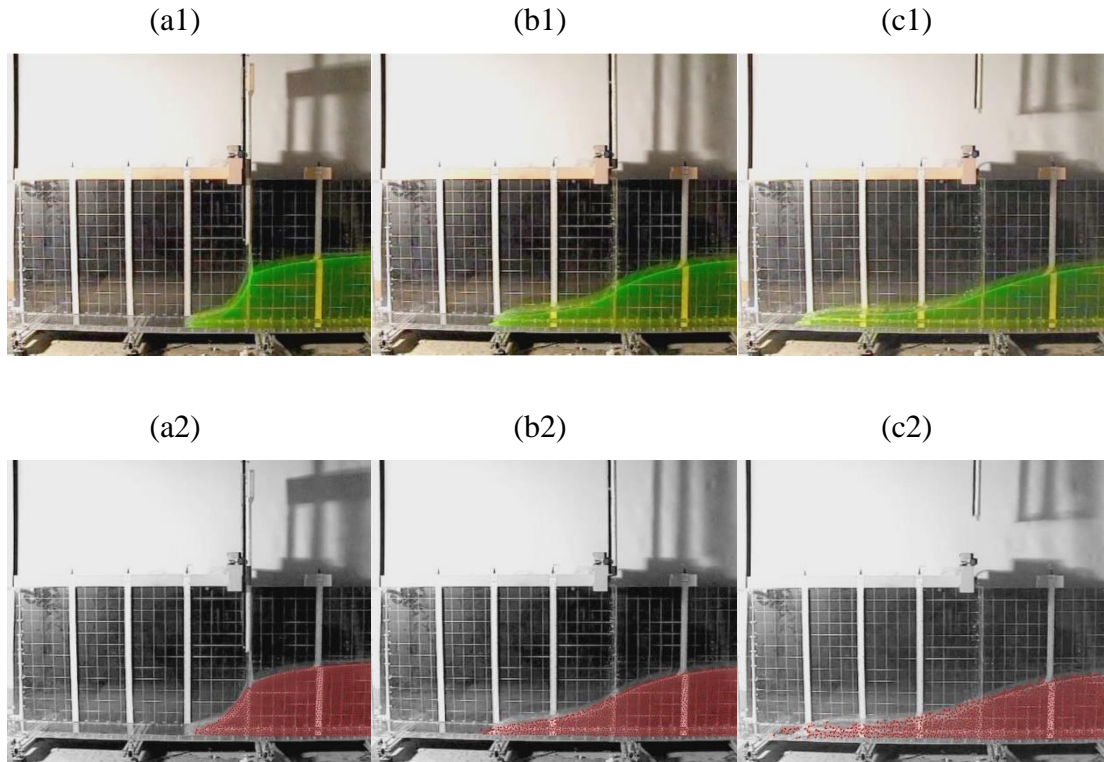


Figure 3.9 Free surface profiles at $t = 0.1599$ (a), 0.2766 (b) and 0.3733 (c) seconds. (Top frames from experiments, bottom frames from simulations, Lobovský et al., 2014).

3.3.2 Velocity Calculations

In Figure 3.10, horizontal velocity values at the downstream side of the gate for an initial reservoir head of 0.30 m are given (LaRocque et al., 2013a). In the figure, measured, SPH, mesh-based laminar flow, RANS and LES results are given for $T = 11.44$. The dimensionless parameters are

$$T = \sqrt{\frac{g}{h_0}} t \quad (3.1)$$

$$X' = \frac{x}{h_0} \quad (3.2)$$

$$X'' = \frac{x}{\sqrt{\frac{g}{h_0}} t} \quad (3.3)$$

$$V' = \frac{v}{\sqrt{\frac{g}{h_0}}} \quad (3.4)$$

where X'' represents the dimensionless distance from the probe. The velocities are determined at 0.045 m above the bottom of the canal and at $X' = 2.00, 2.53, 3.00$ and 4.00 downstream of the gate. Although there is not a significant difference between the results, RANS gives relatively the worst results. The difference between RANS and experimental results is the highest when $X'=2.53$ and approximately equal to 9%. The highest relative differences between the results of SPH, mesh-based laminar and LES simulations and measurements are approximately 6.5%, 5.4% and 5.7%, respectively. The relative differences in percentage according to measurement locations are given in Table 3.3. The results closest to the experiments are obtained with laminar flow and LES turbulence model. According to LaRocque et al. (2013a) downstream of the gate, the flow is turbulent and turbulence models should be used in the simulations. However, the simulations without turbulence also match with the experimental measurements. LaRocque et al. (2013a) proposed that RANS with k- ϵ turbulence model may not be appropriate for dam break problems. Although free surfaces obtained from k- ϵ turbulence model closely match with the measured data, the velocity profiles show differences.

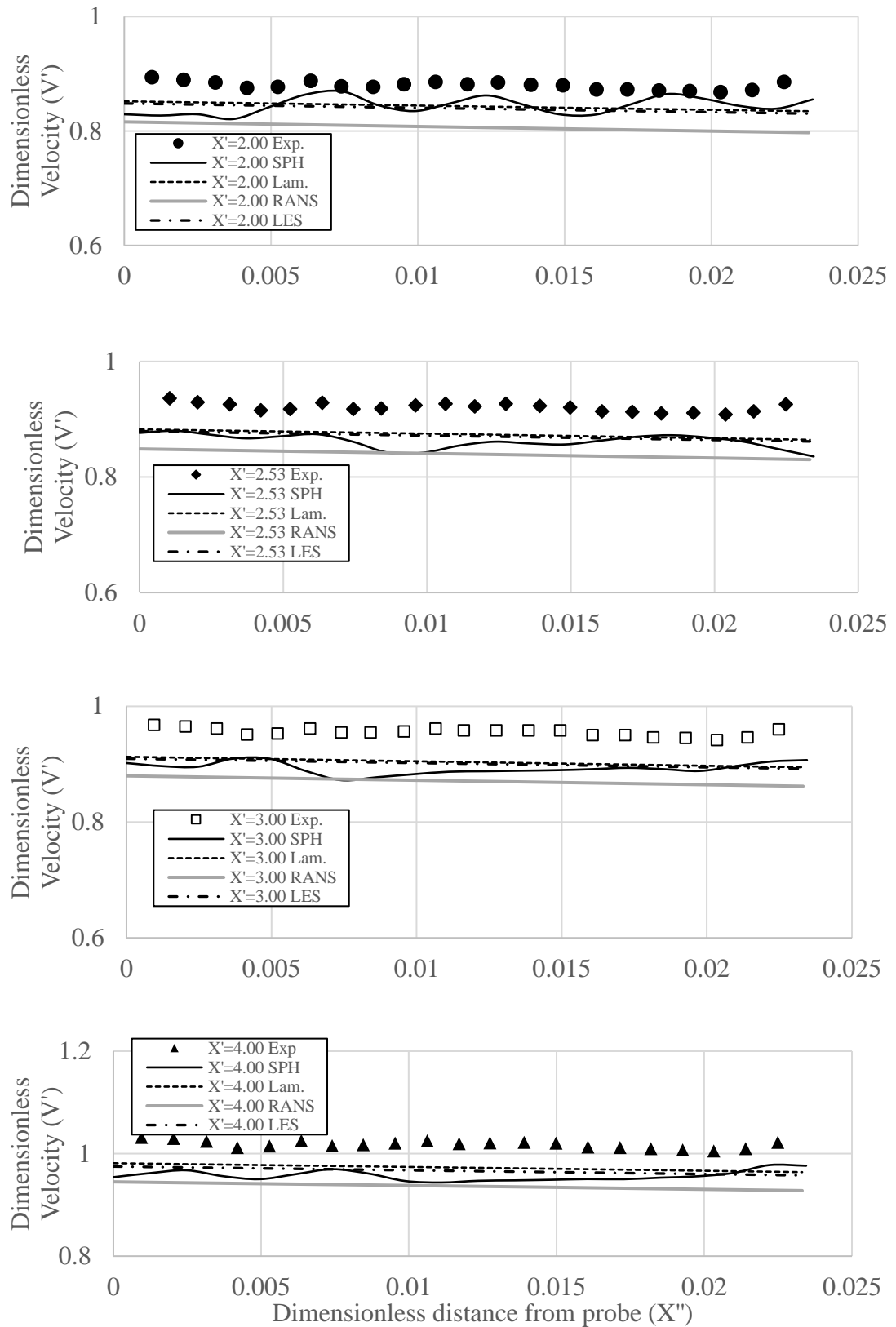


Figure 3.10 Downstream velocity profiles for $T = 11.44$ and $h_0=0.30$ m of LaRocque et al. (2013a)

Table 3.3 Relative approximate difference between numerical and experimental results for (in %)

X'	% relative differences between			
	SPH-exp.	lam-exp.	RANS-exp.	LES-exp.
2.00	4.02	4.12	8.29	4.57
2.73	4.02	5.08	8.79	5.42
3.00	6.52	5.40	8.84	5.70
4.00	5.99	4.44	8.00	5.08

The causes that make the results of RANS with k- ϵ turbulence model deviate should be investigated. One of the reasons is deemed to be the channel slope. However, currently there is not sufficient evidence to support this claim. This is going to be a subject matter for a follow-up study. Just to provide some insight into whether or not the channel slope has some effect, laminar flow, RANS and LES models were run again by assuming that the channel has no slope. In Figure 3.11, the results of the simulations for $X''=2.00$ and $X''=4.00$ which are the closest and the furthest measurement locations to the gate are shown. When there is no slope, the three models give the similar results for both locations. However, when there is a channel slope of 0.93%, RANS with k- ϵ turbulence model gives slightly underestimated results. In fact, in the experiments of Ozmen-Cagatay and Kocaman (2010), the channel had no slope and RANS with k- ϵ turbulence model gave the closest results to the measured data. However, LaRocque et al. (2013a) used a channel with 0.93% slope and k- ϵ turbulence model gave the furthest results from the measured data in terms of velocity profile.

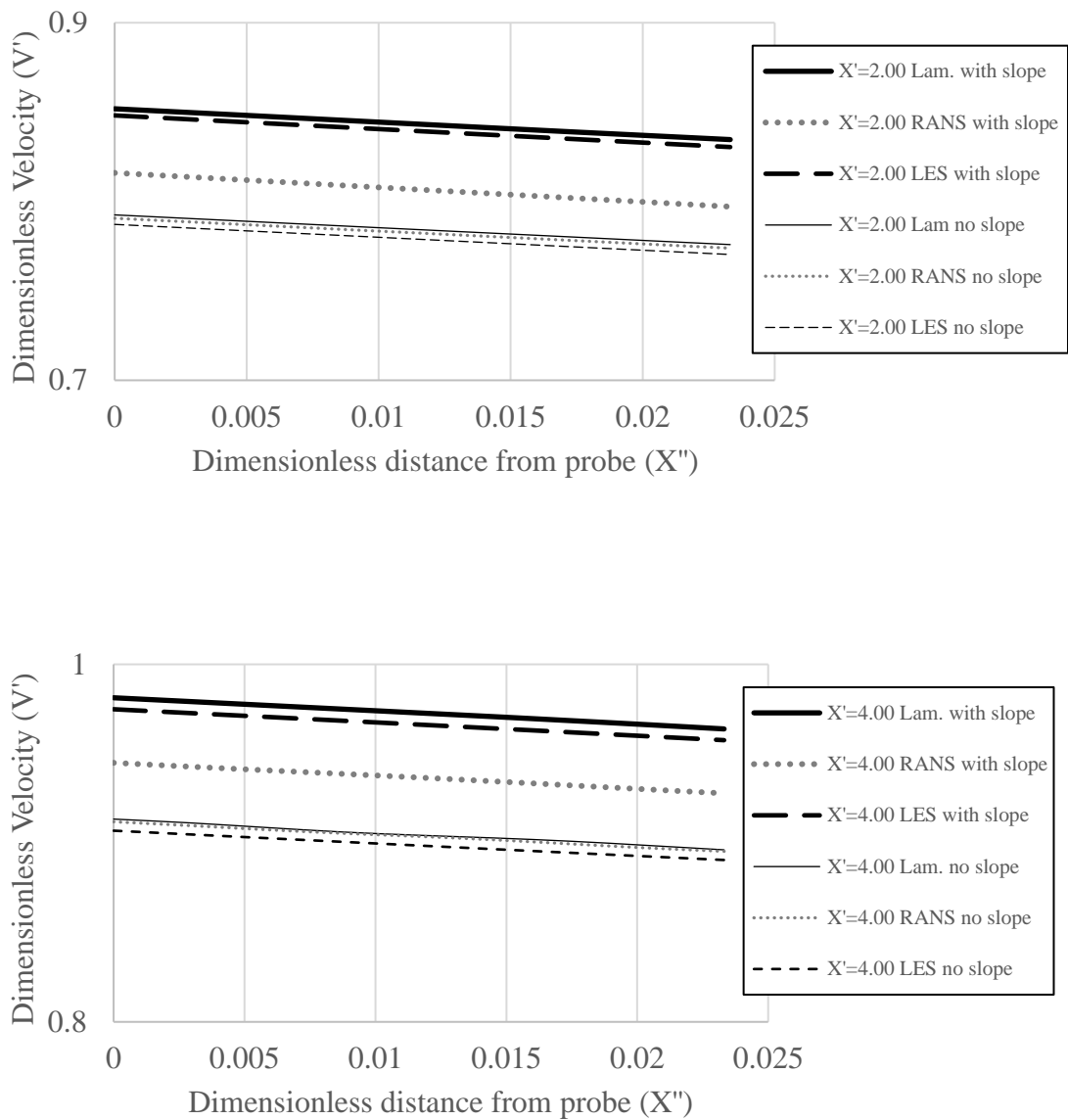


Figure 3.11 Numerical simulation of velocity profiles for different bed slopes

3.3.3 Pressure Calculations

For the experiments of Lobovský et al. (2014), the forces or pressures calculated from the Lagrangian multiplier boundary method can be seen in Figure 3.12. The measured pressures at transducer shown in Figure 3.3 were used to validate the simulation results. The calculated and simulated water-front reaches to the wall located at the end of the channel approximately at the same time. The calculated and measured impact

pressures are in good agreement. Minor oscillations in the numerical results are observed.

Calculation of the forces on structure, or boundary in this case, will lead to interaction between fluid and solid. Although the mechanism of fluid structure interaction (FSI) method is beyond the scope for this study, it can be said that by defining an interaction mechanism between solid nodes and water particles, the proposed boundary allows FSI simulations which will be covered in a follow-up study.

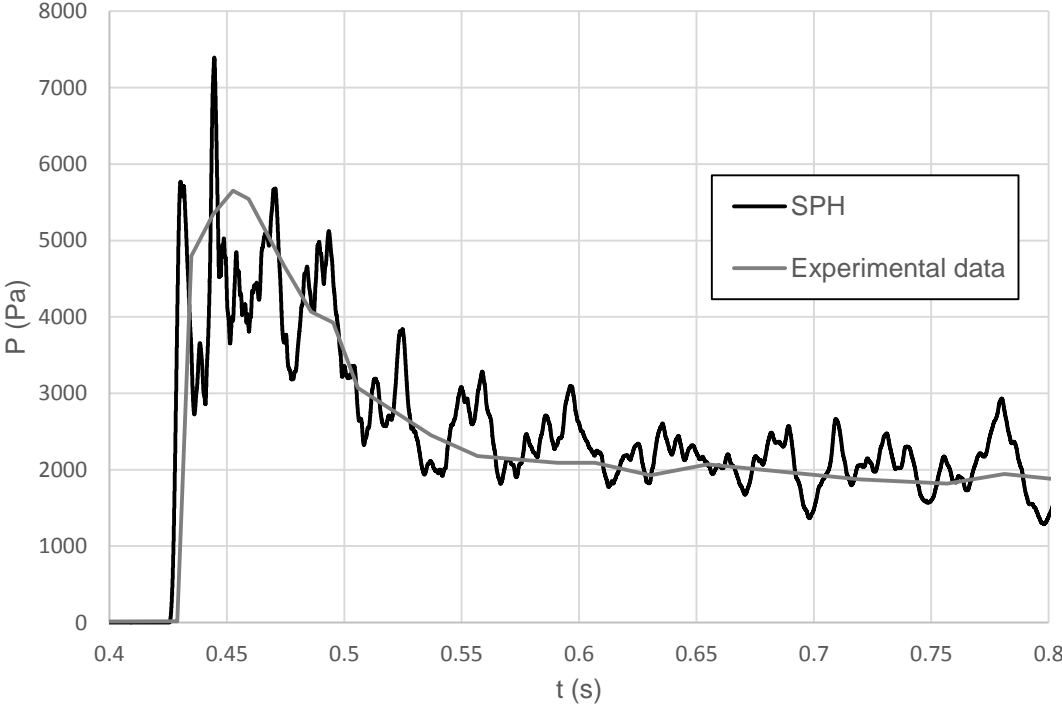


Figure 3.12 Impact pressures measured and calculated at pressure sensor for experimental data of Lobovský et al. (2014)

3.4 Discussion of Results

In this part, two idealized dam break problems were simulated by using both mesh-free and mesh-based methods. The turbulence effects in dam-break problems were also investigated with a $k-\epsilon$ turbulence model and a LES model. SPH with a novel boundary method was used as the mesh free-method. In the literature, although the calculation of free surfaces is widespread within the particle methods, the analysis of the velocities

is rarely found (Fu & Jin, 2014). In the present study, both the velocities and the free-surface profiles calculated from SPH, Eulerian, mesh-based laminar, RANS with $k-\varepsilon$ turbulence model and LES model were investigated. The free surface profiles can be predicted satisfactorily with all the methods. However, the downstream velocities show slight differences. LaRocque et al. (2013a) proposed that $k-\varepsilon$ turbulence modelling may not be applicable for dam-break problems. In fact, the relatively worst results (maximum average of 8% deviation from measured data in the downstream velocity) were found with $k-\varepsilon$ turbulence modelling in the simulations of the experiments of LaRocque et al. (2013a) whose channel had a slope. On the other hand, for the simulation of free-surface profiles in the experiments of Ozmen-Cagatay and Kocaman (2010), $k-\varepsilon$ turbulence modelling gave the relatively best results. While the experimental setup of LaRocque et al. (2013a) has a slope, the channel in the setup of Ozmen-Cagatay and Kocaman (2010) is horizontal. When the experiment of LaRocque et al. was simulated without a slope, it was seen that the $k-\varepsilon$ turbulence model gave similar results with the other numerical models. This slope effect is to be investigated further in the follow up studies.

Computational time with the proposed boundary is less than that of a traditional boundary used in SPH simulations. The main reason is since boundary particles are not used, total number of particles decreases. Moreover, in proposed boundary all particles invading the boundary are pushed out by solving Equation (2.72) which is a rapidly solvable identity type of matrix.

In SPH boundary methods in literature, the water particles cannot touch the real boundary due to either the force exerted from the boundary particles or pressure difference between water and ghost particles. In the proposed boundary, no force is applied if water particle does not invade the boundary. Therefore, water particles can freely move no matter how much close to boundary, which is not possible in many other boundary types.

The main drawback of the method is the boundary deficiency, which is the decrease in the accuracy of an SPH approximation when a fluid particle approaches the boundary since there is no particle outside the boundary (Liu & Liu, 2003). To overcome boundary deficiency, dummy particles may be put outside the boundary by

instantaneously mirroring a nearby fluid particle which is referred as ghost particle technique. However, the position and number of particles change at every time step leading to inefficiency of computational time and problems in the implementation. Moreover, the technique is problematic when irregular boundaries exist in the domain. Monaghan type of boundary condition (repulsive force method) is advantageous on the problems with irregular boundaries. However, boundary deficiency is also encountered since, there is no particle outside the boundary. In addition, a high repulsive force is exerted to a fluid particle which is very close to boundary leading to disturbances in pressure distribution near the wall. In the proposed method, no improvements have been recommended to overcome the boundary deficiency. On the other hand, pressure distribution near the wall is smooth since no external force is applied near the boundary. Moreover, the implementation of the complex boundaries is easier. The main advantage of the proposed boundary is that the method can be easily extended to fluid-structure interaction problems. In fact, the boundary is mainly designed for that reason.

In conclusion, SPH method and investigated mesh-based methods were satisfactorily used in the simulations of dam-break flow. Turbulence modelling did not improve the results significantly over the other models used in the study. It should be noted that SPH has superiority in terms of tracking the large free surface deformation, although the computational time is higher compared to mesh-based methods. However, with the proposed boundary method, the computational time of SPH decreases nearly 15% for the experiments investigated here.

CHAPTER 4

APPLICATION OF SPH ON PIPE FLOWS

In this part, for the application of SPH on closed-conduit flows, liquid slug flow driven by pressurized air in inclined and horizontal pipes with a downstream elbow is investigated numerically. As the liquid slug hits the elbow, the impact pressure and the associated force generated at the elbow may damage pipe supports as well as the pipe itself. It is essential for the design engineers of pipeline systems to accurately predict the pressure trace during the impact for safe operation. The slug arrival velocity and slug length (i.e. mass) at the elbow directly affect that pressure. In order to calculate these slug parameters just before the impact an improved one-dimensional model proposed in the literature is used. At the elbow, pressure variation with respect to time is calculated with a two-dimensional SPH method. In the first numerical setup, two representative initial slug lengths, one for short slugs and one for long slugs, and three different initial air tank pressures are used. Second numerical setup is generated for two different initial slug lengths and three different initial air tank pressures. The obtained numerical data are validated with experimental results. For both short and long slugs, calculated peak pressures show great agreement with measured peak pressures.

4.1 Introduction to Slug Flow in a Pipe

There are different steady gas-liquid flow regimes classified in the literature (Mandhane, Gregory, & Aziz, 1974). Liquid slug flow is one of the flow regimes that has caused problems in power plants (Kim, 1987; Kim et.al, 1988). In this study, instead of a steady slug flow, a single slug accelerated along an initially voided pipeline is investigated. Liquid slug motion is frequently observed in piping systems with high-pressure steam. The slugs in these systems may reach high velocities and

damage the piping when they hit obstructions such as tees, partially open valves, elbows, etc. The impact force and the impact duration are proportional to the square of the speed of the slug and the length of the slug, respectively (Tijsseling et.al. 2016). In order to prevent damage on critical sections and maintain safe operation the estimation of impact forces is very important. The nature of the problem is very complex. There is not a wide range of studies on this topic. Fenton (1989) and Fenton and Griffith (1990) experimentally investigated the behavior of unsteady slug flow by measuring the impact forces at the elbow and developed two analytical models. The pipe used in the experiments was slightly inclined upward and the water was trapped in its lower part. The pipe was connected to a tank and a valve was located between the tank and the pipeline. By opening the valve suddenly, trapped water was accelerated to the elbow located at the upper end of the pipe. The water hit the elbow and the magnitude of the impact force with respect to time was measured with a transducer connected to the elbow. By changing the volume of the trapped water and the air pressure in the tank, the experiments were repeated. They found that if the travel length of the initial slug is seven or more times higher than the initial slug length, due to the high holdup, the forces experienced by the bend dropped dramatically.

Neumann (1991) and Neumann and Griffith (1992) studied the forces on a pipe bend due to the pressurized clearing a pool of liquid. They used a water pool with varying depth instead of trapped water occupying the full pipe cross-section. They found that if the transition from stratified to slug flow does not occur, the generated forces are negligible. They defined a dimensionless length $D^* = L/L_0$, referred to as dispersion distance, where L_0 is the initial slug length and L is the distance from the upstream end of the slug to the bend. When the dispersion distance was equal to six, air was entrained into the slug so much that the generated forces at the bend were greatly reduced, and when it was higher than six, the force generated at the elbow was nearly negligible.

Another significant contribution is the work of Bozkuş (1991) and Bozkuş and Wiggert (1997). They carried out experiments and presented an analytical solution for a slug flow in a 5 cm diameter horizontal pipe having a 90-degree elbow at the downstream end. The pipe was connected to an air tank at the upstream end and a ball valve was located in between them. There was a pipe section between the air tank and the valve

called slug-generating pipe by which it was possible to form slugs of various lengths for a given experiment. By opening the valve suddenly, the slug was accelerated by the pressurized air in the initially voided line and eventually hit the elbow. The downstream side of the elbow was open to the atmosphere. The experimental setup will be explained in the next parts in detail. Data obtained from the experiments were scattered largely because of the manual opening of the valve by hand. In order to overcome this, each experiment was repeated 8 to 10 times. Pressure at the elbow was recorded with two pressure transducers. In their analytical study, the method of characteristics (MOC) was employed to solve the partial differential equations of motion of the compressible gas between the upstream end of the slug and the air tank. They also included the mass loss from the slug, called holdup, due to gravity and shearing effects. For short slugs, the air entrainment was so large that they broke up even before reaching the elbow. On the other hand, for long slugs, two peak pressures were observed at the elbow. Bozkuş explained this phenomenon as the break-up of a single slug into two pieces due to a short-lived water-hammer which occurred due to the very rapid valve opening at the beginning of the slug motion. The calculated peak pressures at the elbow were in agreement with the measured ones.

Owen and Hussein (1994) also studied slug motion experimentally and numerically. The main difference of their experimental setup with that of Bozkuş was the usage of a large air reservoir so that the air pressure drop in each experiment was less than 3%. They also recorded the velocities of the slug which helped determine the impact force. As advised by Bozkuş and Wiggert (1997) for any future research, Owen and Hussein (1994) eliminated the manual valve operation.

Yang and Wiggert (1998) developed a quasi-two dimensional model which allowed air entrainment. The water slug was treated as a number of concentric cylinders sliding through each other. The air penetrated into the slug front via the outer cylinders, since the inner cylinders moved faster than the outer cylinders. They did not include gravity effects so that the computed flow remained axi-symmetric. Numerical results were compared with the experiments of Bozkuş (1991) and it appeared that the quasi-2D model largely overestimated the experimental impact pressures.

Bozkuş, Baran, and Ger (2004) carried out experiments in a 10 cm diameter pipe which was twice the diameter of the pipe in a previous study (Bozkuş & Wiggert, 1997). Since the frictional force is reduced by increasing the pipe diameter, this experiment resembles more real power plant piping. They also derived a mathematical model which underestimated the measured peak pressures. This was mainly because they did not include the mass loss from the slug body during its motion. This specific experimental setup is explained in detail in the next sections.

Kayhan and Bozkuş (2011) developed a numerical model in which the holdup coefficient was a coordinate-dependent function. Although relatively closer agreement with the experimental data were obtained, there was still discrepancy with the measurements.

Hou et al. (2014) numerically investigated the slug flow to better predict the slug dynamics. Before arriving at the elbow, they used the analytical model derived by Bozkuş (1991). At the elbow, they used SPH method. As another novelty, they considered the flow separation at the bend. They compared the numerical model to the experimental studies of Bozkuş (1991). The calculated and the measured results were in good agreement.

Tijsseling et.al. (2016) derived a one-dimensional improved model to investigate the slug flow. The model was able to predict the acceleration and the shortening of the liquid slug. It also included holdup of the slug and flow separation at the bend. Their numerical model was compared to the experimental studies of Bozkuş et al. (2004). Although for long slugs the experimental results were underestimated, for other slugs the magnitudes of the impact pressures were predicted more or less correctly.

In this part, the experiments of Bozkuş (1991) and Bozkuş et al. (2004) are used to validate the developed numerical model for slug motion. In order to calculate the slug parameters such as velocity, length and driving pressure, just prior to slug impact on the elbow, the improved one-dimensional model proposed by Tijsseling et.al. (2016) is used. Upon arrival at the elbow and during the slug passage through the elbow, the SPH method is utilized. At the elbow, pressure variation with respect to time is calculated. The pressure or the force at the elbow occurs due to momentum transfer as

the flow direction changes. Calculated peak pressures show great agreement with recorded peak pressures. In fact, to the knowledge of the authors, the new 2-D SPH model gives closer peak pressure values than all other numerical models proposed in the literature so far. The organization of this part is as follows: the governing equations used in the improved 1-D model proposed by Tijsseling et.al. (2016) are presented first, followed by the description of the experimental setup of Bozkuş (1991) and Bozkuş et al. (2004) and the present numerical model. The comparison between the recorded data and calculated results is given later and conclusions are drawn last.

4.2 Improved One-Dimensional Model

The equations derived in this model are used to calculate the slug velocity and length just before arrival at the elbow. Details of derivation of the equations is given by Tijsseling et.al. (2016). In terms of front velocity, v_1 , slug length, L , and the slug front position, x_1 , the governing equations are:

$$L(t) \frac{dv_1}{dt}(t) \frac{1 - \frac{1}{2}\beta}{1 - \beta} = v_1^2(t) \frac{\beta}{1 - \beta} + \frac{P_2(t) - P_1(t)}{\rho} - L(t)v_1^2(t) \frac{1 - \beta + \frac{1}{3}\beta^2}{(1 - \beta)^2} \frac{f}{2D} + gL(t)\sin\theta \quad (4.1)$$

$$\frac{dL}{dt}(t) = -\frac{\beta}{1 - \beta} v_1(t) \quad (4.2)$$

$$\frac{dx_1}{dt}(t) = v_1(t) \quad (4.3)$$

where β is the holdup coefficient which is assumed to be constant throughout the slug's motion. In the numerical model it is taken as 0.05 or 0.1. The factor β multiplied with the full pipe area, A , that is βA , physically means that slug mass is lost and left behind across 5% or 10% of the cross-sectional area of the pipe, respectively. Figure 4.1, a slug with holdup is shown (Bozkuş & Wiggert, 1997). The control volume in that figure was used to derive Equations (4.1), (4.2) and (4.3).

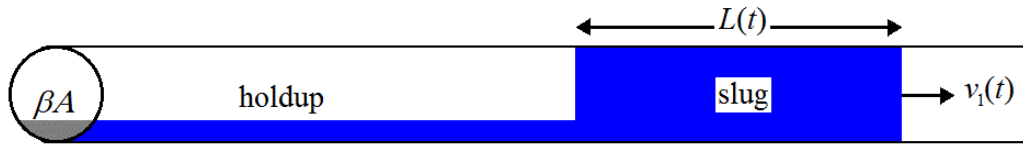


Figure 4.1 Slug motion with holdup (taken from Tijsseling et al., 2016)

4.3 Experimental Setups

The experiments of Bozkuş (1991) and Bozkuş et al. (2004) are used for validation of the SPH slug impact model introduced. The experimental setup of Bozkuş et al. (2004) is displayed in Figure 4.2. The steel test pipe is inclined with an angle of 4.6 degrees with respect to the horizontal plane and has 12 m length and 0.1 m inside diameter. There was a cylindrical tank with a volume of 0.5 m³ connected to the pipe. A ball valve was located between the tank and the pipe. In order to mimic pressurized steam, the tank was filled with pressurized air. Water slugs with different masses and different lengths were trapped in the lower elbow just downstream of the ball valve, Figure 4.3. A transducer aligned with the pipe axis was placed at the upper elbow to record the impact pressures. Just below the upper elbow a short vertical pipe was connected to discharge the slug into the open atmosphere. Roughly, the initial slug mass, distance travelled by the slug front, skin friction and initial air tank pressure determine the impact pressure at the elbow. In the experiments, initial slug mass and initial tank pressure were varied. The distance travelled by the slug could not be changed because of the physical limitations of the experimental setup. However, it varied in proportion to the initial slug length. The tests were run for initial air tank pressures of 3, 4 and 5 bar and initial slug masses of 24, 32, 40 and 48 kg. Two initial slug masses of 24 kg and 40 kg representing a relatively short and a relatively long slug were selected for comparison with the numerical results. They are equivalent to one-dimensional initial slug lengths of 3.0 m and 5.1 m, respectively.

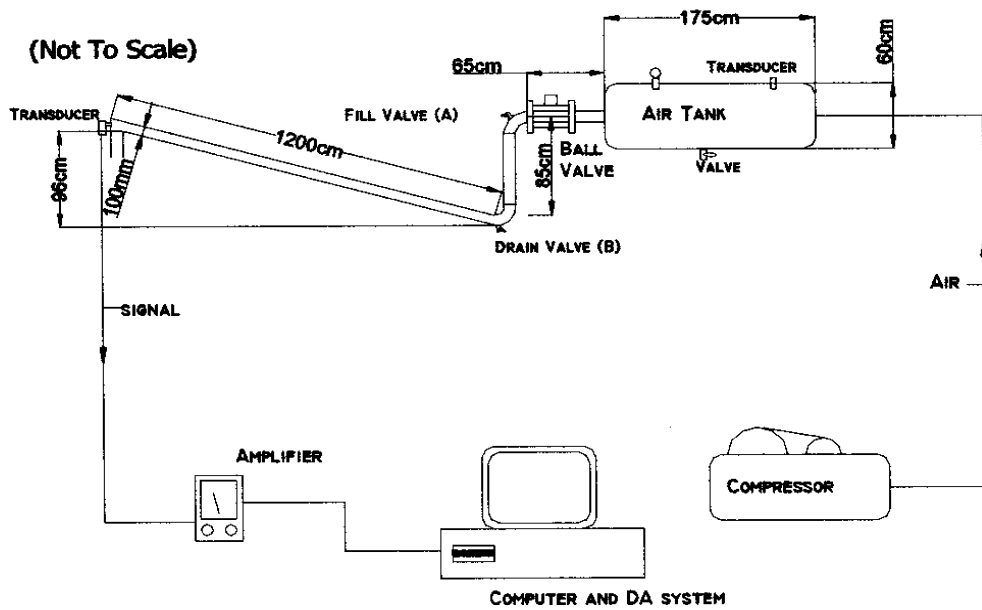


Figure 4.2 Experimental setup used in Bozkuş et al. (2004)

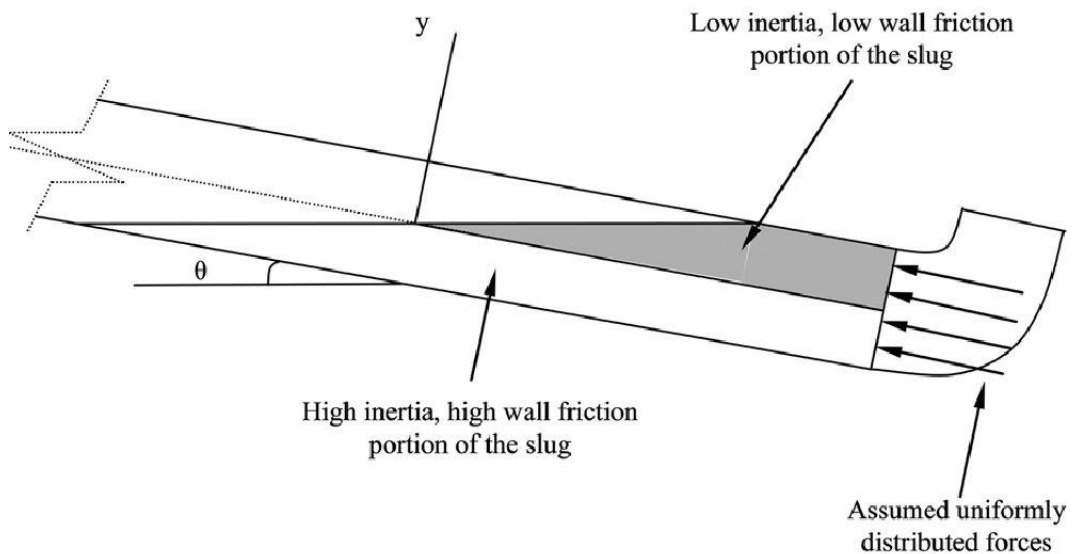


Figure 4.3 Initial liquid slug in an inclined pipe Bozkuş et al. (2004)

In Figure 4.4, the experimental setup of Bozkuş (1991) is shown. As can be seen from the figure, a horizontal, PVC pipe with a length of 9.45 m and a diameter of 50 mm is connected to a pressurized air tank and between them a ball valve is located. A slug generating pipe (SGP) is used to adjust the initial slug length before each experiment.

By opening the valve the slug is accelerated due to the pressurized air at the tank and hits 90° degree elbow located at the downstream end of the pipe. After the elbow, the system is open to atmosphere with a short pipe segment. The pipe is rigidly attached to air tank and concrete floor. Due to extensive anchoring, the pipe can be assumed to be rigid and constrained from axial movement induced by the slug impact. To measure the pressure history, two pressure transducers are installed on the elbow. The experiments were conducted for five initial slug lengths of 1.22 m, 1.52 m, 2.13 m, 2.74 m and 3.35 m and four initial air pressures of 69 kPa, 138 kPa, 207 kPa and 276 kPa.

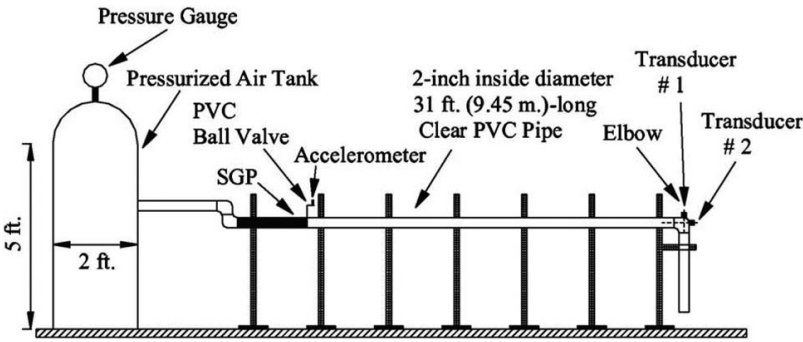


Figure 4.4 Experimental setup of Bozkuş (1991) in original work

4.4 Numerical Models

Two numerical models are used to simulate the slug motion. The improved one-dimensional model proposed by Tijsseling et.al. (2016) is used to calculate the slug parameters in the pipeline which are the input values for the second model, i.e. the two-dimensional SPH model for impact at the elbow. In the first model the ordinary differential Equations (4.1), (4.2) and (4.3) are solved with an explicit fourth-order Runge-Kutta formula. For the validation of the proposed model for two representative slugs, with initial mass of 24 kg and 40 kg, the β values are taken as 0.05 and 0.1, respectively in the simulation of the experiments of Bozkuş et al. (2004).

At the elbow, SPH is used to calculate the impact pressure. Slug length, slug velocity and driving pressure behind the slug just before impact at the elbow are the input values for the SPH code. The initial spacing of the water particles and boundary particles is

0.005 m and 0.0025 m, respectively. The initial density of the water particles is 1000 kg/m³. The mass of a particle is calculated by multiplying its density with the volume (or area in 2D) which is taken as the product of the initial particle spacing in x, y and z directions. Since the slug length just before arrival at the elbow is different in different tests, the number of water particles varies in each run. However, nearly 3000 boundary particles and 10000 water particles are used for the slug with an initial mass of 24 kg and nearly 4000 boundary particles and 18000 water particles are used for the slug with the an initial mass of 40 kg for the experimental setup of Bozkuş et al. (2004). To illustrate the number of particles for the simulations of experimental setup of Bozkuş (1991), for a slug of 207 kPa of initial air pressure and 3.35 m of initial length, 5600 water particles are used. The number of boundary particles is approximately 3000, in this case.

The initial and boundary conditions are shown in Figure 4.5. The smoothing length or kernel length is taken equal to the initial particle spacing, i.e. 0.005 m. Since the initial velocities are different in each run, the time steps are also different. With increasing velocities, the maximum time step decreases. The maximum velocity occurs for the slug with initial air pressure of 5 bar and initial mass of 24 kg. The maximum velocity in this case is 45 m/s and the time step is 2×10^{-6} s according to the CFL condition, where the time step is proportional to the smallest spatial particle resolution. In SPH this is the smoothing length which is assumed to be constant herein (Liu & Liu, 2003-p.142). The time step has to be very small, mainly because all SPH equations are solved explicitly. In the SPH method, the flow separation at the elbow is obtained naturally. Therefore, there is no need to define a flow contraction coefficient as in the improved 1D model.

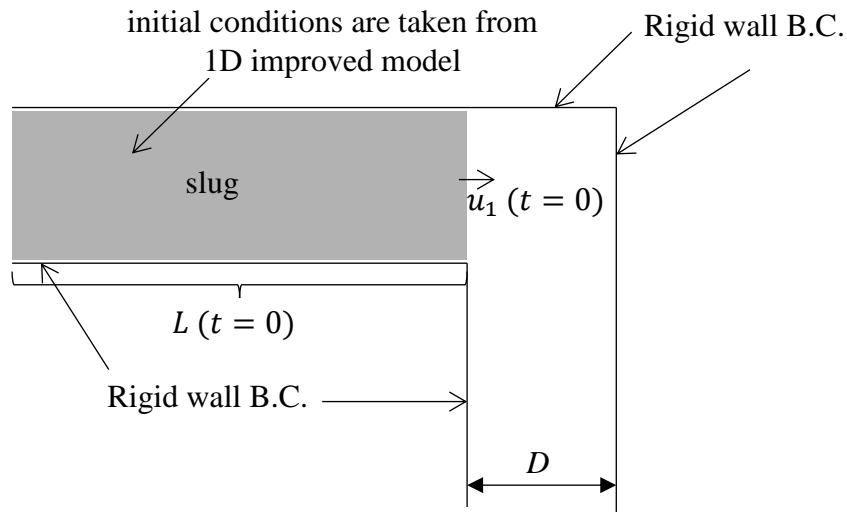


Figure 4.5 Boundary and initial ($t=0$) conditions used in SPH setup (not to scale)

4.5 Results of the simulations for the Experiments of Bozkuş et al. (2004)

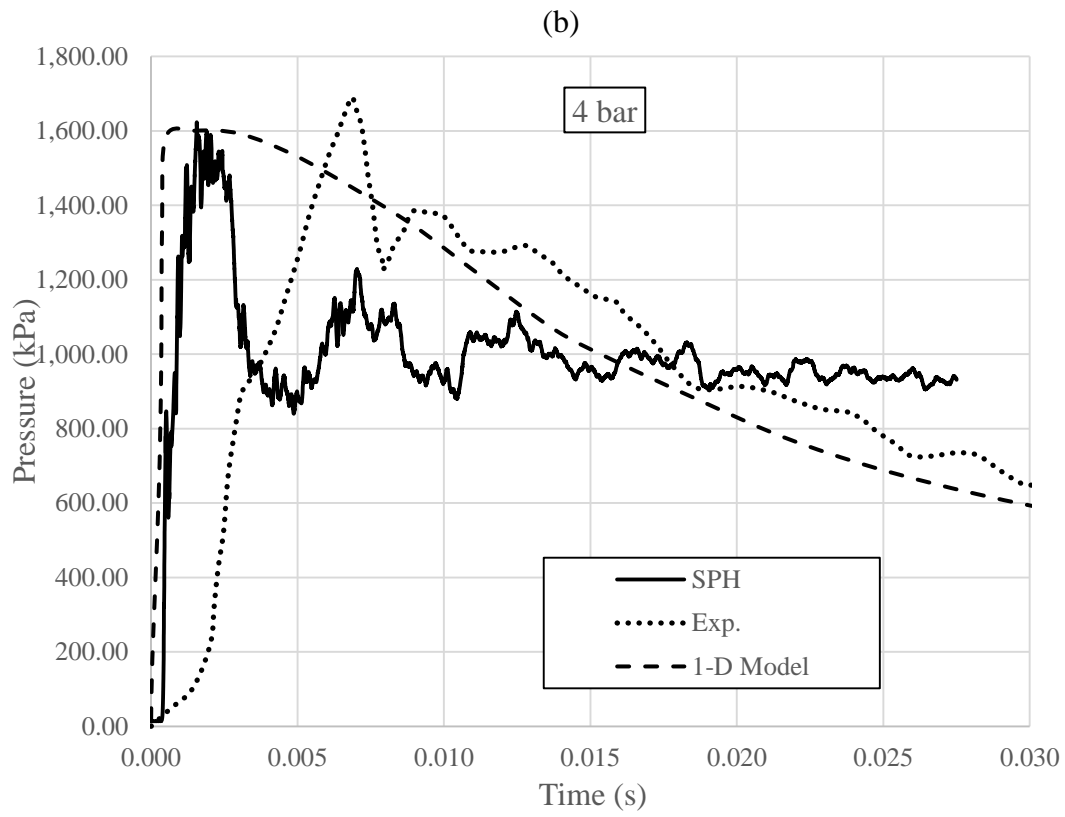
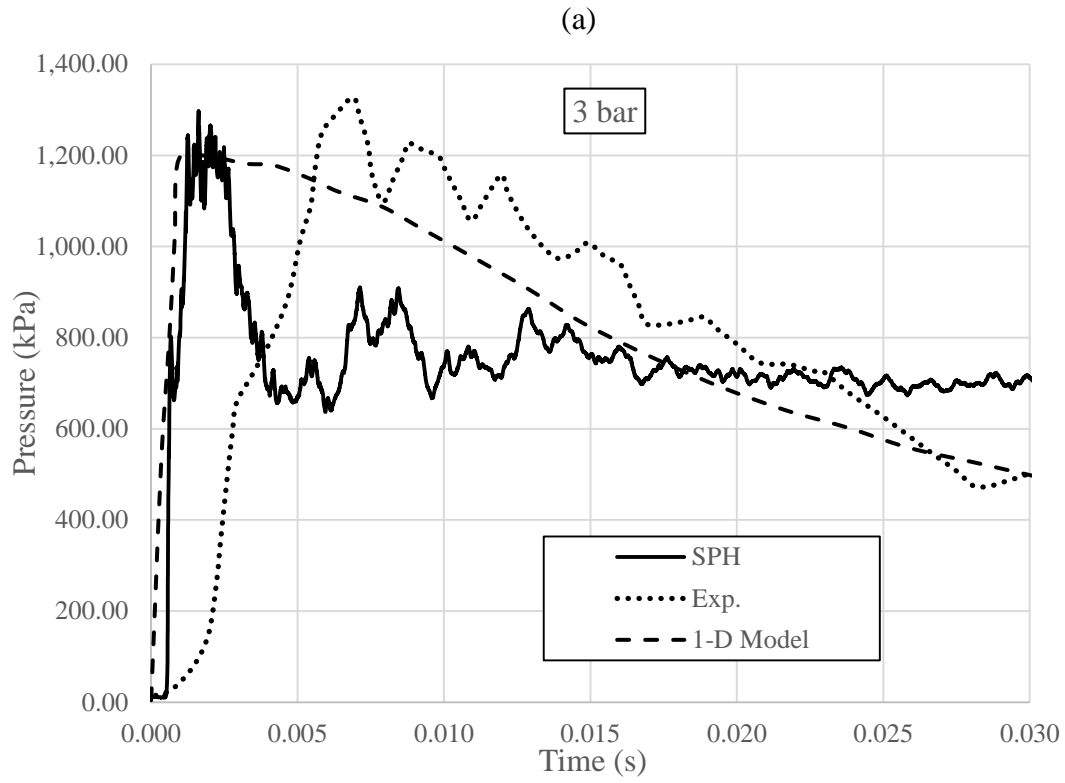
Although the one-dimensional improved model gives the velocity and length of the slug just before arrival at the elbow, it does not give the impact pressure in a direct way. Tijsseling et.al. (2016) estimated the impact peak pressure from ρv_1^2 and they introduced a term to model flow contraction at the elbow. In Figure 4.6 (a), (b) and (c) the impact pressure histories at the elbow are shown for a slug with an initial mass of 24 kg and initial air pressures of 3, 4 and 5 bar, respectively. In the figures, for a meaningful comparison, slug arrival times at the elbow were set equal to zero, to be understood as the time at which the 2D slug impact begins. The observed shapes and magnitudes of the pressure histories obtained with both methods agree reasonably well with the experimental results. The theoretical and experimental peak pressures are nearly the same. Figure 4.7 shows pressure histories of a slug with 40 kg initial mass. The general trends of simulations and experiments can be said to agree well. The calculated peak pressures from the one-dimensional improved method are largely under-predicting: for a slug driven by an initial air pressure of 5 bar, there is a 60% difference between the peak pressures of the one-dimensional improved model and the experiment. On the other hand, SPH predicts the peak pressure magnitudes almost

perfectly. It can be concluded that although the one-dimensional improved model predicts the peak pressures well for short slugs, it does not do so well when the slug is long.

2D SPH simulations usually suffer from pressure noise. In other 2D SPH work, this drawback is also seen (Hou et al., 2014; Korzilius, 2016). In addition, the decreasing trend in Figure 4.6 also shows differences with the experiments. For plotting the pressure histories calculated with SPH, the spatially averaged pressure at the elbow is used, instead of using the pressure at the point where the transducer is located. This average is based on approximately 40 particles in a square box around the transducer location. Although, using average pressure at the elbow reduces pressure noise in the SPH method, it causes small differences in the decreasing trend in Figure 4.6 and Figure 4.7.

Since in the experiments an inclined pipe setup is used, an initial free surface line with 41 % of the total length of the slug of 24 kg initial mass ($L_0 = 3.0$ m, short slug) occurs as previously shown in Figure 4.3 (Bozkuş et al., 2004). Due to a uniform driving pressure force, the upper and lower layers of the slug will be exposed to different accelerations and the slug flow steepens (Korzilius, 2016). Consequently, the pressure at the elbow might gradually reach its peak values if the wave front is not flat. However, in the present 2D model, the evolution of this initial free surface is ignored. The flat slug front causes a nearly instantaneous pressure rise at the square bend.

In Figure 4.8, the positions of the 10000 water particles at the elbow for the slug with 24 kg initial mass and 4 bar initial tank pressure are shown. The figure shows the water particle positions 0.015 s after the simulation started. In the figure, the flow contraction of the water particles when they leave the elbow is evident and the flow contraction coefficient is about 0.54 which is close to the theoretical value of 0.53.



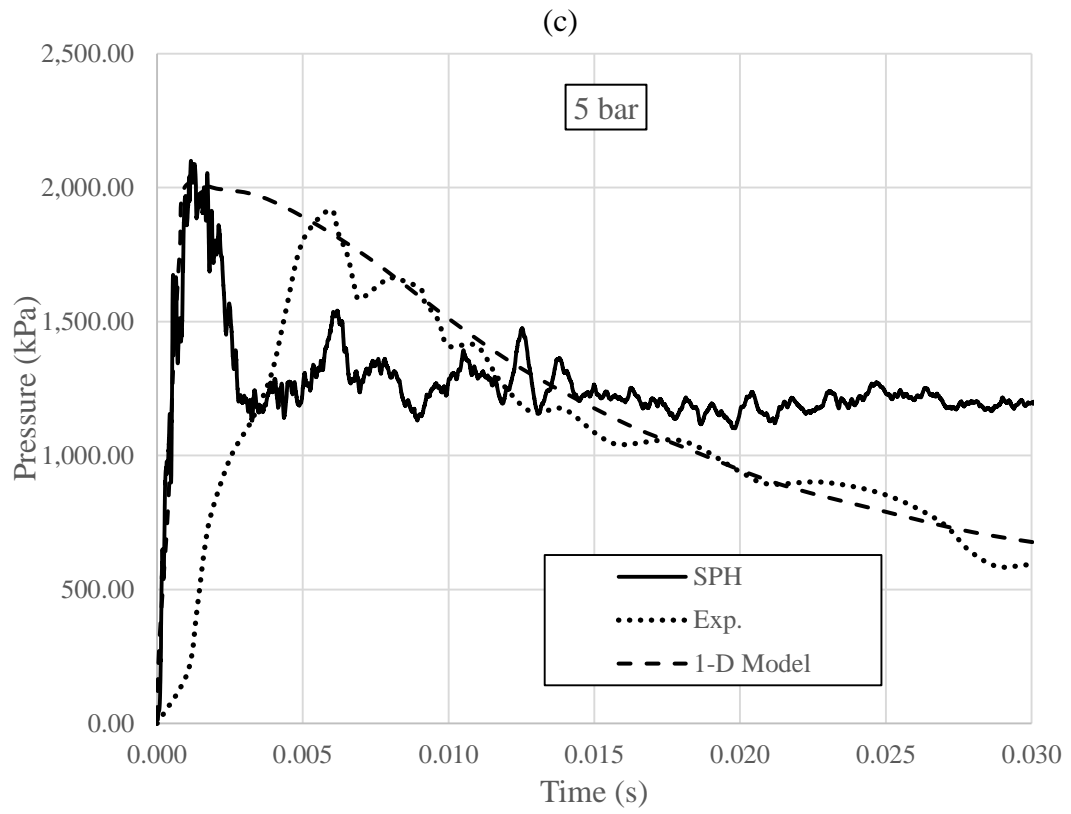
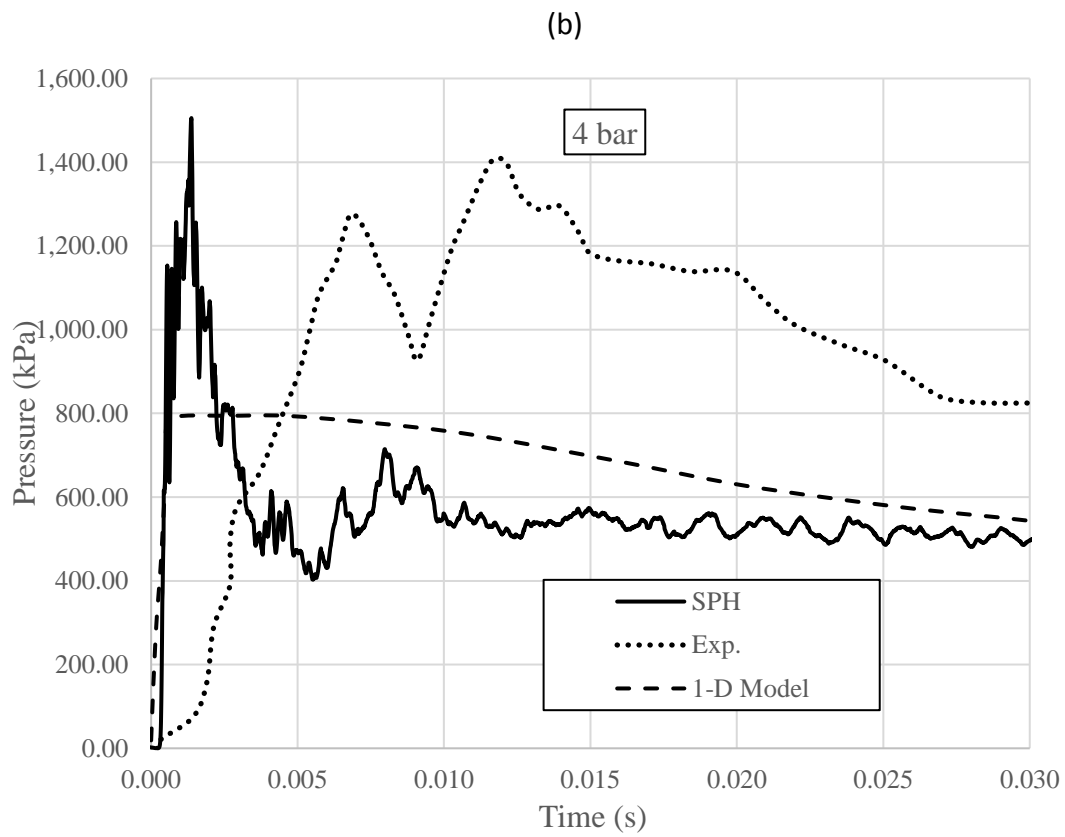
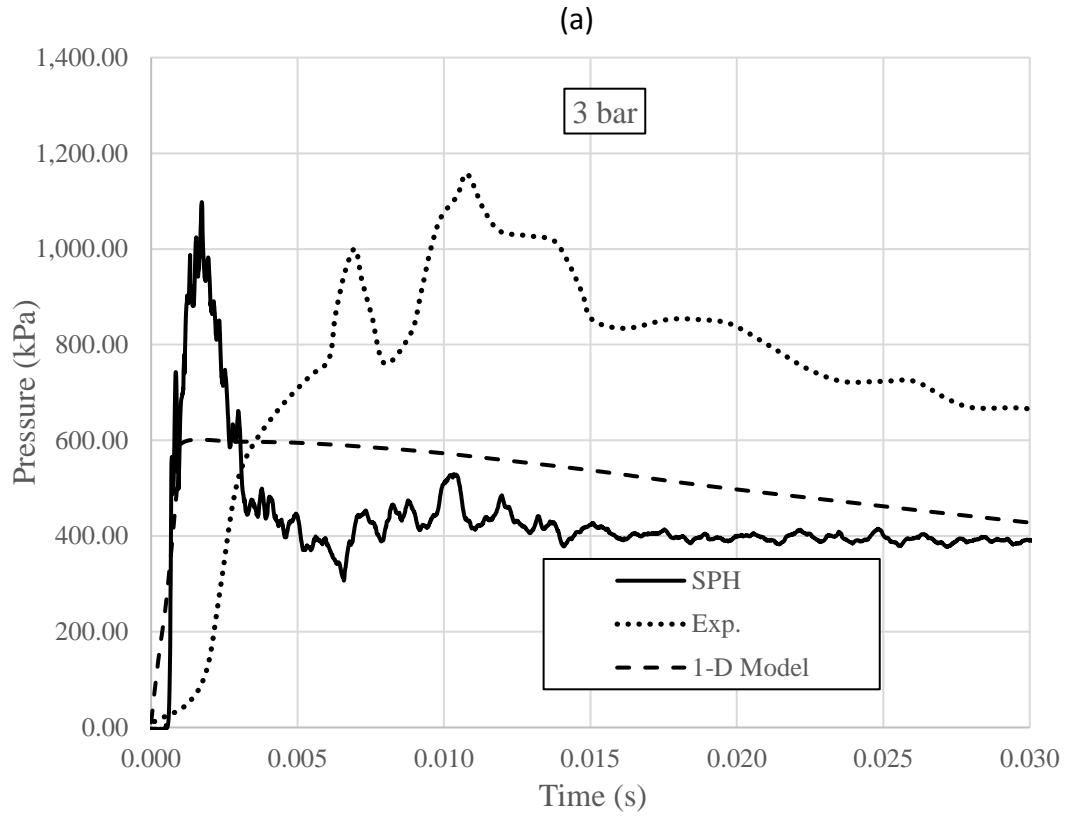


Figure 4.6 Pressure history at the elbow for a 24 kg slug and driving pressures of: (a) 3 bar, (b) 4 bar and (c) 5 bar



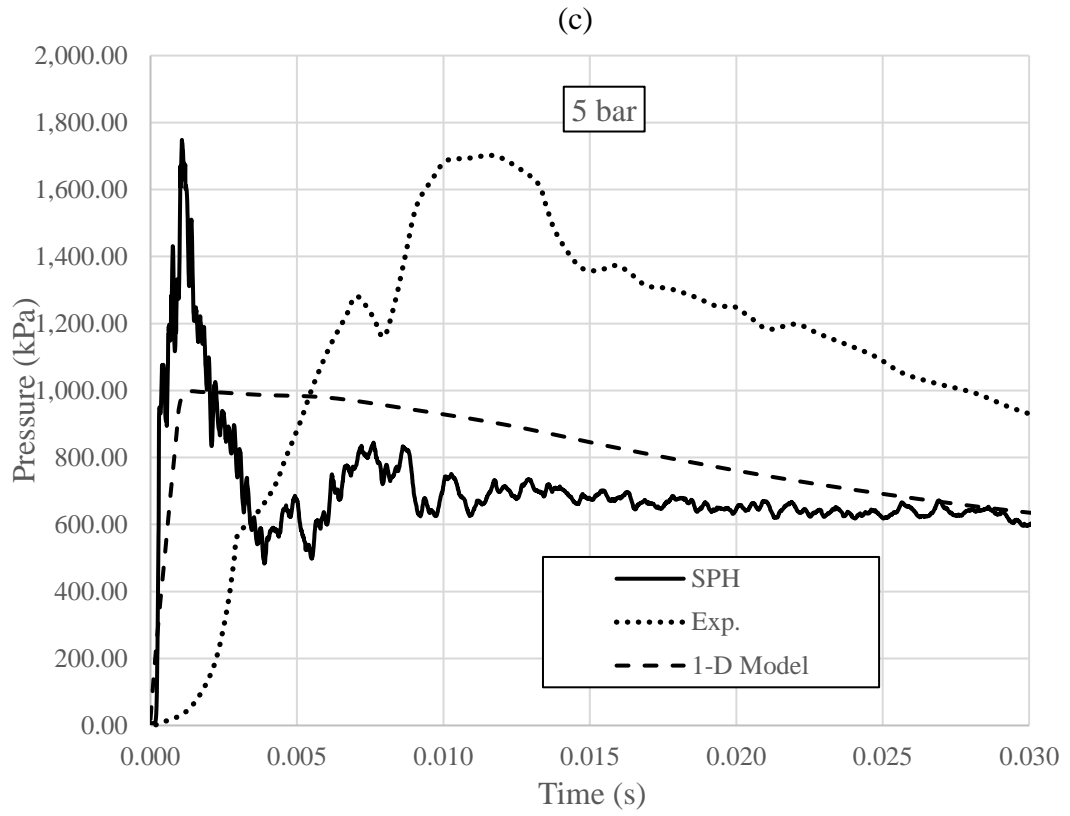


Figure 4.7 Pressure history at the elbow for a 40 kg slug and driving pressures of:
(a) 3 bar, (b) 4 bar and (c) 5 bar

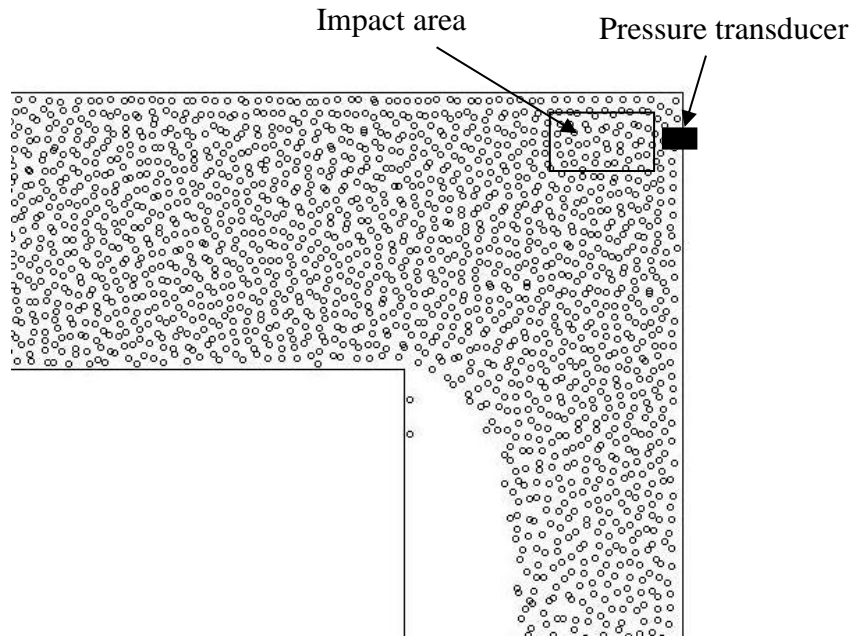


Figure 4.8 Particle distribution and flow separation at the elbow at $t = 0.015$ s (not to scale)

4.6 Results of the simulations for the Experiments of Bozkuş (1991)

In Figure 4.9, the experimental and the numerical results of Bozkuş (1991) and the results of SPH for the case of 138 kPa of initial air pressure and 2.74 m of initial slug length are given. As can be seen from the figure, the simulated peak pressures from SPH are in great agreement with the experimental data. However, time to the peak pressure show slight differences. SPH simulations also represent the general trend of the pressure variation at the elbow satisfactorily. At this point it should be mentioned that double peak in pressures are observed in the experiments of Bozkuş (1991). He pointed out that the slugs were put into motion by opening a ball valve located just downstream of the slug and the location of the valve may affect the slug dynamics to some degree since the valve was opened by hand and the operation of valve may not be the same in each run. As a result of that, Bozkuş (1991) indicated that for longer slugs, the slug separated into two pieces, moving as two slugs in the pipe.

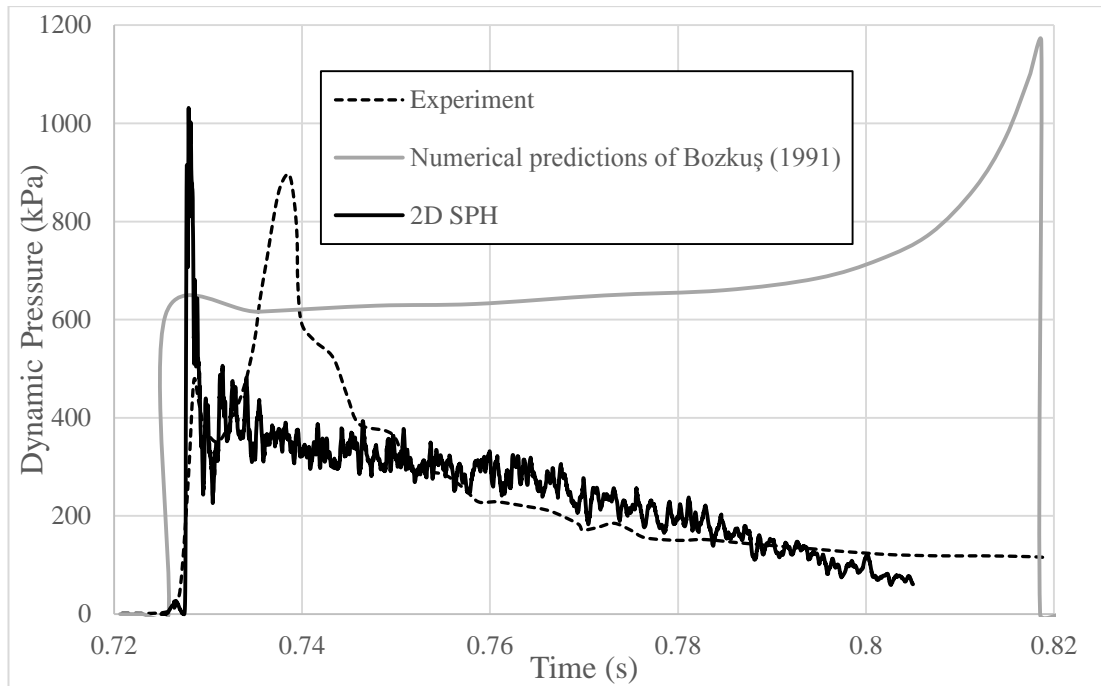


Figure 4.9 Pressure history at the elbow for an initial slug length of 2.74 m and an initial air pressure of 138 kPa.

In Figure 4.10, the simulations of the slug with an initial air pressure of 69 kPa and initial length of 2.74 m are shown. Instead of using the numerical predictions of Bozkuş (1991), the simulations of Kayhan and Bozkuş (2011) are used, because more accurate results were obtained in the latter one. Again the peak pressures are predicted well with SPH.

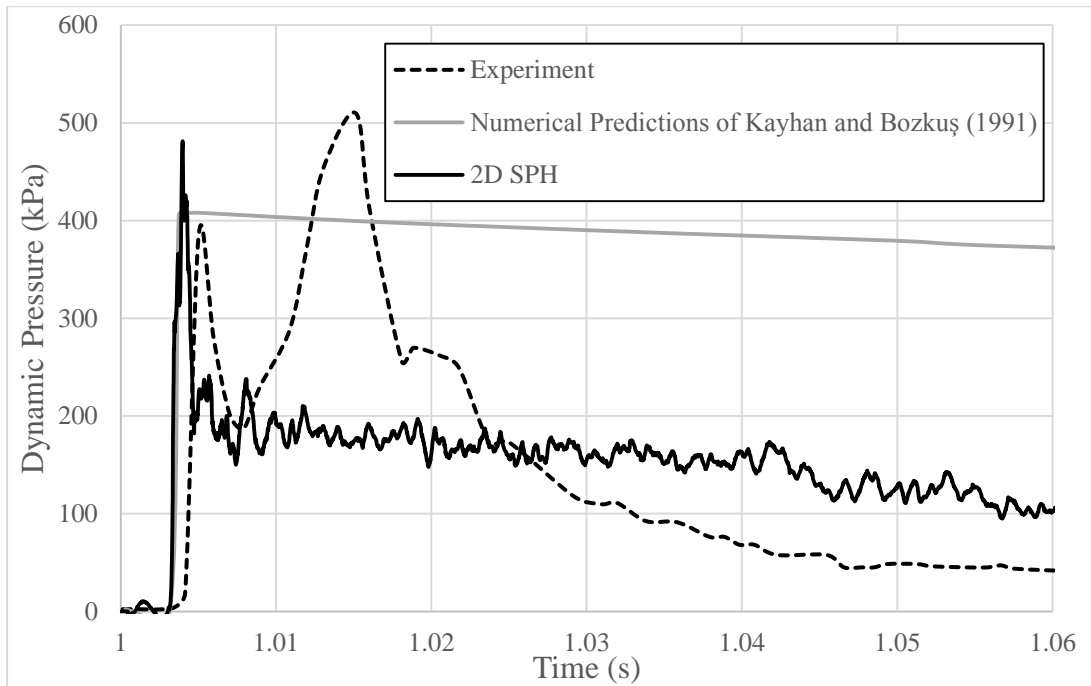


Figure 4.10 Pressure history at the elbow for an initial slug length of 2.74 m and an initial air pressure of 138 kPa.

In Figures 4.11 (a) & (b), the impact pressures due to the slugs with an initial length of 3.35 m and initial air pressure of 138 kPa and 207 kPa are shown, respectively. SPH predicts the peak pressures well.

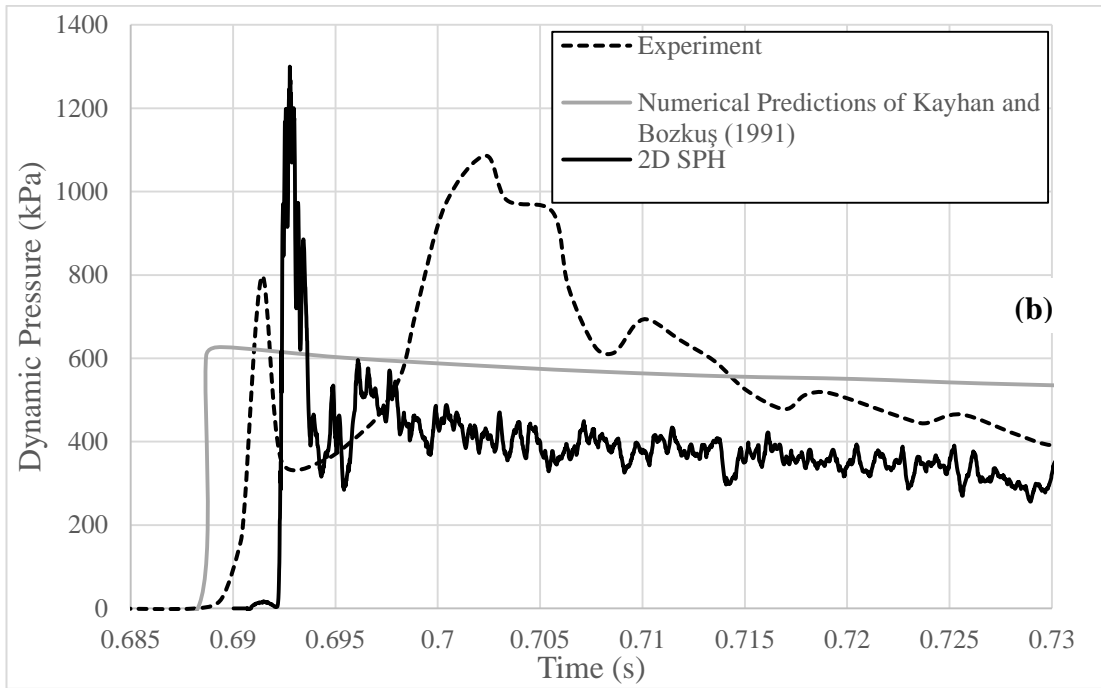
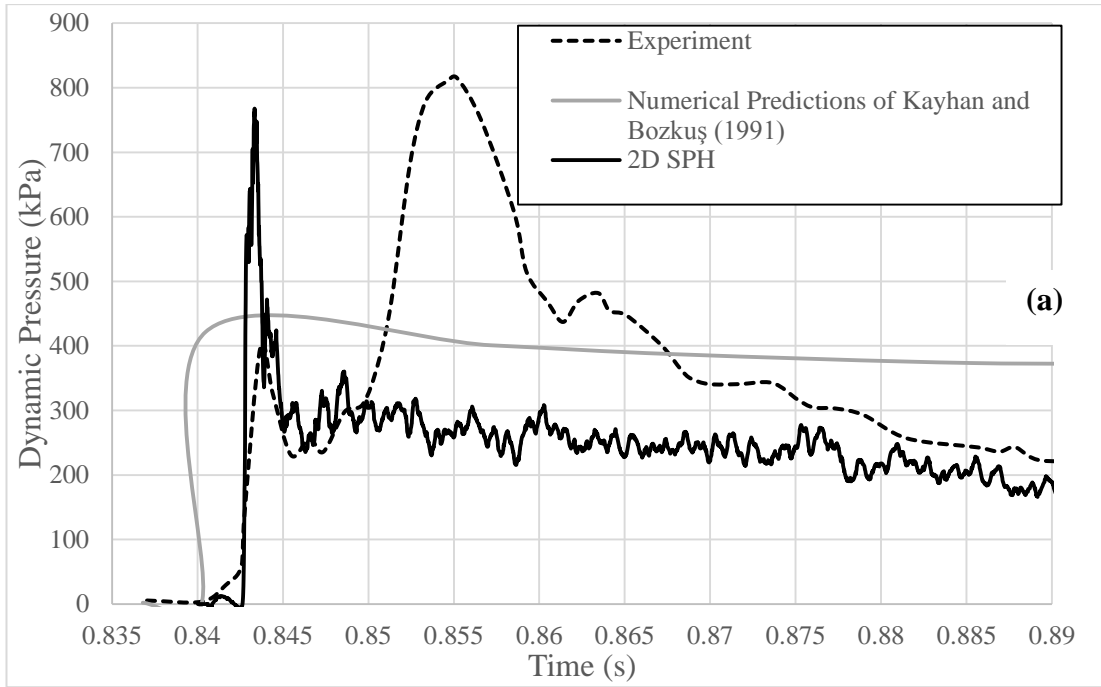


Figure 4.11 Pressure history at the elbow for an initial slug length of 3.35 m and an initial air pressure of (a) 138 kPa, (b) 207 kPa.

4.7 Discussion of Results

The dynamic pressure at an elbow due to liquid slug motion in a pipe with an upward slope has been investigated numerically. In order to validate the numerical model, the experiments of Bozkuş (1991) and Bozkuş et al. (2004) have been used. In the simulations, an improved one-dimensional model proposed by Tijsseling et al., (2016) has been used to calculate the parameters of the slug (length, velocity) just before the impact at the elbow. The proposed analytical model is applicable when the pipe slope is constant. At the elbow a two-dimensional SPH method has been used. In the simulation of slug motion using the one-dimensional model, peak pressures for short slugs agree well with experimental data. However, as stated by Tijsseling et al., (2016), the method systematically underestimates the peak pressures for long slugs. On the other hand, in the present study, the peak pressures computed using the improved one-dimensional method in combination with the two-dimensional SPH model agree very well with the experimental results even for long slugs.

CHAPTER 5

CONCLUSIONS

5.1 Summary and Conclusions

In the present study, a computer code is developed to implement SPH method to free-surface flows and closed-conduit systems. The developed two-dimensional code is validated with five experimental studies: 3 for the free-surface flow and 2 for the closed-conduit part, available in literature.

In free-surface flow part, two dimensional dam break problems are investigated numerically. The results of three recently published experimental studies are used to validate the numerical solutions. In addition to particle method, experimental studies are also simulated with mesh-based methods using turbulence models i.e. large eddy simulation (LES) and k- ϵ , a laminar and Eulerian models. Turbulence models are used since downstream of the dam, turbulence may be deemed to be effective. Both free-surfaces, velocity profiles and pressures are numerically simulated. In literature, the numerical modelling of velocity profiles with SPH method in dam-break induced flows is relatively rare. The general trend of the free-surface profile and the velocity profiles of the simulation results of the SPH method with a novel boundary method are pretty close with the results of the experiments. Turbulence modelling does not improve the results significantly. It is seen that the SPH method and laminar, Eulerian, RANS with k- ϵ turbulence and LES models can be used for the prediction of dam break flows. However, the inclination angle of the channel may somewhat adversely affect the accuracy of k- ϵ turbulence model. In addition, for a novelty, the computational time of SPH decreases with the proposed boundary model. Proposed

boundary model is promising for fluid-structure interaction problems with SPH.

For the closed-conduit part, the experiments of Bozkuş (1991) and Bozkuş et.al. (2004) about slug flow were simulated with the developed code. The results were also compared with the numerical simulations found in literature. According to the results, for both short and long slugs, calculated peak pressures show great agreement with measured peak pressures. In fact, the developed two-dimensional SPH model gives the closer peak pressure values than all other numerical models proposed in the literature, to the best knowledge of the author.

It is known that SPH uses more CPU time than regular mesh-based methods. The CPU time may be shortened by using parallel processors or various different algorithms as proposed in the study of Korzilius (2016). Since SPH is a relatively new subject, it is expected to mature over time through practical implementation and theoretical considerations. It is also known that using virtual boundary particles may be cumbersome to deal with and some modifications similar to boundary model proposed in this study may be implemented to shorten the CPU time.

5.2 Future Works

In fluid mechanics problems, the flow is usually turbulent. Therefore, the implementation of turbulence models to the developed SPH code is useful. In fact, the author has started to implement $k-\varepsilon$ turbulence model to the code.

In the present study, it is seen that RANS with $k-\varepsilon$ turbulence model give slightly underestimated results when the channel is inclined. This phenomena will be investigated in detail.

Lagrange multipliers for SPH boundaries method is mainly developed for the fluid-structure-interaction problems. In this study, a simplified version of the boundary method in which the boundary is fixed, is explained. By expanding the method, FSI problems including the deformation of the solid can be solved. In these problems, the fluid is simulated with particle methods whereas the solid is simulated with mesh-based methods.

Additional experimental studies will be conducted for the slug flow to better understand the mechanism of the slug by modifying the experimental setup of Bozkuş et al., (2004).

REFERENCES

- Aleixo, R., Soares-Frazão, S., & Zech, Y. (2011). Velocity-field measurements in a dam-break flow using a PTV Voronoï imaging technique. *Experiments in Fluids*, 50(6), 1633–1649. <https://doi.org/10.1007/s00348-010-1021-y>
- Anderson, J. D. (1995). *Computational Fluid Dynamics: The Basics with Applications*. McGraw-Hill Inc. <https://doi.org/10.1017/CBO9780511780066>
- Aureli, F., Dazzi, S., Maranzoni, A., Mignosa, P., & Vacondio, R. (2015). Experimental and numerical evaluation of the force due to the impact of a dam-break wave on a structure. *Advances in Water Resources*, 76, 29–42. <https://doi.org/10.1016/j.advwatres.2014.11.009>
- Aziz, M. (2000). Dam Breaching Model. In *Building Partnerships* (pp. 1–9). Reston, VA: American Society of Civil Engineers. [https://doi.org/10.1061/40517\(2000\)56](https://doi.org/10.1061/40517(2000)56)
- Barreiro, A., Crespo, A. J. C., Domínguez, J. M., & Gómez-Gesteira, M. (2013). Smoothed Particle Hydrodynamics for coastal engineering problems. *Computers & Structures*, 120, 96–106. <https://doi.org/10.1016/j.compstruc.2013.02.010>
- Bell, S. W., Elliot, R. C., & Chaudry, M. H. (1992). Experimental results OF 2-dimensional DAM-BREAK flows. *Journal of Hydraulic Research*, 30(2), 225–252.
- Bozkuş, Z. (1991). *The hydrodynamics of an individual transient slug in a voided line (Doctoral dissertation)*. Michigan State University, East Lansing, MI, USA.
- Bozkuş, Z., Baran, O. U., & Ger, M. (2004). Experimental and Numerical Analysis of Transient Liquid Slug Motion in a Voided Line. *Journal of Pressure Vessel Technology*, 126(2), 241. <https://doi.org/10.1115/1.1688781>

Bozkuş, Z., & Wiggert, D. C. (1997). Liquid slug motion in a voided line. *Journal of Fluids and Structures*, 11(8), 947–963. <https://doi.org/DOI 10.1006/jfls.1997.0112>

Chen, J. K., Beraun, J. E., & Jih, C. J. (1999). Improvement for tensile instability in smoothed particle hydrodynamics. *Computational Mechanics*, 23(4), 279–287. <https://doi.org/10.1007/s004660050409>

Colagrossi, A., & Landrini, M. (2003). Numerical simulation of interfacial flows by smoothed particle hydrodynamics. *Journal of Computational Physics*, 191(2), 448–475. [https://doi.org/10.1016/S0021-9991\(03\)00324-3](https://doi.org/10.1016/S0021-9991(03)00324-3)

Crespo, A. J., Gómez-Gesteira, M., & Dalrymple, R. A. (2008). Modeling Dam Break Behavior over a Wet Bed by a SPH Technique. *Journal of Waterway, Port, Coastal, and Ocean Engineering*, 134(6), 313–320. [https://doi.org/10.1061/\(ASCE\)0733-950X\(2008\)134:6\(313\)](https://doi.org/10.1061/(ASCE)0733-950X(2008)134:6(313))

Dalrymple, R. A., & Knio, O. (2001). SPH modelling of water waves. *Coastal Dynamics '01: Proceedings*, 779–787. [https://doi.org/10.1061/40566\(260\)80](https://doi.org/10.1061/40566(260)80)

Dressler, R. F. (1952). Hydraulic resistance effect upon the dam-break. *Journal of Research of the National Bureau of Standards*, 49(3), 217–225. <https://doi.org/10.6028/jres.049.021>

Elliot, R. C., & Chaudhry, M. H. (1992). A wave propagation model for two-dimensional dam-break flows. *Journal of Hydraulic Research*, 30(4), 467–483. <https://doi.org/10.1080/00221689209498895>

Fennema, R. J., & Chaudhry, M. H. (1990). Explicit Methods for 2-D Transient Free Surface Flows. *Journal of Hydraulic Engineering*, 116(8), 1013–1034. [https://doi.org/10.1061/\(ASCE\)0733-9429\(1990\)116:8\(1013\)](https://doi.org/10.1061/(ASCE)0733-9429(1990)116:8(1013))

Fenton, R. M. (1989). *The forces at a pipe bend due to the clearing of water trapped upstream (master's thesis)*. Massachusetts Institute of Technology, Cambridge, USA.

Fenton, R. M., & Griffith, P. (1990). The Force at a Pipe Bend Due to the Clearing of Water Trapped Upstream. *Transient Thermal Hydraulics and Resulting Loads on Vessel and Piping Systems, ASME*, 190, 59–67.

Ferrari, A., Dumbser, M., Toro, E. F., & Armanini, A. (2009). A new 3D parallel SPH scheme for free surface flows. *Computers and Fluids*, 38(6), 1203–1217. <https://doi.org/10.1016/j.compfluid.2008.11.012>

Fu, L., & Jin, Y. C. (2014). Simulating Velocity Distribution of Dam Breaks with the Particle Method. *Journal of Hydraulic Engineering*, 140(10), 4014048. [https://doi.org/10.1061/\(ASCE\)HY.1943-7900.0000915](https://doi.org/10.1061/(ASCE)HY.1943-7900.0000915)

Gingold, R. A., & Monaghan, J. J. (1977). Smoothed particle hydrodynamics-theory and application to non-spherical stars. *Monthly Notices of the Royal Astronomical Society*, 181, 375–389. <https://doi.org/10.1093/mnras/181.3.375>

Hernquist, L., & Katz, N. (1989). TREESPH - A unification of SPH with the hierarchical tree method. *The Astrophysical Journal Supplement Series*, 70, 419. <https://doi.org/10.1086/191344>

Hirohisa, N., Kawashima, T., & Miyamura, T. (2000). Element free analyses of shell and spatial structures. *International Journal for Numerical Methods in Engineering*, 47(6), 1215–1240. [https://doi.org/10.1002/\(SICI\)1097-0207\(20000228\)47:6<1215::AID-NME834>3.0.CO;2-M](https://doi.org/10.1002/(SICI)1097-0207(20000228)47:6<1215::AID-NME834>3.0.CO;2-M)

Hirt, C. W., & Nichols, B. D. (1981). Volume of fluid (VOF) method for the dynamics of free boundaries. *Journal of Computational Physics*, 39(1), 201–225. [https://doi.org/10.1016/0021-9991\(81\)90145-5](https://doi.org/10.1016/0021-9991(81)90145-5)

Hockney, R. W., & Eastwood, J. W. (1988). Computer Simulation Using Particles. *SIAM Review*. <https://doi.org/10.1137/1025102>

Hogg, A. J., & Woods, A. W. (2001). The transition from inertia- to bottom-drag-dominated motion of turbulent gravity currents. *Journal of Fluid Mechanics*, 449, 201. <https://doi.org/10.1017/S0022112001006292>

Hou, D. Q. (2012). *Simulating unsteady conduit flows with smoothed particle hydrodynamics (Doctoral dissertation)*. Eindhoven University of Technology, Eindhoven, The Netherlands. Retrieved from <http://repository.tue.nl/733420>

Hou, D. Q., Tijsseling, A. S., & Bozkuş, Z. (2014). Dynamic Force on an Elbow Caused by a Traveling Liquid Slug. *Journal of Pressure Vessel Technology*, *136*(3), 31302. <https://doi.org/10.1115/1.4026276>

Hu, X. Y., & Adams, N. A. (2006). A multi-phase SPH method for macroscopic and mesoscopic flows. *Journal of Computational Physics*, *213*(2), 844–861. <https://doi.org/10.1016/j.jcp.2005.09.001>

Johnson, G. R., Stryk, R. A., & Beissel, S. R. (1996). SPH for high velocity impact computations. *Computer Methods in Applied Mechanics and Engineering*, *139*(1–4), 347–373. [https://doi.org/10.1016/S0045-7825\(96\)01089-4](https://doi.org/10.1016/S0045-7825(96)01089-4)

Johnsson, P. (2011). *Smoothed particle hydrodynamic modelling of hydraulic jump (Master`s thesis)*. Lulea University of Technology, Lulea, Sweden.

Jones, D. A., & Belton, D. (2006). *Smoothed Particle Hydrodynamics: Applications within DSTO*. Victoria, Australia: DSTO Defence Science and Technology Organisation.

Kao, H. M., & Chang, T. J. (2012). Numerical modeling of dambreak-induced flood and inundation using smoothed particle hydrodynamics. *Journal of Hydrology*, *448–449*, 232–244. <https://doi.org/10.1016/j.jhydrol.2012.05.004>

Kayhan, B. A., & Bozkuş, Z. (2011). A New Method for Prediction of the Transient Force Generated by a Liquid Slug Impact on an Elbow of an Initially Voided Line. *Journal of Pressure Vessel Technology*, *133*(2), 21701. <https://doi.org/10.1115/1.4002626>

Kim J. H. (1987). Water Hammer Prevention, Mitigation, and Accommodations: A perspective. Trans. American Nuclear Society, September.

Kim, J. H., Merilo, M., and Sursock, J.P. (1988). The second EPRI workshop on water hammer in nuclear power plants. Boston.

Korzilius, S. P. (2016). *Second derivatives, particle collisions and travelling liquid slugs within smoothed particle hydrodynamics (Doctoral dissertation)*. Eindhoven University of Technology, East Lansing, MI.

Larocque, L. A., Imran, J., & Chaudhry, M. H. (2013). 3D numerical simulation of partial breach dam-break flow using the LES and $k-\epsilon$ turbulence models. *Journal of Hydraulic Research*, 51(October 2013), 145–157. <https://doi.org/10.1080/00221686.2012.734862>

LaRocque, L. A., Imran, J., & Chaudhry, M. H. (2013). Experimental and Numerical Investigations of Two-Dimensional Dam-Break Flows. *Journal of Hydraulic Engineering*, 139(6), 569–579. [https://doi.org/10.1061/\(ASCE\)HY.1943-7900.0000705](https://doi.org/10.1061/(ASCE)HY.1943-7900.0000705)

Lauber, G., & Hager, W. H. (1998). Experiments to dambreak wave: Horizontal channel. *Journal of Hydraulic Research*, 36(3), 291–307. <https://doi.org/10.1080/00221689809498620>

Lauder, B. E., & Spalding, D. B. (1974). The numerical computation of turbulent flows. *Computer Methods in Applied Mechanics and Engineering*, 3(2), 269–289. [https://doi.org/10.1016/0045-7825\(74\)90029-2](https://doi.org/10.1016/0045-7825(74)90029-2)

Lee, E. S., Moulinec, C., Xu, R., Violeau, D., Laurence, D., & Stansby, P. (2008). Comparisons of weakly compressible and truly incompressible algorithms for the SPH mesh free particle method. *Journal of Computational Physics*, 227(18), 8417–8436. <https://doi.org/10.1016/j.jcp.2008.06.005>

Lin, H., & Atluri, S. N. (2001). Analysis of incompressible Navier-Stokes flows by the meshless MLPG method. *Computer Modeling in Engineering & Sciences*, 2(2), 117–142.

Liu, G. G. R., & Liu, M. B. (2003). *Smoothed Particle Hydrodynamics: A Meshfree Particle Method*. *World* (Vol. 68).
<https://doi.org/10.1142/9789812564405>

Liu, G. R., & Gu, Y. T. (2001). A point interpolation method for two-dimensional solids. *International Journal for Numerical Methods in Engineering*, 50(4), 937–951.
[https://doi.org/10.1002/1097-0207\(20010210\)50:4<937::AID-NME62>3.0.CO;2-X](https://doi.org/10.1002/1097-0207(20010210)50:4<937::AID-NME62>3.0.CO;2-X)

Liu, G. R., & Quek, S. S. (2013). *The Finite Element Method: A Practical Course: Second Edition*. *The Finite Element Method: A Practical Course: Second Edition*. Retrieved from <http://www.scopus.com/inward/record.url?eid=2-s2.0-84904033550&partnerID=40&md5=506df17f75c35e4d0063463dbdff37f3>

Liu, G. R., & Tu, Z. H. (2002). An adaptive procedure based on background cells for meshless methods. *Computer Methods in Applied Mechanics and Engineering*, 191(17–18), 1923–1943. [https://doi.org/10.1016/S0045-7825\(01\)00360-7](https://doi.org/10.1016/S0045-7825(01)00360-7)

Lobovský, L., Botia-Vera, E., Castellana, F., Mas-Soler, J., & Souto-Iglesias, A. (2014). Experimental investigation of dynamic pressure loads during dam break. *Journal of Fluids and Structures*, 48, 407–434.
<https://doi.org/10.1016/j.jfluidstructs.2014.03.009>

Lucy, L. B. (1977). A numerical approach to the testing of the fission hypothesis. *The Astronomical Journal*, 82(12), 1013–1024. <https://doi.org/10.1086/112164>

Mandhane, J. M., Gregory, G. A., & Aziz, K. (1974). A flow pattern map for gas-liquid flow in horizontal pipes. *International Journal of Multiphase Flow*, 1(4), 537–553. [https://doi.org/10.1016/0301-9322\(74\)90006-8](https://doi.org/10.1016/0301-9322(74)90006-8)

- Martin, J. C., & Moyce, W. J. (1952). Part IV. An Experimental Study of the Collapse of Liquid Columns on a Rigid Horizontal Plane. *Philosophical Transactions of the Royal Society of London. Series A, Mathematical and Physical Sciences*, 244(882), 312–324. <https://doi.org/10.1098/rsta.1952.0006>
- Miller, S., & Chaudhry, H. M. (1989). Dam-break Flows in Curved Channel. *Journal of Hydraulic Engineering*, 115(11), 1465–1478. [https://doi.org/10.1061/\(ASCE\)0733-9429\(1989\)115:11\(1465\)](https://doi.org/10.1061/(ASCE)0733-9429(1989)115:11(1465))
- Monaghan, J. J. (1985). Particle methods for hydrodynamics. *Computer Physics Reports*, 3(2), 71–124. [https://doi.org/10.1016/0167-7977\(85\)90010-3](https://doi.org/10.1016/0167-7977(85)90010-3)
- Monaghan, J. J. (1989). On the problem of penetration in particle methods. *Journal of Computational Physics*, 82(1), 1–15. [https://doi.org/10.1016/0021-9991\(89\)90032-6](https://doi.org/10.1016/0021-9991(89)90032-6)
- Monaghan, J. J. (1992). Smoothed Particle Hydrodynamics. *Annual Review of Astronomy and Astrophysics*, 30, 543–274. <https://doi.org/10.1017/CBO9781107415324.004>
- Monaghan, J. J. (1994). Simulating free surface flows with SPH. *Journal of Computational Physics*. <https://doi.org/10.1006/jcph.1994.1034>
- Monaghan, J. J. (2005). Smoothed particle hydrodynamics. *Reports on Progress in Physics*, 68(8), 1703–1759. <https://doi.org/10.1088/0034-4885/68/8/R01>
- Monaghan, J. J., & Gingold, R. A. (1983). Shock simulation by the particle method SPH. *Journal of Computational Physics*, 52(2), 374–389. [https://doi.org/10.1016/0021-9991\(83\)90036-0](https://doi.org/10.1016/0021-9991(83)90036-0)
- Monaghan, J. J., & Kajtar, J. B. (2009). SPH particle boundary forces for arbitrary boundaries. *Computer Physics Communications*, 180(10), 1811–1820. <https://doi.org/10.1016/j.cpc.2009.05.008>

Monaghan, J. J., & Kos, A. (1999). Solitary Waves on a Cretan Beach. *Journal of Waterway, Port, Coastal, and Ocean Engineering*, 125(3), 145–155. [https://doi.org/10.1061/\(ASCE\)0733-950X\(1999\)125:3\(145\)](https://doi.org/10.1061/(ASCE)0733-950X(1999)125:3(145))

Monaghan, J. J., & Lattanzio, J. (1985). A refined particle method for astrophysical problems. *Astronomy and Astrophysics*, 149, 135–143. <https://doi.org/10.1017/CBO9781107415324.004>

Morris, J. P. (2000). Simulating surface tension with smoothed particle hydrodynamics. *International Journal for Numerical Methods in Fluids*, 33(3), 333–353. [https://doi.org/10.1002/1097-0363\(20000615\)33:3<333::AID-FLD11>3.0.CO;2-7](https://doi.org/10.1002/1097-0363(20000615)33:3<333::AID-FLD11>3.0.CO;2-7)

Morris, J. P., Fox, P. J., & Zhu, Y. (1997). Modeling Low Reynolds Number Incompressible Flows Using SPH. *JOURNAL OF COMPUTATIONAL PHYSICS*, 136, 214–226. <https://doi.org/10.1006/jcph.1997.5776>

Nelson, A. F., Wetzstein, M., & Naab, T. (2009). Vine—a Numerical Code for Simulating Astrophysical Systems Using Particles. II. Implementation and Performance Characteristics. *The Astrophysical Journal Supplement Series*, 184(2), 326–360. <https://doi.org/10.1088/0067-0049/184/2/326>

Neumann, A. (1991). *The forces exerted on a pipe bend due to a pipe clearing transient (Master`s thesis)*. Massachusetts Institute of Technology, Cambridge, USA.

Neumann, A., and Griffith, P., (1992). Forces on a pipe bend resulting from clearing a pool of liquid upstream. *Transient Thermal-Hydraulics and Structural Mechanics*, ASME PVP Vol. 231, ASME, New York.

Owen, I., & Hussein, I. B. (1994). The propulsion of an isolated slug through a pipe and the forces produced as it impacts upon an orifice plate. *International Journal of Multiphase Flow*, 20(3), 659–666. [https://doi.org/10.1016/0301-9322\(94\)90036-1](https://doi.org/10.1016/0301-9322(94)90036-1)

Ozmen-Cagatay, H., & Kocaman, S. (2010). Dam-break flows during initial stage using SWE and RANS approaches. *Journal of Hydraulic Research*, 48(5), 603–611. <https://doi.org/10.1080/00221686.2010.507342>

Piomelli, U. (1999). Large-eddy simulation: achievements and challenges. *Progress in Aerospace Sciences*, 35(4), 335–362. [https://doi.org/10.1016/S0376-0421\(98\)00014-1](https://doi.org/10.1016/S0376-0421(98)00014-1)

Pohle, F. V. (1950). *The Lagrangian equations of hydrodynamics: solutions which are analytic functions of the time (Doctoral dissertation)*. New York University, New York, USA.

Ritter, A. (1892). Die Fortpflanzung der Wasserwellen. *Vereine Deutscher Ingenieure Zeitschrift*, 36(2), 947–954.

Schlatter, B. (1999). *Modeling fluid flow using smoothed particle hydrodynamics (Master's thesis)*. Oregon State University, Oregon, USA.

Springel, V., White, M., & Hernquist, L. (2001). Hydrodynamic Simulations of the Sunyaev-Zeldovich Effect(s). *The Astrophysical Journal*, 549(2), 681–687. <https://doi.org/10.1086/319473>

Stansby, P. K., Chegini, A., & Barnes, T. C. D. (1998). The initial stages of dam-break flow. *Journal of Fluid Mechanics*, 374, 407–424. <https://doi.org/10.1017/S0022112098009975>

Staubach, D. (2010). *Smoothed particle hydrodynamics real-time fluid simulation approach (Doctoral dissertation)*. Friedrich-Alexander-Universität Erlangen-Nürnberg.

Stoker, J. J. (1957). *Water waves: The mathematical theory with applications*. Wiley-Interscience, New York.

Tijsseling, A.S., Hou, Q. & Bozkuş, Z., (2016). An improved one-dimensional model for liquid slugs traveling in pipelines. *Journal of Pressure Vessel Technology*, 138(1). <https://doi.org/10.1115/1.4029794>

Viccione, G., Bovolín, V., & Carratelli, E. P. (2008). Defining and optimizing algorithms for neighbouring particle identification in SPH fluid simulations. *International Journal for Numerical Methods in Fluids*, 58(6), 625–638. <https://doi.org/10.1002/flid.1761>

Weller, H. G., Tabor, G., Jasak, H., & Fureby, C. (1998). A tensorial approach to computational continuum mechanics using object-oriented techniques. *Computers in Physics*, 12(6), 620. <https://doi.org/10.1063/1.168744>

Whitham, G. B. (1955). The Effects of Hydraulic Resistance in the Dam-Break Problem. *Proceedings of the Royal Society A: Mathematical, Physical and Engineering Sciences*, 227(1170), 399–407. <https://doi.org/10.1098/rspa.1955.0019>

Wilcox, D. C. (1998). *Turbulence Modeling for CFD (Second Edition)*. DCW Industries.

Yang, J., & Wiggert, D. C. (1998). Analysis of Liquid Slug Motion in a Voided Line. *Journal of Pressure Vessel Technology*, 120(1), 74. <https://doi.org/10.1115/1.2841889>

Yildiz, M., Rook, R. A., & Suleman, A. (2009). SPH with the multiple boundary tangent method. *International Journal for Numerical Methods in Engineering*, 77(10), 1416–1438. <https://doi.org/10.1002/nme.2458>

Zhang, H., Nakagawa, H., Kawaike, K., & Baba, Y. (2009). Experiment and simulation of turbulent flow in local scour around a spur dyke. *International Journal of Sediment Research*, 24(1), 33–45. [https://doi.org/10.1016/S1001-6279\(09\)60014-7](https://doi.org/10.1016/S1001-6279(09)60014-7)

Zhiyin, Y. (2015). Large-eddy simulation: Past, present and the future. *Chinese Journal of Aeronautics*, 28(1), 11–24. <https://doi.org/10.1016/j.cja.2014.12.007>

Zienkiewicz, O. C., Taylor, R. L., & Zhu, J. Z. (2013). The Finite Element Method: its Basis and Fundamentals. *The Finite Element Method: Its Basis and Fundamentals*, 493–543. <https://doi.org/10.1016/B978-1-85617-633-0.00015-0>

CURRICULUM VITAE

Name Dr. Ali Ersin Dinçer
E-mail aliersindincer@gmail.com



Education

- **Ph. D.**
(2013-2017) Middle East Technical University
Civil Engineering / Hydromechanics

Thesis: Numerical Investigation of Free Surface and Pipe Flow Problems by Smoothed Particle Hydrodynamics
- **M. Sc.**
(2010-2013) Middle East Technical University
Civil Engineering / Hydromechanics

Thesis: Investigation of Waterhammer Problems in the Penstocks of Pumped-Storage Hydropower Plants
- **B. Sc.**
(2006-2011) Anadolu University
Department of Business
- **B. Sc.**
(2005-2010) Middle East Technical University
Civil Engineering

Work Experience

- **Research Assistant (2011 -2017)** Middle East Technical University
Civil Engineering / Hydromechanics
- **Project Engineer (2010-2011)** GF Project

Project Work

- 2014-2015** Kaleköy Barajı ve Hidroelektrik Enerji Santrali Dolusavak Hidrolik Model Çalışmaları. **Researcher.**
- 2014-2014** İncir Barajı ve Hidroelektrik Enerji Santrali Hidrolik Model Çalışmaları 2013.03.03.2.00.60. **Researcher.**
- 2013-2014** Artvin Barajı ve Hidroelektrik Enerji Santrali Dipsavak Model Çalışmaları 2013.03.03.2.00.12. **Researcher.**
- 2012-2013** Beyhan 1 Barajı ve Hidroelektrik Enerji Santrali Su Alma Yapıları Hidrolik Model Çalışmaları. **Researcher.**

Awards

1. Water-loss Reduction of Keçiören N8.1 Region (Ankara) Water Distribution Network by means of Pressure Drop at Night, 2014, United Nations Development Programme (UNDP)
2. Evaporation Shield, 2014, United Nations Development Programme (UNDP)